Technische Universität München

Fakultät für Medizin

Institut für medizinische Mikrobiologie, Immunologie und Hygiene

# Histopathological and functional analysis of the tumor suppressor RNF43 during gastric carcinogenesis

Victoria Diana Neumeyer, M.Sc.

Vollständiger Abdruck der von der Fakultät für Medizin der Technischen Universität München zur Erlangung des akademischen Grades eines

**Doktors der Naturwissenschaften (Dr. rer. nat.)**

genehmigten Dissertation.

| | |
|---|---|
| Vorsitzender: | Prof. Dr. Wilko Weichert |
| Prüfende der Dissertation: | 1. Prof. Dr. Markus Gerhard |
| | 2. Prof. Dr. Percy A. Knolle |
| | 3. Prof. Dr. Andreas Jung |

Die Dissertation wurde am 24.04.2020 bei der Technischen Universität eingereicht und durch die Fakultät für Medizin am 16.02.2021 angenommen.

The work presented herein was performed at the Institute of Microbiology, Immunology and Hygiene of the Technical University of Munich under the direction of Prof. Dr. Markus Gerhard in the period of January 2016 to March 2020.

Parts of this thesis have already been published in scientific journals.

**Victoria Neumeyer***, Martina Grandl*, Alisa Dietl, Anna Brutau-Abia, Michael Allgäuer, Behnam Kalali, Yang Zhang, Kai-Feng Pan, Katja Steiger, Michael Vieth, Martina Anton, Raquel Mejías-Luque*, Markus Gerhard*.; Loss of Endogenous RNF43 Function Enhances Proliferation and Tumour Growth of Intestinal and Gastric Cells.; Carcinogenesis 40 (4), 551-559, 2019 Jun 10.; DOI: 10.1093/carcin/bgy152

**Victoria Neumeyer**, Michael Vieth, Markus Gerhard, Raquel Mejías-Luque.; Mutated Rnf43 Aggravates Helicobacter Pylori-Induced Gastric Pathology.; Cancers (Basel) 11 (3), 2019 Mar 16.; DOI: 10.3390/cancers11030372

**Victoria Neumeyer**, Anna Brutau-Abia, Michael Allgäuer, Nicole Pfarr, Wilko Weichert, Christina Falkeis-Veits, Elisabeth Kremmer, Michael Vieth, Markus Gerhard, Raquel Mejías-Luque.; Loss of RNF43 Function Contributes to Gastric Carcinogenesis by Impairing DNA Damage Response.; Cellular and Molecular Gastroenterology and Hepatology. 2021;11(4):1071-1094. doi: 10.1016/j.jcmgh.2020.11.005

**Pánta chorei kaì oudèn ménei**

Plato, 427 – 347 B.C.

## Table of content

# 1 Summary

Mutations in the E3 ubiquitin ligase RING finger protein 43 (RNF43) have been described as driving mutations for gastric cancer important for the transition from adenoma to carcinoma. In the colon and the pancreas, RNF43 acts as a tumor suppressor by negatively regulating Wnt signaling. In the stomach, studies have shown that RNF43 was negatively correlated with proliferation and that its overexpression impaired stem-like properties in gastric cancer cell lines. Yet, the mechanism by which RNF43 acts as a tumor suppressor in the stomach has not been determined.

In this study, we aimed at deciphering the role of endogenous RNF43 during gastric carcinogenesis and the molecular mechanisms behind. Loss of RNF43 expression in gastric cancer cells was induced by a lentiviral knock down as well as CRISPR/Cas9 technology. RNF43 depleted cells showed a higher tumorigenic potential *in vitro* and *in vivo* in a xenograft mouse model. In *Rnf43*$^{\Delta Exon8}$ and Rnf43$^{H292R/H295R}$ mice bearing mutations that lead to loss of function in Rnf43, we could detect gastric multifocal hyperplasia which worsened over time. However, we could not detect enhanced expression of Wnt target genes in the stomach of these mice, indicating that RNF43 acts independent of Wnt in the gastric epithelium. A study in pancreatic duct cells suggested that RNF43 could also be involved in DNA damage response (DDR). To explore this, we treated gastric cancer cells with ionizing radiation and chemotherapy. RNF43 loss of function lead to reduced activation of DDR, resistance to apoptosis and reduced susceptibility to chemotherapy.

*Helicobacter pylori* infection is the major risk factor for gastric cancer and this infection can directly induce DNA damage. Loss of Rnf43 function in mice increased inflammation and worsened *H. pylori*-driven pathology. Additionally, DDR activation was reduced in *Rnf43*$^{\Delta Exon8}$ mice compared to wild type mice upon infection. Moreover, *RNF43* was mutated in gastric tumors, upregulated during gastric carcinogenesis and correlated with DDR activation in human gastric samples.

Taken together, we could show that RNF43 is a tumor suppressor that is involved in DDR in the stomach.

## Zusammenfassung

Mutationen in der E3-Ubiquitin-Ligase RING-Fingerprotein 43 (RNF43) sind als treibende Mutationen für Magenkrebs beschrieben worden, die für den Übergang vom Adenom zum Karzinom wichtig sind. Im Dickdarm und in der Bauchspeicheldrüse wirkt RNF43 als Tumorsuppressor, indem es den Wnt-Signalweg reguliert. Im Magen haben Studien gezeigt, dass RNF43 negativ mit der Zellproliferation korreliert war und dass die Überexpression die Stammzell-ähnlichen Eigenschaften in Magenkrebszelllinien beeinträchtigte. Der Mechanismus, durch den RNF43 als Tumorsuppressor im Magen wirkt, ist jedoch noch nicht geklärt.

In der vorliegenden Studie zielten wir darauf ab, die Rolle des endogenen RNF43 während der Magenkarzinogenese und die molekularen Mechanismen dahinter zu entschlüsseln. Der Verlust der RNF43-Expression in Magenkrebszellen wurde durch einen lentiviralen Knockdown sowie durch die CRISPR/Cas9-Technologie induziert. Zellen mit verringerter RNF43 Expression zeigten *in vitro* und *in vivo* in einem Xenotransplantat-Mausmodell ein höheres tumorerzeugendes Potenzial. In *Rnf43*$^{\Delta Exon8}$ und in Rnf43$^{H292R/H295R}$ Mäusen, die Mutationen tragen, die zum Funktionsverlust von Rnf43 führen, konnten wir eine gastrische multifokale Hyperplasie nachweisen, die sich mit der Zeit verschlimmerte. Wir konnten jedoch keine verstärkte Expression von Wnt-Zielgenen im Magen dieser Mäuse nachweisen, was darauf hinweist, dass RNF43 im Magenepithel unabhängig von Wnt wirkt. Eine Studie an Zellen des Pankreasgangs deutete darauf hin, dass RNF43 auch an der DNA-Schadensantwort (DDR) beteiligt sein könnte. Um dies zu untersuchen, haben wir Magenkrebszellen mit ionisierender Strahlung und Chemotherapie behandelt. Der Funktionsverlust von RNF43 führte zu einer verminderten Aktivierung der DDR, zu einer Resistenz gegen Apoptose und zu einer verminderten Anfälligkeit für Chemotherapie.

Die Infektion mit *Helicobacter pylori* ist der wichtigste Risikofaktor für Magenkrebs, und diese Infektion kann direkt eine DNA-Schädigung hervorrufen. Der Verlust der Rnf43-Funktion bei Mäusen führte zu einer verstärkten Entzündung und einer Verschlechterung der durch *H. pylori* verursachten

Pathologie. Zusätzlich war die DDR-Aktivierung bei *Rnf43*$^{\Delta Exon8}$ Mäusen im Vergleich zu Wildtyp-Mäusen nach der Infektion reduziert. Darüber hinaus war RNF43 in Magentumoren mutiert, während der Magenkarzinogenese hochreguliert und korrelierte mit der DDR-Aktivierung in menschlichen Magenproben.

Zusammengefasst konnten wir zeigen, dass RNF43 ein Tumorsuppressor ist, der im Magen an der DDR beteiligt ist.

# 2 Introduction

## 2.1 Gastric cancer

Gastric cancer is the 5th most prevalent cancer in the world and the 3rd leading cause of cancer related death with an estimated number of 780,000 deaths per year worldwide [1]. Over 70 % of the cases occur in developing countries. 90 – 95 % of gastric cancers are adenocarcinomas, while lymphomas account for 4 % and neuroendocrine tumors for 3 % of the cases, respectively. Metastases of gastric carcinoma are commonly found in the supraclavicular lymph nodes, the liver and the lung. Gastric cancer is a multifactorial disease which can be caused by several environmental factors, such as smoking, diet, especially nitrate and nitrite rich diet, and the chronic infection with the pathogen *Helicobacter pylori* [2].

### 2.1.1 Gastric mucosal homeostasis and stem cell renewal

The stomach is part of the gastrointestinal tract and plays an important role in the digestion of food. It is located in the upper abdomen between the esophagus and the duodenum. Its main functions are the retention and digestion of food, killing of bacteria and the production of the intrinsic factor which is essential for vitamin $B_{12}$ uptake. The stomach can be divided into five parts that have distinct functions: the cardia, fundus, corpus, pyloric antrum and the pylorus (**Figure 1**). The cells located in the cardiac glands produce mucus to build up a mucus barrier between the stomach and the esophagus. The glands in this part are shallower than those in the corpus and pylorus [3].

In the corpus and fundus, the foveola represents one third of the gastric glands and contains mucus producing foveolar cells. Parietal and mucous neck cells are located in the neck region. Parietal cells are responsible for the secretion of HCl and the intrinsic factor, a glycoprotein that is essential for vitamin $B_{12}$ uptake in the ileum. These cells contain numerous mitochondria and the $H^+/K^+$ ATPase, the proton pump that exchanges $K^+$ ions for $H^+$ ions against a strong concentration gradient. Mucous neck cells produce the mucin MUC6 and trefoil factors. Furthermore, multipotent gastric stem cells

are found in the neck region which contrasts with the location of the stem cells in the antrum and the intestine, where stem cells are located at the bottom of the glands. The main cell type found at the base of the glands are chief cells, which produce and secrete lipase and pepsinogens. In the acidic gastric juice, the inhibitory peptide is cleaved, and the resulting active form pepsin can break down proteins in the chyme. The secretion of pepsinogens is induced by the parasympathetic nervous system and gastrin that is produced in the antrum. Beneath the epithelium especially in the vicinity of parietal cells, enterochromaffin-like cells (ECL cells) can be found. These ECL cells secrete histamine which then stimulates the production of acid. In the pyloric antrum, the pits reach deeper, making up about half of the pyloric gland. In these glands, MUC6 producing cells can be found as well as gastrin producing G cells and somatostatin producing D cells. By secreting these molecules, G and D cells play an important role in acid production and pepsinogen secretion. In the antrum, the gastric stem cells are found in the base of the glands (**Figure 1**) [4] .

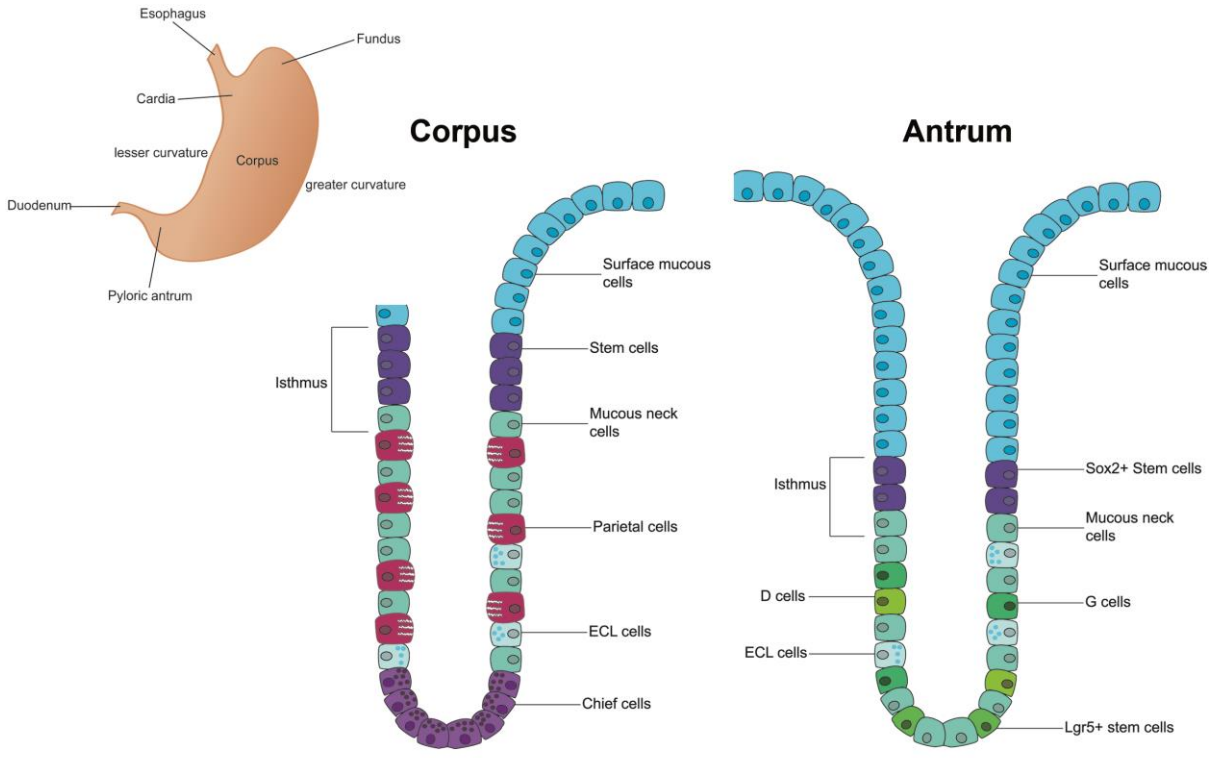


**Figure 1: Schematic representation of the composition and cell types of gastric glands in the corpus and fundus.**

While the stem cell niche has been characterized extensively in the intestinal epithelium, little is known about tissue homeostasis and stem cell renewal in the gastric epithelium. Gastric multipotent

stem cells have been described to be located at the neck of fundic glands and at the base of pyloric glands, and to sequentially differentiate into all gastric cell types [5]. Epithelial growth factor (EGF) and Indian hedgehog (Ihh) trigger the differentiation into surface mucous cells, which have a life span of 3 to 5 days [6], while gastrin, Sonic hedgehog (Shh) and Bone morphogenetic protein 4 (BMP4) lead to differentiation into parietal cells, which are exchanged after 8 weeks [7]. Furthermore, stem cells can give rise to mucous neck cells, which then further differentiate into Mist1 expressing chief cells with a life span of several months [6].

Numerous studies have tried to identify signaling pathways that are important for maintenance of the stem cell niche as well as markers by which stem cells can be defined. In the antrum, Wnt signaling, the key regulator of intestinal stem cells, was described to be involved in cell renewal [8]. Cells positive for Leucine-rich repeat-containing G-protein coupled receptor 5 (LGR5), a receptor involved in Wnt signaling, and the Wnt target gene Axin2 were shown to divide frequently and to be able to repopulate antral glands under homeostatic conditions [9]. In contrast, more recent studies showed that LGR5-positive cells have a low proliferation rate and that a population of LGR5-negative Axin2-positive cells divide frequently and are also able to give rise to all antral gland cells under homeostatic conditions as well as upon injury [10, 11]. These cells were suggested to be LGR4-positive, a receptor that can also activate Wnt signaling, and were found at the bottom of antral glands as well [12, 13]. Mice with hyperactivated Wnt signaling developed tumors in the antrum but not in the corpus, further supporting an important role for this signaling pathway in the antral stem cell niche [14]. In contrast, less is known about the stem cell compartment of the corpus. Tamoxifen, which is frequently used to perform lineage tracing experiments, was shown to damage parietal cells and induce metaplasia, making it difficult to trace corpus gland repopulation under homeostatic conditions with these methods [15]. However, when performing tamoxifen-based lineage tracing a population of LGR5-positive gland base chief cells was shown to be able to repopulate corpus glands upon injury [16]. Furthermore, LGR5-negative stem cells in the isthmus region were shown to regenerate the glands bidirectionally [17].

SRY (sex determining region Y)-box 2 (SOX2) is a transcription factor that regulates embryonic development. SOX2 was shown to be expressed in corpus and antral glands of the adult stomach, however, its expression is not restricted to a specific gland zone. Furthermore, SOX2 positive cells were shown to be able to repopulate gastric glands and to differentiate into all cell types and ablation of SOX2 expressing cells hampered renewal of the gastric epithelium [18, 19]. This suggests, that SOX2-positive cells mark a gastric stem cell population distinct from LGR5-positive cells.

### 2.1.2 Gastric cancer stem cells

The cancer stem cell theory describes a hierarchical organization of the cancer tissue with stem cell-like cells that can generate all subpopulations of tumor cells. These cells were found to be more tumorigenic and more resistant to chemotherapy [20]. Several markers have been proposed to identify cancer stem cells, which are shared by tumor types including gastric cancer. One of these markers is the cell surface glycoprotein CD44. CD44 was shown to be expressed on tumor-initiating gastric cancer cells and conferred resistance to chemotherapy [21]. Furthermore, certain splice variants of CD44 were shown to have a prognostic value on cancer recurrence in early gastric cancer patients [22]. In mice, it was shown that CD44 was highly expressed in dysplastic gastric epithelium upon *H. pylori* infection and was enriched in invasive cells, while it was only expressed at the base of antral glands in normal murine gastric tissue [21]. CD133 (also known as Prominin1) is another cell surface protein that was described to be expressed on gastric cancer stem cells. CD133 is frequently expressed in gastric tumors and was positively correlated with cancer progression and poor prognosis, and negatively with disease free survival [23, 24]. Furthermore, CD133 was suggested to confer resistance to chemotherapeutic treatment by activation of PI3K/Akt signaling, thereby preventing apoptosis. Both, CD44 and CD133 were shown to drive epithelial-mesenchymal transition (EMT) through downregulation of E-cadherin and upregulation of vimentin [25]. Additionally, Aldehyde dehydrogenase 1 (ALDH1) has been described as a marker for cancer stem cells and especially its subtype ALDH1A1 was shown to modulate cell differentiation and survival and to mediate EMT. ALDH1 expression in gastric cancer patients was associated with tumor progression [25, 26]. Taken

together, gastric cancer stem cells defined by the markers described above display higher tumorigenic potential and have a prognostic value for gastric cancer patients.

### 2.1.3 Classification of gastric tumors

Gastric cancers display high inter- and intraindividual heterogeneity [27] and several models have been proposed to classify subtypes of gastric tumors. Former classifications are based on histological features; however, these hardly guide therapy and therefore have little clinical utility.

The WHO suggested to subdivide cancers into 5 subtypes: papillary, tubular, mucinous or mixed adenocarcinoma as well as poorly cohesive carcinoma containing signet-ring cells [28]. A more commonly used distinction is the Laurén classification that divides gastric cancers into intestinal, diffuse, mixed or indeterminant gastric cancer. Intestinal-type gastric cancer resembles neoplasms of the intestinal mucosa expressing intestinal markers such as Caudal Type Homeobox 2 (CDX2), and can be well, moderately or poorly differentiated. Diffuse-type gastric cancer on the other hand appears poorly differentiated with lost cell-cell adhesion. The cancer cells produce mucus that is secreted into the interstitium or is retained inside of signet-ring cells [29]. When comparing WHO and Laurén classification, poorly cohesive carcinoma and diffuse-type gastric cancer describe the same pathology, while intestinal-type cancer comprises papillary, tubular and mucinous adenocarcinoma.

As described above, these classifications have little influence on therapy since they are solely based on histological appearance. Therefore, a more recent study tried to subdivide gastric cancers according to their molecular features [30]. Samples were analyzed for presence of Epstein-Barr-Virus (EBV), micro-satellite instability (MSI) and chromosomal instability (CIN). $EBV^+$ tumors accounted for around 9 % of cases and were more commonly found in the fundus or corpus. These tumors showed a high CpG island methylator phenotype (CIMP) with promoter hypermethylation of the cell cycle regulator Cyclin-dependent kinase inhibitor 2A (*CDKN2A*), for example, and amplification of genes involved in immune response, such as Programmed death-ligand 1 and 2 (*PD-L1/2*). 22 % of cases were MSI tumors displaying hypermethylation of the DNA repair gene MutL homolog 1 (*MLH1*)

resulting in a high mutation burden. Among the genes mutated in these tumors, tumor suppressors and oncogenes such as *p53* or *KRAS* are commonly found. The most common type is CIN tumors, which represent about 50 % of cases. These tumors are often found in the gastroesophageal junction and the cardia, and mainly include intestinal-type cancers. These tumors often harbor mutations in *p53* and gene amplifications in the receptor tyrosine kinase (RTK) pathways such as epidermal growth factor receptor (EGF). Tumors negative for all these features are defined as genomically stable and represent diffuse-type gastric cancers according to the Laurén classification. On a molecular basis, these tumors display a loss of E-cadherin expression caused by mutations in the corresponding *CDH1* gene as well as in other genes related to cell adhesion and motility, such as Claudin 18 or Ras homolog gene family, member A (RhoA). This molecular classification might help to select specific targeting agents based on the expression and mutation profiles to improve therapy, for example the use of specific antibodies and inhibitors of RTKs in CIN tumors.

### 2.1.4 Development of gastric cancer

Gastric cancer is a multifactorial disease and many environmental factors such as diet or smoking can influence malignant transformation of the stomach epithelium. For intestinal-type gastric cancer, the transition of normal gastric mucosa to cancer has been described in the Correa's pathway (**Figure 2**) [31]. Here, chronic gastritis serves as a trigger for tissue transformation. This chronic gastritis presents with an infiltration of lymphocytes and plasma cells and is defined by the Sydney classification according to its location, infiltration of immune cells, presence of atrophy and intestinal metaplasia and bacterial load of *H. pylori* [32]. Chronic gastritis can be caused by several agents. Autoimmune (type A) gastritis is caused by autoreactive T cells and antibodies against parietal cells, resulting in anacidity of the gastric juice. This loss of acid production can induce hyperplasia of G and ECL cells, and parietal atrophy and metaplasia. Chemical (C type) gastritis is induced by damaging agents such as alcohol or non-steroidal anti-inflammatory drugs (NSAIDs) or by reflux of bile acid into the stomach. This type of gastritis is characterized by increased epithelial regeneration and foveolar hyperplasia. However, 80 to 90 % of all gastritis cases are caused by infection with *H. pylori* infection (type B

gastritis). This type of gastritis mainly occurs in the antrum but can develop into pangastritis that spreads to the corpus [2]. Here, chronic inflammation can lead to parietal atrophy and intestinal metaplasia during tissue regeneration. Furthermore, the production of reactive oxygen species (ROS) as well as pathogen induced DNA damage can favor the acquisition of mutations in the epithelium [33]. Additionally, several pathways related to inflammation, such as Signal transducer and activator of transcription 3 (STAT3) or nuclear factor kappa-light-chain-enhancer of activated B cells (NF-κB) signaling can drive cell proliferation and survival [34, 35]. The mechanisms, by which *H. pylori* can colonize the stomach, induce inflammation and cause tissue damage will be discussed in section 2.2. B type and, in rare cases, A type gastritis can progress to intestinal metaplasia (IM). During chronic inflammation and subsequent regenerative processes in the gastric mucosa, gastric stem cells can differentiate into cells of the intestinal epithelium. In this IM, the foveolar epithelium and the stomach specific glands are replaced by tubular glands of the intestine. In these glands, microvilli carrying enterocytes, goblet cells and Paneth cells can be found. Furthermore, predominant mucins of the intestine, such as MUC2, as well as the intestinal transcription factor CDX2 are expressed [2]. These characteristics usually serve as markers for detection of IM in the stomach. A second type of metaplasia that has been described to occur in the stomach is spasmolytic polypeptide expressing metaplasia (SPEM). SPEM is characterized by a loss of parietal cells and chief cells and high levels of trefoil factor 2 (TFF2) at the base of the glands. During this type of metaplasia, chief cells lose their maturity markers, such as Mist1, reenter the cell cycle and start to express TFF2, while they still express pepsinogens. SPEM is usually triggered by parietal cell loss and can occur during *H. pylori* infection since this bacterium leads to an expansion of the proliferative zone to the gland base [36, 37]. In humans, both metaplasia types are frequently found during malignant transformation of the stomach, whereas in mice, mostly SPEM occurs after gastric tissue damage [38]. Additionally, it has been shown that bone marrow-derived cells infiltrating the epithelium during inflammation can also repopulate the gastric tissue and transition to metaplasia and dysplasia [39, 40]. Taken together, these responses to ongoing tissue damage can then further deregulate tissue homeostasis and accumulate

genomic alterations resulting in dysplasia and finally intestinal-type gastric cancer. Additionally, remodeling of the gastric tissue disrupts the equilibrium between acid production and protection of the epithelium. A less acidic environment in the stomach can then lead to bacterial overgrowth, which can further drive inflammatory processes and lead to the production of harmful bacterial metabolites such as carcinogenic nitrosamines [41, 42].

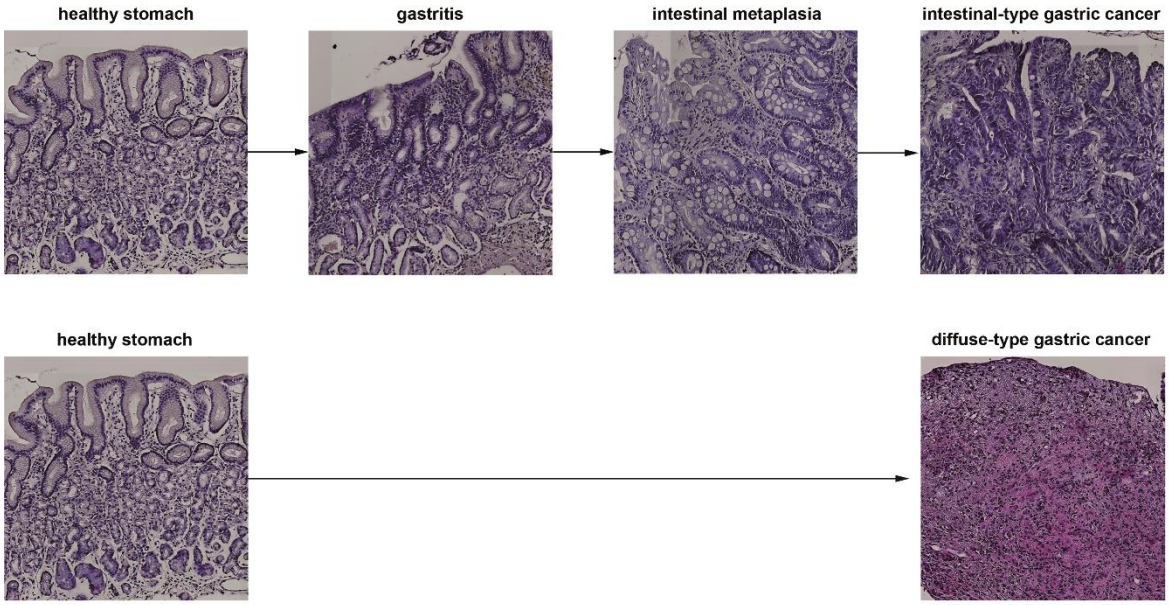


**Figure 2: Histological representation of the Correa's pathway.** The Correa's pathway describes the stepwise progression of healthy gastric tissue to gastric cancer. Upon inflammatory stimulus, gastritis will occur that may develop to intestinal metaplasia which can further progress to intestinal-type gastric cancer. Possible steps for the development of diffuse-type gastric cancer remain unclear.

To date, less is known about the development of diffuse-type gastric cancer. As described above, this subtype is characterized by loss of cell-cell adhesion due to genes involved in this mechanism, such as *CDH1*. Individuals with a germline mutation in *CDH1* show an increased risk for the development of hereditary diffuse-type gastric cancer. E-cadherin binds β-catenin to the cellular membrane and its loss leads to increased levels of this molecule which finally results in increased Wnt signaling. More recently, it has been suggested, that infection with EBV or *H. pylori* can not only induce the Correa's cascade, but can also favor the development of diffuse-type gastric cancer [2]. This is due to the fact, that *H. pylori* can also disrupt cell-cell adhesion and E-cadherin – β-catenin interaction [43] and

additionally can hypermethylate the *CDH1* gene, thereby leading to a loss of cell adhesion and integrity [44, 45].

### 2.1.5 Gastric cancer therapy

Gastric cancer remains asymptomatic in early stages and can lead to rather vague symptoms such as absence of appetite or nausea at later stages. Because of this, it is often diagnosed at late stages, especially in Western countries, where screening examinations focus on more prominent cancers, such as breast or colon [27]. To date, the only curative therapy is complete tumor resection; however, tumors diagnosed at late stages are often unresectable [46]. Neoadjuvant chemo- or radiotherapy were shown to improve survival. However, not all patients respond to this treatment, and more than 50 % of patients relapse locally or with distant metastases. Taken together, this leads to overall poor prognosis with a median survival of less than 12 months and a 5-year survival of less than 10 % [27, 46]. Thus, to increase prognosis and improve therapy, numerous attempts have been made to identify new potential biomarkers that could stratify patients for therapy. Human epidermal growth factor receptor 2 (HER2/ERBB2), which can be found in 20 – 25 % of patients, was found to be a reliable marker for therapy selection, since treatment with specific antibodies against HER2 improved survival [47, 48]. Additionally, MSI and expression of Programmed Cell Death 1 Ligand 1 (PD-L1) were shown to predict response to immune checkpoint blockade, thereby serving as a biomarker for the selection of this therapy [49, 50].

## 2.2 *Helicobacter pylori* infection

*H. pylori* infection is the main risk factor for gastric cancer development. *H. pylori* is a gram-negative, microaerophilic bacterium that colonizes the stomach of half of the world's population [51]. It has a helix shape and carries flagella, which allow high motility. It was discovered in 1983 by Robin Warren and Barry Marshall and was then linked to gastritis and gastric ulcers as well as duodenal ulcers and gastric cancer [52]. In 1994, the International Agency for Research on Cancer (IARC) classified *H. pylori* as class I carcinogen, and this was reconfirmed by the IARC in 2011 [53, 54]. *H. pylori* prevalence is

highly variable with less than 40 % in many developed countries and more than 70 % in developing countries [55]. Its transmission route is not well defined, however, oral-oral or fecal-oral transmission at early age within the family has been suggested. *H. pylori* infection leads to a chronic gastritis that stays asymptomatic in 80 – 90 % of cases, whereas 10 – 20 % of infected individuals develop peptic ulcer disease and around 1 - 2 % develop gastric cancer [56]. Peptic ulcer disease is caused by increased acid production resulting from a loss of somatostatin producing D cells and can be located in the stomach or the duodenum. These ulcers carry a risk of malignant transformation and their spontaneous remission can induce IM in the regenerative epithelium [57]. Additionally, mucosa-associated lymphoid tissue (MALT) lymphoma in the stomach, which occurs in less than 1 % of infected individuals [56], has been highly associated with *H. pylori* infection. The risk for malignant transformation of the gastric tissue varies across regions and has been linked to several virulence genes. Strains carrying the cytotoxin-associated gene (cag) pathogenicity island (PAI) encoding for a type IV secretion system (T4SS) and CagA, and a certain combination of alleles in the gene of vacuolating cytotoxin A (VacA) were associated with high risk for the development of gastric cancer [58]. These virulent strains are commonly found in countries with high gastric cancer prevalence, for example in East Asia, and less common in Western countries [59]. In individuals with peptic ulcer disease, eradication of *H. pylori* is recommended since this can completely cure ulcers [57]. Eradication is mostly performed through a triple therapy containing proton pump inhibitors and the antibiotics clarithromycin and amoxicillin or metronidazole. However, rising evidence suggests that asymptomatic *H. pylori* infection can be beneficial, since it was negatively correlated with other diseases such as asthma, allergies or inflammatory bowel disease [60-62].

### 2.2.1 *H. pylori* virulence factors

*H. pylori* has developed several strategies to be able to colonize the harsh environment of the stomach, which is characterized by a very low pH and the presence of digestive enzymes. To counteract low pH levels, *H. pylori* secretes urease (UreA), an enzyme that hydrolyses urea into carbon dioxide and ammonia, thereby raising the pH in the surrounding of the bacterium [63]. Furthermore,

it uses chemotaxis to move to areas with higher pH levels, such as the epithelial surface. The higher pH value around the bacterium leads to a change in mucus viscosity, thereby facilitating penetration of the mucus layer and entering the less hostile environment at the epithelium [64, 65]. Additionally, it is able to directly block acid secretion of parietal cells through VacA and lipopolysaccharide mediated suppression of the $H^+/K^+$ ATPase [66-68]. Furthermore, cytokines secreted during infection were also shown to downregulate acid production [69, 70].

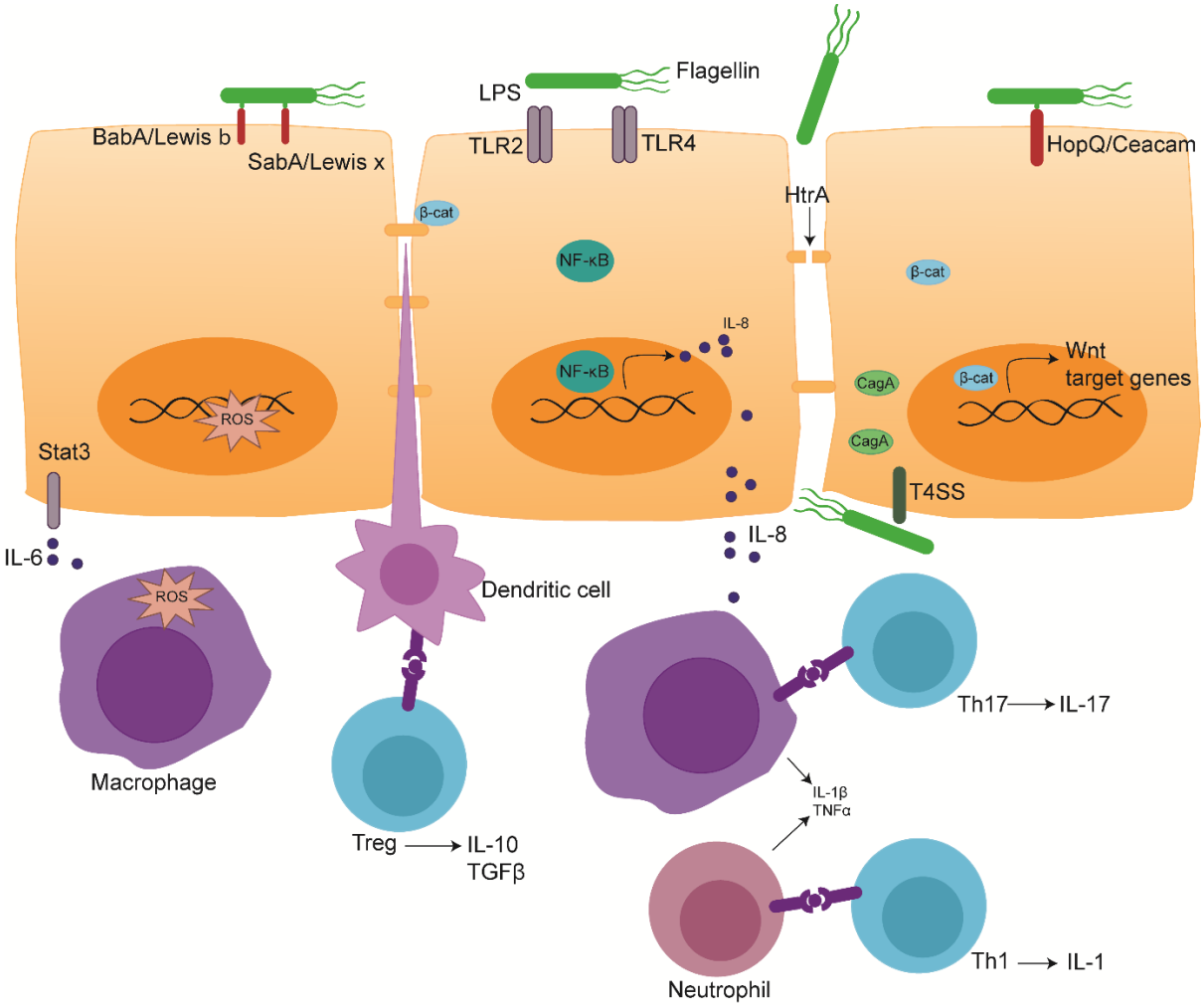


**Figure 3: Schematic representation of pathways altered by *H. pylori* infection.** *H. pylori* binds to gastric cells via BabA/Lewis$^b$, SabA/Lewis$^x$ and HopQ/Ceacam interaction. LPS and flagellin induce Toll-like receptor (TLR) signaling and thereby IL-8 secretion, which favors the recruitment of macrophages and neutrophils. These innate immune cells drive a Th1 and Th17 differentiation and produce reactive oxygen species (ROS), which can damage host cell DNA. Secreted IL-6 activates STAT3 signaling in gastric cells. Bacterial HtrA protein damages cell-cell junctions leading to loss of cell polarity and increase in free β-catenin, which can then induce expression of Wnt target genes.

*H. pylori* expresses several adhesins by which it can attach to gastric epithelial cells. Thus, BabA and SabA bind Lewis$^{b}$ and Lewis$^{x}$ antigens expressed on the gastric epithelial cells, respectively [71-73], while HopQ binds to Carcinoembryonic antigen-related cell adhesion molecules (CEACAMs) [74, 75]. Furthermore, *H. pylori* secretes the serine protease HtrA that cleaves E-cadherin, a crucial protein of cell-cell junctions, thereby disrupting tight junctions and adherens junctions [76]. By this mechanism, *H. pylori* reaches the basolateral side of the gastric epithelial cells. Integrins are expressed here and were described to be important for T4SS mediated injection of CagA into the host cells [77]. However, more recent literature showed that HopQ – CEACAM interaction but not interaction with integrins is essential for CagA translocation in gastric cancer cells. CagA then further modulates cell-cell junctions leading to a loss of cell adhesion and polarity [78] (**Figure 3**).

### 2.2.2 Immune response elicited by *H. pylori*

Infection with *H. pylori* triggers a complex pro- and anti-inflammatory immune response (**Figure 3**). Bacterial polysaccharide complexes such as lipopolysaccharide (LPS) and peptidoglycan serve as pathogen-associated molecular patterns (PAMPs) that are recognized by several toll-like receptors (TLRs), which subsequently activate the NF-KB signaling pathway. In epithelial cells, this induces secretion of interleukin 8 (IL-8) [79, 80], a chemokine that favors the recruitment of immune cells such as neutrophils and macrophages to the site of infection [81]. These innate immune cells phagocytose *H. pylori,* secrete pro-inflammatory cytokines such as IL-1β and tumor necrosis factor α (TNFα), and present microbial peptides on major histocompatibility complex (MHC) class II molecules to T cells [82]. Furthermore, dendritic cells (DCs) that reside in the gastric epithelium can take up infecting bacteria and migrate to the draining lymph nodes and Peyer's patches where they present microbial peptides loaded onto MHC class II molecules to T cells [83]. This step is crucial for activation of naïve T cells and differentiation of T helper cells into Th1 and Th17 subtypes [82]. Activated T cells then migrate back to the stomach and infiltrate the gastric epithelium. These cells produce cytokines such as interferon γ (IFNγ) or IL-17, which can further stimulate pro-inflammatory cytokine production by stromal and epithelial cells [84, 85]. Infiltration of lymphocytes into the gastric epithelium is one of

the key features of *H. pylori* driven chronic gastritis, which can progress to atrophy and compensatory hyperplasia [86]. However, to be able to persist in the stomach, *H. pylori* also induces an anti-inflammatory immune response to evade clearance. During co-evolution with its host, *H. pylori* LPS and flagellin have undergone modifications, which reduce recognition by TLRs [87, 88]. This lower PAMP-mediated activation in turn can induce differentiation of regulatory T cells (Tregs), which secrete anti-inflammatory cytokines such as IL-10 and Transforming growth factor β (TGFβ) [60, 89]. In DCs, CagA has been shown to inhibit IFNγ production, thereby preventing Th1 differentiation and to induce a semi-mature DC phenotype which favors the induction of Tregs [90]. Additionally, VacA has been shown to block DC maturation [91]. Furthermore, *H. pylori* virulence factors VacA, γ-glutamyltransferase (GGT) and UreA can inhibit T cell activation and proliferation through direct effects as well as through deprivation of nutrients [92-94]. The balance between pro- and anti-inflammatory immune responses has been shown to influence severity of gastritis and whether patients develop ulcers. In asymptomatic patients, Tregs and the cytokines IL-10 and TGFβ were shown to be increased, whereas the amount of infiltrating Th17 cells correlates with severity of gastritis and is increased in ulcers compared to gastritis [95, 96]. This chronic gastritis with increased cellular turnover and apoptosis can lead to a destruction of antral D cells resulting in a lack of somatostatin and increased levels of gastrin. This hypergastrinemia induces acid production and a decrease in pH and can induce duodenal ulcers as described above [97-99]. When the gastritis spreads to the corpus, on the other hand, parietal cell loss can occur leading to gastric atrophy. The resulting rise in pH can furthermore cause dysbiosis, which can favor the overgrowth of other bacteria in the stomach [41, 42].

### 2.2.3 Carcinogenic Signaling pathways altered by *H. pylori*

Several signaling pathways have been shown to be dysregulated during infection, especially those involved in cell proliferation and survival, such as NF-κB or Wnt signaling (**Figure 3**). As described above, *H. pylori* activates canonical NF-κB signaling through TLRs as well as non-canonical NF-κB through members of the TNF family such as Lymphotoxin β receptor (LTβR) [100]. Furthermore, NF-

κB signaling was also described to mediate cell survival [34]. Thus, active NF-κB signaling can prevent apoptosis, for example through upregulation of anti-apoptotic genes [101], and promote cell cycle progression as it regulates expression of several cyclins [102]. Additionally, several interleukins secreted during inflammation, such as IL-6 and IL-11, activate STAT3 signaling during gastritis [103, 104]. This pathway can not only further drive inflammation, but is also associated with cell survival, proliferation and invasion. A direct link between STAT3 signaling and gastric carcinogenesis was established, since mice with constitutive activation of this pathway develop neoplasms in the stomach [35]. *H. pylori* was also shown to interfere with epidermal growth factor (EGF) signaling. Upon infection, this pathway was upregulated in epithelial cells and was shown to be important for *H. pylori*-mediated gastric carcinogenesis in animal models [105, 106]. In addition, *H. pylori* infection can lead to a hyperactivation of Wnt signaling, one of the key regulators of cell proliferation, stemness and survival. The disruption of cell-cell adhesions by *H. pylori* leads to the release of E-cadherin-bound β-catenin and to its accumulation in the cell [43]. Thus, β-catenin can translocate to the nucleus and induce Wnt target gene expression. Furthermore, *H. pylori* was shown to increase secretion of Rspondin3 (RSPO3), a positive regulator of Wnt signaling. Higher Wnt activity then leads to increased number and proliferation of $Axin2^+$ stem and progenitor cells and increased cell survival [11, 107]. Taken together, *H. pylori* directly and indirectly interferes with several signaling pathways that drive cell survival, proliferation and suppress apoptosis. These pathways can then lead to higher tissue turnover and ultimately to malignant transformation of the gastric epithelium.

### 2.2.4 *H. pylori* and DNA damage

Besides chronic inflammation and activation of tumorigenic signaling pathways, infection with *H. pylori* also causes DNA damage that can contribute to malignant transformation of epithelial cells. Infiltrating neutrophils and macrophages produce reactive oxygen and nitrogen species (RNS) to clear the infecting pathogen [108]. However, these components not only target the bacterium, but can also damage gastric epithelial cells. ROS and RNS interact with the cells' DNA and induce point mutations by modifying guanine, and thus induce a guanine to thymidine transversion in the subsequent repair

process. Additionally, ROS and RNS can generate DNA adducts that can lead to DNA single or double strand breaks (SSBs and DSBs, respectively) [33, 109] (**Figure 3**). Furthermore, the CagPAI was shown to upregulate Activation-induced cytidine deaminase (AID) in gastric epithelial cells, an enzyme that converts cytosine into uracil, thereby introducing point mutations into the genome [110]. AID is not expressed in the gastric epithelium under basal conditions but is responsible for somatic hypermutation and immunoglobulin class switching in B cells [111]. Additionally, *H. pylori* was shown to directly induce DNA double strand breaks in host cells. This induction of DNA damage was shown to be independent of ROS and to require contact of live bacteria [112, 113]. However, whether CagPAI or CagA are necessary for induction of DSBs has been controversially discussed. DNA damage caused by *H. pylori* is repaired, but upon persistent infection around 70 % of cells were shown to lose their proliferative capacity, indicating that *H. pylori*-induced DSBs permanently alter gastric cells [112]. A more recent study suggested that activation of NF-κB by T4SS-mediated integrin β1 signaling is responsible for DSB induction. Upon NF-κB activity, components of the nucleotide excision repair (NER) machinery are recruited to p65/RelA complexes in the nucleus. The endonucleases XPG, XPF and the recruitment factor XPA then induce DSBs to facilitate transcription initiation, which is important for IL-8 expression upon *H. pylori* infection. In this study, knock out of any of these XP proteins was shown to prevent formation of DSBs and to reduce IL-8 secretion in *H. pylori*-infected gastric cells. Furthermore, it was shown that NF-κB activity was crucial for cell survival, despite the presence of massive DNA damage in those cells [114]. In addition, it has been shown that *H. pylori* can alter expression of other components of the DNA damage response (DDR). P53, the master regulator of DDR, is first upregulated during infection and subsequently downregulated below basal levels *in vivo* in the stomach of mongolian gerbils infected with *H. pylori*. Degradation of p53 was shown to increase short and long term cell survival and to confer resistance to chemotoxic agents [115]. *H. pylori* also induces epigenetic modifications and thereby upregulation of the DDR activator Ataxia-telangiectasia mutated (ATM) [113], as well as downregulation of other DDR components such as MRE11 or Nibrin (NBS1) [116]. Furthermore, infection with *H. pylori* was shown to downregulate

genes of the DNA repair pathways mismatch repair (MMR) and base excision repair (BER) [117, 118], and to favor the more error-prone non-homologous end joining (NHEJ) instead of homology repair as repair mechanism for DSBs [114]. Taken together, *H. pylori* induces severe DNA damage in its host cells by different mechanisms and at the same time enhances cell survival and proliferation. This combination can then drive gastric carcinogenesis in infected individuals.

## 2.3 Wnt signaling pathway

The Wnt signaling pathway was first discovered in 1982, when infection experiments with murine retroviruses revealed a new proto-oncogene capable of driving the development of breast cancer, which was then named integration 1 (Int1) [119]. Further studies showed that this gene was highly conserved across species and was an orthologue of the known Wingless (Wg) gene of *Drosophila melanogaster*, which was described to be important for embryonic development [120]. Continuous research discovered further Int1 related proteins that were also involved in murine embryonic development and thus, the signaling pathway was renamed across species by the neologism Wingless-related integration site (Wnt) [121]. In mammals, 20 secreted Wnt proteins were discovered that can drive 3 different pathways: Canonical Wnt, non-canonical planar cell polarity, and Wnt/$Ca^{2+}$ signaling [122]. During embryonic development, Wnt signaling has been shown to be important for body axis formation, cell proliferation and differentiation and tissue formation [123]. Furthermore, Wnt signaling regulates cell turnover in several adult tissues, as it is involved in the formation of hair follicles [124], as well as in the control of hematopoietic stem cells [125] and bone density [126]. Additionally, canonical Wnt signaling was shown to regulate the stem cell compartment in the gastrointestinal system. As described above, stem cells of the gastric antrum were shown to be regulated by Wnt signaling. In the intestine, this signaling pathway was shown to be crucial for epithelial turnover. Here, Wnt is produced by the crypt epithelial cells and is the dominant mitogen in intestinal progenitor cells. Wnt also induces differentiation of Paneth cells in the intestinal crypt. Inside the intestinal crypt, a Wnt gradient regulates division of stem cells and proliferation of progenitor cells that then move up the crypt, where they terminally differentiate [127].

### 2.3.1 Regulation of canonical Wnt signaling

Wnt ligands can be secreted by different cell types dependent on the tissue type and have to be palmitoylated by Porcupine (PORCN) in order to elicit their function [128, 129]. In absence of the ligand, a destruction complex consisting of Axin, Adenomatosis polyposis complex (APC) and Glycogen synthase kinase 3 β (GSK3β) binds and phosphorylates β-catenin. Phosphorylated β-catenin is then recognized by β-Transducin repeat containing E3 ubiquitin protein ligase (β-TrCP), subsequently ubiquitinated and thereby targeted for degradation [130]. When secreted, Wnt ligands bind to Frizzled (Fz) receptors on their target cells that build a complex with lipoprotein receptor-related protein (LRP) 5/6 receptors [131]. This complex recruits Axin, which is the scaffold protein of the destruction complex, to the cell membrane thereby abolishing phosphorylation of β-catenin. Thus, β-catenin can accumulate in the cytosol, translocate to the nucleus and bind to T cell factor (TCF)/Lymphoid enhancing factor (LEF) transcription factors [132-134]. In absence of β-catenin, TCF/LEF bind Groucho proteins and thus function as a transcriptional suppressor [135]. However, β-catenin displaces Groucho and binds Tcf/Lef, which then can bind to Wnt responsive elements (WREs) on the genome [136]. This enables transcription of Wnt target genes including cyclins [137] and c-myc [138], which drive proliferation, or Axin2, which provides a negative feedback loop [139]. In addition, Wnt signaling can be modulated by agonists and antagonists. Members of the R-spondin (RSPO) family were shown to bind to LGR4 and LGR5 [140] and this complex subsequently binds the E3 ubiquitin ligase Zinc and Ring Finger 3 (ZNRF3) and its functional homologue RING finger protein 43 (RNF43) [141]. ZNRF3 and RNF43 were shown to ubiquitinate Fz receptors thus targeting the receptors for degradation and downregulating Wnt activity [142]. Upon complex formation with R-spondin and LGR4/5, ZNRF3 and RNF43 are inhibited which leads to a stabilization of Fz receptors on the cell membrane and a potentiation of Wnt signaling (**Figure 4**) [141, 143]. In the stomach, R-spondins were shown to be produced and secreted by the stromal cells of the lamina muscularis mucosae [12].

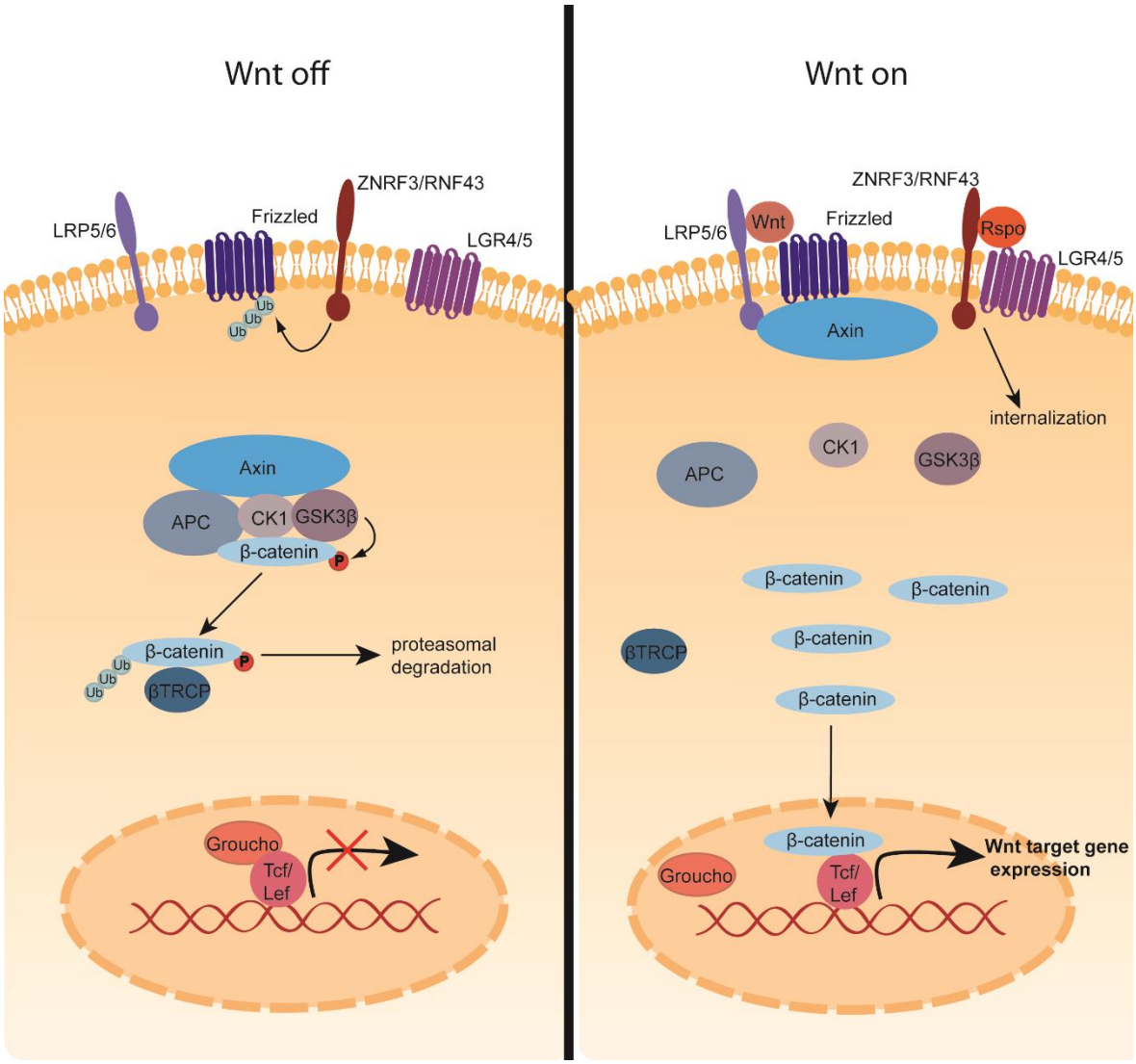


**Figure 4: Schematic representation of the Wnt signaling pathway.** In the absence of Wnt ligand, the degradation complex containing Axin, APC and GSK3β phosphorylates β-catenin and targets it for ubiquitination and degradation. Groucho bound to TCF/LEF transcription factors acts as a suppressor of gene expression. Wnt activity is further negatively regulated by ZNRF3/RNF43 mediated ubiquitination and degradation of Frizzled receptors. Upon Wnt ligand binding, Axin is recruited to the cell membrane and β-catenin is released from the degradation complex. β-catenin translocates to the nucleus, binds TCF/LEF and mediates Wnt target gene expression. Additionally, binding of Rspondin to LGR4/5 receptors and ZNRF3/RNF43 prevents ubiquitination of Frizzled, which further enhances Wnt activity.

### 2.3.2 Wnt signaling during gastric cancer development

Since Wnt signaling regulates processes that are required for cell proliferation and migration and can also enhance stem cell properties, aberrant activity of this pathway has been linked to many tumor entities, including breast or lung cancer [127]. In colorectal cancer, defects in negative Wnt regulators such as APC or Axin, or gain-of-function mutations in *β-catenin* are found in a majority of patients

[122, 144]. A heterozygous mutation in *APC* was directly linked to hereditary Familial adenomatous polyposis (FAP), where patients develop polyps in the large intestine [145]. These benign polyps display a loss of heterozygosity (LOH) in the *APC* gene and can progress to colorectal cancer if they acquire further mutations. In addition, mice carrying a premature stop codon in the *APC* gene ($APC^{min}$) develop adenomas in the small intestine, which further shows the direct association between defective Wnt signaling and malignancies in the intestine [146]. In the stomach, however, the role of Wnt signaling during gastric carcinogenesis is less well defined. Interestingly, it was shown, that $APC^{min}$ mice can also develop gastric adenomas, which have acquired LOH in *APC* and therefore display high Wnt activity [14]. In gastric cancer patients, it was estimated that pathologic dysregulation of Wnt signaling occurs in around 30 % of the cases [147], but these numbers highly vary across studies. Several studies showed, that upregulation of agonists such as Wnt ligand or β-catenin occurred in 30 – 50 % of GC samples [148, 149], whereas frequency of *APC* mutations varied between 7 % and 30 – 34 % [13, 30, 150]. Furthermore, it was shown that *APC* mutations occurred in premalignant lesions such as low-grade dysplasia and were less frequent during malignant transformation [151]. This has been confirmed in mouse models such as the $APC^{min}$ mice, since lesions in these animals do not progress to gastric adenocarcinoma [152]. Additionally, upregulation of Wnt5A was associated with advanced tumor stage and poor prognosis and LGR5 expression was linked to poor survival and high mortality [153, 154]. Taken together, these results suggest that aberrant Wnt signaling is able to induce neoplasms in the stomach. However, since the number of gastric cancer patients with altered Wnt activity varies drastically across studies, it remains to be elucidated whether this signaling pathway is one of the key drivers of gastric carcinogenesis and whether this pathway could be exploited for the development of new therapies.

## 2.4 The E3 ubiquitin ligase RNF43

### 2.4.1 RNF43 function in Wnt signaling

When RNF43 was first discovered, it was described to be overexpressed in hepatocellular carcinoma (HCC). In this study, RNF43 knock down led to a decrease in proliferation and invasion in HCC cells suggesting that RNF43 acts as an oncogene [155]. However, more recent publications have described RNF43 to have a tumor suppressive function. In studies conducted in the colon and pancreas it was shown that RNF43 suppresses autocrine Wnt activity and interacts with Fz and LRP6 receptors. Mechanistically, RNF43 was suggested to be expressed at the cellular membrane and to ubiqitinate Fz receptors similarly to ZNRF3, thereby targeting them for internalization and degradation and thus dampening Wnt activity [142, 156]. Upon active Wnt signaling, RNF43 is bound in a complex of RSPO and LGR5, which prevents RNF43 mediated Fz degradation [141]. Thus, RNF43 acts as a tumor suppressor through negatively regulating Wnt signaling. Furthermore, the promoter region of RNF43 contains WREs suggesting that it is a direct Wnt target gene and serves as a negative feedback loop upon active Wnt signaling [157, 158]. Indeed, it was shown that RNF43 is upregulated upon active Wnt signaling and that this upregulation is β-catenin dependent and therefore attributable to canonical Wnt signaling [157]. Additionally, a second mode of action has been shown for RNF43 function. RNF43 localized in the nucleus regulates Wnt activity downstream of APC or β-catenin mutations by binding to the transcription factor TCF4 and sequestering it to the nuclear membrane, thereby preventing TCF4-mediated Wnt target gene expression [157]. In gastric cells, the regulatory function of RNF43 in Wnt signaling is less clear. It was shown that it also acts as a tumor suppressor in this tissue since overexpression was associated with less proliferation and upregulation of apoptosis [159], while knock down of RNF43 induced downregulation of apoptosis and increased proliferation and LGR5 expression [160]. In the overexpression model, stem cell markers such as CD44 were downregulated in gastric cancer cell lines. Furthermore, higher levels of RNF43 led to decreased levels of β-catenin, TCF4 and LGR5 and overall dampened the self-renewal capacity in these cells [159].

However, whether RNF43 regulates Wnt signaling through the same mechanisms in the stomach as described for colon and pancreas remains to be elucidated.

### 2.4.2 RNF43 mutations in cancer

In several tumor types, sequencing studies showed that *RNF43* is frequently mutated. Thus, *RNF43* mutations were detected in 24 % of colorectal traditional serrated adenomas and these mutations were shown to be enriched in MMR deficient tumors, to be mutually exclusive with RSPO3 fusions and to occur at a later stage in tumorigenesis [161]. Furthermore, an *RNF43* germline mutation (E318fs) was shown to predispose individuals to colorectal cancer and all cancer patients carrying this mutation showed a second hit LOH or other *RNF43* mutations in the polyps. In this study, *RNF43* was mutated in 34 % of sporadic serrated polyps, mostly together with mutations in *BRAF* and mutually exclusive with *APC* mutations [162]. In contrast to the previous study, *RNF43* was described to be an early mutation preceding MSI status. Numerous other studies have analyzed *RNF43* mutation rates in subtypes of colorectal cancer that varied drastically, however, enrichment in MSI tumors and high frequencies of certain hotspot mutations such as RNF43 G659Vfs*41 or R117Pfs*41 were common findings [163-165]. In the pancreas, *RNF43* was found to be most commonly mutated in intraductal papillary mucinous neoplasms indicating that it suppresses neoplasia in this organ [166]. Similar results have been obtained from sequencing studies in gastric cancer patients. In a WGS study, around 5 % of MSS and 55 % of MSI tumors displayed alterations in *RNF43* and most of these were truncating mutations [167]. Another study showed that 35 % of gastric cancers adjacent to an adenoma had newly acquired *RNF43* mutations indicating that this protein might play a critical role in the transition from adenoma to carcinoma [151]. In this study, *RNF43* mutations occurred in high grade dysplasia and gastric cancer supporting the finding that these mutations might be a rater late event in malignant transformation. In more recent studies, enrichment of *RNF43* mutations in MSI tumors was confirmed as well as the high proclivity for truncating frameshift mutations [168-170]. Taken together, high frequency of *RNF43* mutations indicate that the protein plays an important role in the homeostasis of these tissues and might be one of the key events during malignant transformation.

## 2.5 DNA damage response

Genomic stability is essential for a cell's function and for a reliable transmission of information to the progeny. However, every cell encounters thousands of DNA lesions per day [171], and these lesions have to be efficiently eliminated in order to preserve the genomic information. For this, DDR and subsequent repair mechanisms are essential. The majority of DNA lesions are caused by intrinsic factors, such as mismatches, replication arrest and fork stalling, hydrolysis of nucleotides and damage caused by ROS, a byproduct of oxidative respiration or inflammation [172, 173]. These lesions mainly cause SSBs or insertion/deletion (Indel) loops, which can be repaired efficiently through different mechanisms. DSBs, on the other hand, occur less frequently, but display higher toxicity since the cell does not have a complementary strand as a repair template. Intrinsically, DSBs can be caused by SSBs in close proximity or when the DNA replication apparatus encounters a SSB [174]. Additionally, extrinsic factors can cause DNA damage, which is in fact the case for many known carcinogens [175]. Ultraviolet (UV) light for example induces the formation of photoproducts, e.g. crosslinking of pyrimidines [176], whereas ionizing radiation causes DSBs [177]. As mentioned before, infection with *H. pylori* can also lead to DSBs in gastric cells.

### 2.5.1 Regulation of DNA damage response signaling

Dependent on the type of DNA damage, different signaling arms of the DDR will be activated. Tracks of single stranded DNA are recognized by Replication Protein A (RPA) which binds the DNA and recruits the Rad9-Hus2-Rad1 complex to this lesion. This activates Ataxia telangiectasia and Rad3 related (ATR) kinase, which autophosphorylates and subsequently phosphorylates several downstream effectors such as Checkpoint kinase 1 (Chk1) and the key regulator of DDR p53 [178]. Similarly, DSBs are detected and bound by the MRE11-Rad50-Nbs1 (MRN) complex, which then recruits the kinase Ataxia-telangiectasia mutated (ATM) to the damage site. ATM autophosphorylates upon activation and then phosphorylates histone variant H2AX (γH2AX), which clusters in the so called ionizing radiation-induced foci (IRIF). This histone modification was shown to be crucial for the recruitment and retention of repair factors at the damage site. Furthermore, ATM phosphorylates Chk2 and p53

to further initiate downstream signaling [179, 180]. Under basal conditions, p53 is ubiquitinated by Mouse double minute 2 homolog (Mdm2) and thereby targeted for degradation [181]. However, phosphorylation of p53 leads to a conformational change that prevents its ubiquitination and enables its function as transcription factor [182].

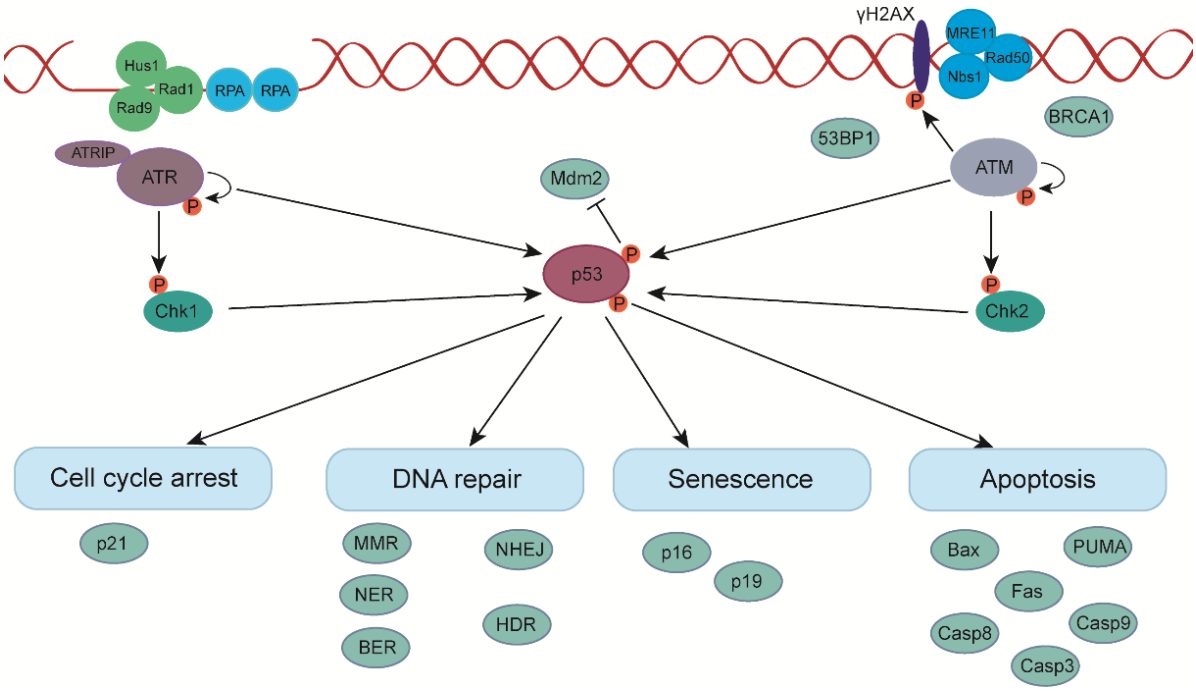


**Figure 5: Schematic representation of DNA damage response and repair signaling.** Tracks of single stranded DNA are recognized by the Rad1-Rad9-Hus1 complex and bound by RPA. This leads to autophosphorylation of ATR, and phosphorylation of Chk1 and p53. Double strand breaks are recognized by MRE11, Rad50 and Nbs1, and leads to ATM recruitment and its autophosphorylation. ATM phosphorylates histone variant H2AX, Chk2 and p53. Phosphorylation of γH2AX leads to the recruitment of the repair factors 53BP1 and BRCA1. P53 induces cell cycle arrest and initiates DNA repair by MMR, NER or BER for SSBs, and NHEJ or HDR for DSBs. If damage burden is too high, cellular senescence or apoptosis is induced.

As a first response, p53 activates cyclin-dependent kinase inhibitor 1 (p21), which will then induce a cell cycle arrest at the checkpoints $G_1$-S, intra-S or $G_2$-M [183]. This allows the cell to activate repair mechanisms to restore genomic integrity [184, 185]. However, if the damage cannot be repaired or the mutational burden is too high, e.g. through chronic exposure to DNA-damaging agents, the cell will undergo p53-mediated apoptosis [186]. Here, p53 upregulates several proteins such as Fas receptors, a member of the death receptors of the tumor necrosis factor receptor (TNF-R) family [187], as well as members of the Bcl-2 protein family or p53 upregulated mediator of apoptosis

(PUMA) [188, 189], which activate the caspases 8 and 9 [190]. These, in turn, cleave the effector caspases 3, 6 and 7 which play a crucial role in the execution-phase of apoptosis [191]. Defects in the induction of apoptosis were shown to promote tumorigenesis [192], indicating that it plays a crucial role in the elimination of potentially malignant cells **(Figure 5**).

### 2.5.2 DNA repair mechanisms

An efficient repair machinery is crucial for the survival of cells that have encountered DNA lesions. Dependent on the type of lesions, different mechanisms and molecules are involved in repairing the damage. Repair of SSBs generally requires nuclease, polymerase and ligase enzymes [177]. Mismatches or loops caused by Indels are removed by mismatch repair (MMR), which functions through single strand excision and involves "Mut" proteins, such as MutL homologs (MLH) [193, 194]. If a single base is damaged, for example by alkylation or deamination, it gets removed by the base excision repair (BER) machinery [33, 195, 196]. On the other hand, helix distorting base lesions that can either be transcription coupled or can occur anywhere on the genome, are repaired by nucleotide excision repair (NER) [197, 198]. Here, a 20 – 30 bp oligomer is excised from the genome and a polymerase is recruited to fill the resulting gap [199, 200]. When a cell encounters DSBs, two repair options are available dependent on the state of the cell cycle. Homology directed repair (HR) is the more reliable mechanism, however, it requires a sister chromatid and is therefore only available when the cell is in S or $G_2$ phase [201]. This repair mechanism is mediated by Breast cancer type 1/2 susceptibility protein (BRCA1/2) proteins, which are recruited by γH2AX to the damage site [202-204]. If no sister chromatid is present in the cell, DSBs are repaired by the error prone Non-homologous end joining (NHEJ). Here, DSBs are recognized by Ku proteins which recruit DNA dependent protein kinases (DNA-PK) as well as end processing enzymes, polymerases and DNA ligase IV [205]. During NHEJ, lose DNA ends are simply ligated back together. This can lead to random insertions or deletions in the genomic DNA [206].

Although different DNA lesions activate a distinct type of DNA repair mechanisms, these signaling pathways are not isolated from each other but share certain markers and effector proteins. During

HR, for example, BRCA1 and 2 initiate single strand resection, which will then be recognized and coated by RPA and activate ATR – Chk1 signaling [207]. Additionally, activated NER can lead to the phosphorylation of H2AX by ATR. These γH2AX positive IRIFs were shown to also be found upon treatment with UV light [208, 209]. Furthermore, NER and HR share the endonuclease complex Excision Repair Cross-Complementation Group 1 (ERCC1)/XPF which is also involved in crosslink repair and telomere maintenance [207].

### 2.5.3 DNA damage response in gastric cancer

Since the acquisition of mutations is a critical step in carcinogenesis, a functional DDR is an important barrier to prevent malignant transformation. It was suggested that possibly all cancer cells have a defect in at least one aspect of DDR due to selective pressure [177]. Furthermore, patients with hereditary defects in DDR components present with higher susceptibility for the development of cancers, as it is the case in ataxia–telangiectasia syndrome (ATM deficiency) [210] or Li-Fraumeni syndrome (p53 mutations) [211]. Overall, around 50 % of all cancers display mutations in *p53* [212], and such mutations were shown to occur in 50 to 65 % of gastric tumors [30, 151, 213]. Additionally, defects in genomic stability have been described to occur in more than 70 % of gastric tumors. The more frequent alteration type of the genome is CIN (50 %) [30], which occurs in the presence of telomere defects [214, 215]. In a healthy cell, the open DNA ends of chromosomes, which present as DSBs, are covered by the shelterin complex and this prevents recognition by the DDR machinery [216]. However, DDR components are important for the formation of this complex. Thus, defects can cause shortening and dysfunction of telomeres and thereby trigger fusions that can result in CIN [217, 218]. Furthermore, activated oncogenes can induce DNA-replication stress that can also lead to unrepaired DSBs and trigger chromosome fusions [219]. The second most frequent genomic instability present in gastric cancer is MSI which is characterized by a deficiency in MMR components, such as downregulation of MLH proteins, and leads to mutations especially in tandem repeats [193]. MSI tumors are characterized by a very high mutational burden [30]. Additionally, the carcinogens mainly associated with gastric cancer have been shown to induce DNA damage. As described above, *H. pylori*

can cause DNA lesions directly as well as through the elicited inflammation. Intake of nitrosamines via food, e.g. cured meat is associated with gastric cancer risk and these organic compounds induce DNA lesions via alkylation [3, 220]. Moreover, excessive p53 activation has been shown to induce cellular senescence, which normally functions as a barrier against malignant transformation [221]. However, senescent cells were shown to secrete growth-promoting and proinflammatory cytokines and chemokines such as IL-6 or IL-8 as well as Vascular endothelial growth factor (VEGF). These proteins lead to the infiltration of macrophages, neutrophils and natural killer (NK) cells [222]. In the stomach, where carcinogenesis is most commonly driven by chronic inflammation, this so-called senescence-associated secretory phenotype (SASP) could further enhance active gastritis and thereby increase gastric cancer risk. Interestingly, the chemotherapeutics recommended and commonly used for gastric cancer therapy [223] act through the induction of DNA damage and subsequent apoptosis in cancer cells. Platinum compounds such as cisplatin or oxaliplatin crosslink DNA at several sites, interfere with mitosis and lead to DSBs [177, 224, 225]. Fluoropyrimidines such as 5-fluorouracil (5-FU) inhibit thymidylate synthase, which leads to a deprivation of thymidine [226]. In addition, 5-FU is incorporated into the DNA and RNA instead of pyrimidine bases and this causes defective base pairing, base damage and replication lesions, which can ultimately also result in DSBs [227]. Taken together, activation and dysfunction of DDR play a major role during gastric carcinogenesis and therapy response.

### 2.5.4 E3 ubiquitin ligases in DDR

Activation of DDR relies on several posttranslational modification (PTMs), especially phosphorylation. However, other modifications such as ubiquitination of histones have been shown to be crucial for induction and maintenance of DDR signaling. A complex of Ring finger protein 2 and 51 (RNF2 and RNF51) was shown to monoubiquitinate the histone H2AX at the lysines K119/K120 and this is crucial for the recruitment of ATM to the damage site as well as ATM-dependent phosphorylation of H2AX [166, 228]. Moreover, a second pair of E3 ubiquitin ligases is important for the recruitment of repair factors to the damage site. RNF8 attaches K63 linked ubiquitin to γH2AX upon DNA damage [229]. This

leads to the recruitment of RNF168 [230] which in turn ubiquitinates γH2AX at the lysines K13/K15 [231]. These PTMs were shown to be necessary for maintenance of DDR signaling and especially for the recruitment of the repair factors BRCA1 and 53 binding protein 1 (53BP1) to the site of DNA damage [230] (**Figure 6**).

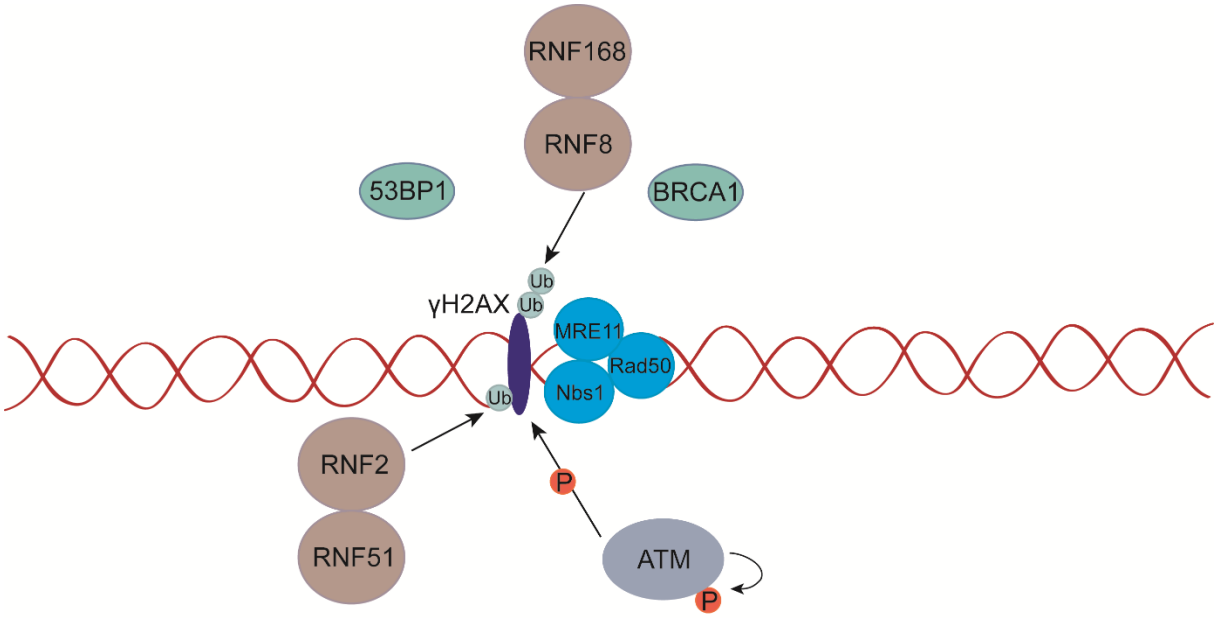


**Figure 6: Role of E3 ubiquitin ligases during DNA damage response.** A complex of RNF2 and RNF51 ubiquitinates H2AX at K119/120 which is crucial for ATM mediated phosphorylation. Furthermore, RNF8 and RNF168 ubiquitinate γH2Ax K63-linked and at K13/15 which is important for recruitment of the repair factors BRCA1 or 53BP1.

### 2.5.5 RNF43 and DDR

Despite its role in Wnt signaling, RNF43 was suggested to have a different function completely independent of negative regulation of this pathway. Upon treatment with UV light, pancreatic duct cells were shown to induce DDR as measured by phosphorylation of H2AX and Chk1. However, when RNF43 was knocked down in these cells, DDR activation was dampened indicating that RNF43 might be important for DDR signaling [232]. This potential role of RNF43 in DDR is supported by the fact that RNF43 mutations are highly enriched in MSI tumors [167, 168, 170]. Thus, high mutational burden in the RNF43 locus could not only be a consequence of MSI but could be also the cause for it since the cells deficient for RNF43 cannot activate DDR appropriately upon DNA damage. Yet, how RNF43 might be involved in DDR and whether this is the case also in gastric cancer needs further investigation.

# 3 Aims of this study

RNF43 has been suggested to have a tumor suppressive function in the stomach, however, those studies were conducted under overexpression conditions. Thus, the first aim of this thesis was to analyze whether endogenous RNF43 has a tumor suppressive function in the stomach. Since Rnf43 knock out mouse models solely concentrated on changes in the intestine and colon, we further analyzed the effect of loss of RNF43 function on gastric homeostasis and its effect on Wnt activity in the stomach of these mice.

The second aim was to elucidate whether RNF43 is involved in DDR signaling in the stomach. A study has hinted towards a role for RNF43 in this signaling pathway. However, this has not been followed up. Especially in gastric tumors, where DDR alterations are more common than those in Wnt activity and RNF43 is frequently mutated, it would be highly interesting to determine whether RNF43 might be important for DDR. Furthermore, we analyzed whether loss of RNF43 could confer resistance to DNA damaging radio- and chemotherapy and could therefore be used as a marker for therapy selection.

*H. pylori* is the major risk factor for gastric cancer and has been shown to target Wnt signaling as well as DDR. Therefore, as a third aim, we investigated how loss of RNF43 function could alter the outcome of *H. pylori* infection in terms of inflammation, DDR and histopathology.

Several studies have been conducted to either analyze RNF43 mutations in gastric cancer patients or to associate RNF43 expression levels with clinicopathological data. However, how RNF43 is expressed during malignant transformation of the gastric tissue and whether RNF43 expression levels could be associated with the activation of DDR has not been investigated. Additionally, it remains to be shown how RNF43 mutation could influence its expression levels and DDR activation. Thus, in the fourth aim, we established a cohort of gastric biopsies from different stages of the carcinogenesis cascade and conducted a comprehensive study that included RNF43 expression, DDR signaling and mutation analysis.

# 4 Material and Methods

## 4.1 Materials

### 4.1.1 Consumables

| | |
|---|---|
| Blotting Paper | Whatman, Dassel, Germany |
| Cell culture flasks | Th.Geyer, Renningen, Germany |
| Coverslips | Menzel-Gläser, Braunschweig, Germany |
| Cryotubes (Nalgene) | Th.Geyer, Renningen, Germany |
| Labsolute reaction tubes 1.5, 2.0 ml | Th.Geyer, Renningen, Germany |
| Novex gel cassettes | Invitrogen, Carlsbad, USA |
| Novex gel combs | Invitrogen, Carlsbad, USA |
| Polypropylene reaction tubes 15, 50 ml | Greiner Bio-one, Frickenhausen, Germany |
| Polypropylene round bottom tubes | BD Bioscience, Franklin Lakes, USA |
| Precellys tubes | Bertin Instruments, Montigny-le-Bretonneux, France |
| Protran Nitrocellulose Transfer membrane | GE Healthcare, Chicago, USA |
| Serological pipette | Greiner Bio-one, Frickenhausen, Germany |
| Superfrost plus microscope slides | Menzel, Braunschweig, Germany |
| Syringe with Sub-Q Needle 1mL, 26 gauge | Becton Dickinson, Franklin Lakes, USA |
| TipOne Graduated Filter Tips | Starlab, Hamburg, Germany |
| Tissue culture plates | Corning, Corning, USA |
| Transwells, 8 µm pore | Sigma, Deisenhofen, Germany |

### 4.1.2 Equipment

| | |
|---|---|
| Aria III Cell sorter | Becton Dickinson, Franklin Lakes, USA |

| | |
|---|---|
| Biofuge fresco centrifuge | Heraeus, Hanau, Germany |
| Biophotometer | Eppendorf, Hamburg, Germany |
| Bio-Rad CFX384 system | Bio-Rad, Hercules, USA |
| Cell culture incubator, HeraCell 240 | Heraeus, Hanau, Germany |
| $Co_2$ Incubator Forma Series II | Thermo Fisher Scientific, Waltham, USA |
| ChemoCam Imager 3.2 | Intas Science Imaging, Göttingen, USA |
| CyAn ADP analyzer | Beckmann Coulter, Brea, USA |
| Electrophoresis chamber | Bio-Rad, Hercules, USA |
| Electrophoresis power supply | Bio-Rad, Hercules, USA |
| Fluoview FV10i confocal microscope | Olympus, Shinjuku, Japan |
| Freezer – 20 °C | Liebherr, Bulle, Switzerland |
| Freezer – 80 °C | Thermo Fisher Scientific, Waltham, USA |
| Heatable magnetic stirrer | IKA, Staufen, Germany |
| Homogenizer T10 Ultra Turrax | IKA, Staufen, Germany |
| Ice machine | Ziegra, Isernhagen, Germany |
| Irradiation source $Cs^{137}$ | Buchler, Braunschweig, Germany |
| Laboratory scale | Kern, Balingen, Germany |
| Laboratory precision scale | Sartorius, Göttingen, Germany |
| Laminar airflow cabinet | Heraeus, Hanau, Germany |
| Maxwell 16 Instrument | Promega, Madison, USA |
| Megafuge 2.0 RS centrifuge | Heraeus, Hanau, Switzerland |
| Mini gel tank | Invitrogen, Carlsbad, USA |
| 4D-Nucleofector X Unit | Lonza, Basel, Switzerland |
| Ph--Electrode | Mettler-Toledo, Columbus, USA |
| Pipetboy | Corning, Corning, USA |

| | |
|---|---|
| Precellys Homogenizer | Bertin Instruments, Montigny-le-Bretonneux, France |
| Refrigerator | Liebherr, Bulle, Switzerland |
| Rocker-Shaker MR-12 | BioSan, Riga, Latvia |
| Shaker, Titramax 100 | Heidolph, Schwabach, Germany |
| Single channel pipettes | Corning, Corning, USA |
| Sonovex Digitec ultrasound waterbath | Bandelin, Berlin, Germany |
| SpectraMax plate reader | Molecular Devices, San José, USA |
| Spectrophotometer NanoDrop 1000 | Thermo Fisher Scientific, Waltham, USA |
| Sunrise Microplate reader | Tecan, Männedorf, Switzerland |
| Thermal cycler C1000 Touch | Bio-Rad, Hercules, USA |
| Thermomixer compact | Eppendorf, Hamburg, Germany |
| Transblot SemiDry Transfer Cell | Bio-Rad, Hercules, USA |
| UV Transilluminator, Eagle Eye | Bio-Rad, Hercules, USA |
| Virtual Slide Microscope | Olympus, Shinjuku, Japan |
| Vortex Genie 2 | Schultheiss, Munich, Germany |

### 4.1.3 Software

| | |
|---|---|
| Adobe Illustrator CS3 | Adobe, San José, USA |
| Adobe Photoshop CS3 | Adobe, San José, USA |
| CFX384 PCR machine software | Bio-Rad, Hercules, USA |
| CLC Workbench 7 | Qiagen, Hilden, Germany |
| FlowJo 10 | FlowJo, Ashland, USA |
| Fluoview Software | Olympus, Shinjuku, Japan |
| GraphPad Prism 8 | GraphPad Software, San Diego, USA |

| | |
|---|---|
| ImageLab 1D | Kapelan, Halle, Germany |
| ImageLab 5.2.1 | Bio-Rad, Hercules, USA |
| SpectraMax Software | Molecular Devices, San José, USA |
| VS-Desktop | Olympus, Shinjuku, Japan |

### 4.1.4 Chemicals

| | |
|---|---|
| Acetic acid | Merck, Darmstadt, Germany |
| Acetone | Merck, Darmstadt, Germany |
| Acrylamide, 40 % | Bio-Rad, Hercules, USA |
| Agarose | Carl Roth, Karlsruhe, Germany |
| Albumin | AppliChem, Darmstadt, Germany |
| Ammonium persulfate, APS | AppliChem, Darmstadt, Germany |
| Ampicillin | AppliChem, Darmstadt, Germany |
| β-Mercaptoethanol | Sigma Aldrich, St. Louis, USA |
| Cisplatin | Sigma Aldrich, St. Louis, USA |
| Crystal Violet | Merck, Darmstadt, Germany |
| Cultrex Basement Membrane Extract | Trevigen, Gaithersburg, USA |
| Diaminobenzidine reagent | Cell Signaling, Danvers, USA |
| Difco Noble Agar | Becton Dickinson, Franklin Lakes, USA |
| 3-(4,5-dimethylthiazol-2-yl)-2,5-diphenyltetrazolium bromide (MTT) | Sigma Aldrich, St. Louis, USA |
| Dimethyl sulfoxide | AppliChem, Darmstadt, Germany |
| Disodium hydrophosphate | Merck, Darmstadt, Germany |
| Dithiothreitol, DTT | AppliChem, Darmstadt, Germany |
| D-Sorbitol | Carl Roth, Karlsruhe, Germany |

| | |
|---|---|
| Eosin | Morphisto, Frankfurt a. M., Germany |
| Ethanol, absolute | AppliChem, Darmstadt, Germany |
| Ethylenediaminetetraacetic acid, EDTA | AppliChem, Darmstadt, Germany |
| Fat-free milk powder | Carl Roth, Karlsruhe, Germany |
| 5-fluorouracil | Sigma Aldrich, St. Louis, USA |
| Glutaraldehyde | AppliChem, Darmstadt, Germany |
| Glycerin | AppliChem, Darmstadt, Germany |
| Glycin | Merck, Darmstadt, Germany |
| Hematoxylin | Carl Roth, Karlsruhe, Germany |
| Hexadimethrine bromide | Sigma Aldrich, St. Louis, USA |
| Hydrochloric acid | Merck, Darmstadt, Germany |
| Hydrogen peroxide, 30 % | Sigma Aldrich, St. Louis, USA |
| Isopropanol | Merck, Darmstadt, Germany |
| Lipofectamine 2000 | Invitrogen, Carlsbad, USA |
| Monopotassium phosphate | Merck, Darmstadt, Germany |
| Nu7026 | Sigma Aldrich, St. Louis, USA |
| Periodic acid | Carl Roth, Karlsruhe, Germany |
| PhosStop phosphatase inhibitor cocktail tablets | Roche, Basel, Switzerland |
| Potassium chloride | Merck, Darmstadt, Germany |
| Ponceau S | Sigma Aldrich, St. Louis, USA |
| Protease inhibitor cocktail tablets | Roche, Basel, Switzerland |
| Protein A agarose beads | Roche, Basel, Switzerland |
| Puromycin | Merck, Darmstadt, Germany |
| Restore Western Blot Stripping buffer | Thermo Fisher Scientific, Waltham, USA |
| Roti-Clear | Carl Roth, Karlsruhe, Germany |
| Roti-Mount | Carl Roth, Karlsruhe, Germany |

| | |
|---|---|
| Roti-Safe | Carl Roth, Karlsruhe, Germany |
| Saponin | Carl Roth, Karlsruhe, Germany |
| Schiff reagent | Carl Roth, Karlsruhe, Germany |
| SignalStain Antibody Diluent | Cell Signaling, Danvers, USA |
| Sodium chloride | Merck, Darmstadt, Germany |
| Sodium citrate | Carl Roth, Karlsruhe, Germany |
| Sodium dodecyl sulfate | Carl Roth, Karlsruhe, Germany |
| Sodium hydroxide | Merck, Darmstadt, Germany |
| Sucrose | Merck, Darmstadt, Germany |
| Tetramethylethylenediamine (TEMED) | Sigma Aldrich, St. Louis, USA |
| Trichostatin A | Sigma Aldrich, St. Louis, USA |
| Tris Ultrapure | Carl Roth, Karlsruhe, Germany |
| Triton-X 100 | AppliChem, Darmstadt, Germany |
| Tween 20 | AppliChem, Darmstadt, Germany |
| Vectashield mounting medium with DAPI | Vector Laboratories, Burlingame, USA |

### 4.1.5 Standards and Kits

| | |
|---|---|
| Benchtop DNA ladder 100 bp, 1 kb | Promega, Madison, USA |
| Cell Counting Kit-8 | Sigma Aldrich, St. Louis, USA |
| Cell Titer Glo 3D | Promega, Madison, USA |
| DNA-free DNAse Kit | Invitrogen, Carlsbad, USA |
| GenElute manmalian total RNA Kit | Sigma Aldrich, St. Louis, USA |
| GoTaq Green Mastermix | Promega, Madison, USA |
| GoTaq qPCR Mastermix | Promega, Madison, USA |
| Maxwell 16 LEV simplyRNA Tissue Kit | Promega, Madison, USA |

| | |
|---|---|
| Precision Plus Protein Dual Color Standard | Bio-Rad, Hercules, USA |
| QiaAmp FFPE Tissue Kit | Qiagen, Hilden, Germany |
| Quick-DNA Miniprep Kit | Zymoresearch, Irvine, Germany |
| PureYield Plasmid Miniprep System | Promega, Madison, USA |
| RNAse free DNAse Kit | Qiagen, Hilden, Germany |
| Wizard SV Gel and PCR Clean Up | Promega, Madison, USA |

#### 4.1.6 Cell Culture

| | |
|---|---|
| A-83-01 TGFβ inhibitor | Tocris, Bristol, UK |
| Corning Matrigel Basement Membrane Matrix | Corning, Corning, USA |
| Fetal Calf Serum (FCS) | Invitrogen, Carlsbad, USA |
| FGF-10 | Peprotech, Hamburg, Germany |
| Gastrin | Sigma Aldrich, St. Louis, USA |
| Gibco B27 supplement | Invitrogen, Carlsbad, USA |
| Gibco collagen Type I rat tail | Invitrogen, Carlsbad, USA |
| Gibco Advanced DMEM/F12 | Invitrogen, Carlsbad, USA |
| Gibco DMEM | Invitrogen, Carlsbad, USA |
| Gibco GlutaMAX | Invitrogen, Carlsbad, USA |
| Gibco HEPES 1M | Invitrogen, Carlsbad, USA |
| Gibco IMDM | Invitrogen, Carlsbad, USA |
| Gibco N2 supplement | Invitrogen, Carlsbad, USA |
| Gibco OptiMEM | Invitrogen, Carlsbad, USA |
| Gibco Penicillin/Streptamycin | Invitrogen, Carlsbad, USA |
| Gibco Trypan blue | Invitrogen, Carlsbad, USA |
| Gibco Trypsin/EDTA | Invitrogen, Carlsbad, USA |

| | |
|---|---|
| Gibco Trypsin/EDTA | Invitrogen, Carlsbad, USA |
| N-acetyl-cysteine | Sigma Aldrich, St. Louis, USA |
| Nicotinamide | Sigma Alrdich, St. Louis, USA |
| P38 inhibitor | Sigma Aldrich, St. Louis, USA |
| Recombinant EGF | Peprotech, Hamburg, Germany |

### 4.1.7 Enzymes

| | |
|---|---|
| BsmA1 | New England Biolabs, Ipswich, USA |
| DpnI | Agilent Technologies, Santa Clara, USA |
| M-MLV reverse transcriptase | Promega, Madison, USA |
| Q5 High-Fidelity DNA polymerase | New England Biolabs, Ipswich, USA |
| Proteinase K | Sigma Aldrich, St. Louis, USA |
| T4 DNA Ligase | Promega, Madison, USA |

## 4.2 Cellular assays

### 4.2.1 Cell culture

AGS (ATCC CRL-1739; 2011) and MKN45 (RCB1001; 2009) as well as Wnt3A-, Rspondin 3- and Noggin producing L-WRN (ATCC CRL-3276; 2013) cells were cultured in Dulbecco's Modified Eagle Medium (DMEM, Gibco) supplied with 10 % fetal calf serum (FCS) and 1 % Penicillin-Streptomycin (5000 U/ml) at 37 °C and 5 % $CO_2$. For subculture, cells were washed in PBS (pH 7.4, **Table 1**) and incubated with 0.05 % Trypsin-EDTA (Gibco) for 5 – 10 minutes. When cells were detached, medium was added in order to stop trypsinization and cells were transferred to a 15 ml falcon tube and centrifuged at 1000 rpm for 5 minutes. The supernatant was aspirated, and the cells were resuspended in medium and seeded into a new culture flask at adequate density. From L-WRN cells, medium was collected after 4 – 5 days of confluent culture and was passed through a 0.22 µm filter.

**Table 1: Composition of 1X PBS.**

| Component | Final concentration |
|---|---|
| NaCl | 13.7 mM |
| KCl | 0.27 mM |
| $Na_2HPO_4$ | 10 mM |
| $KH_2PO_4$ | 0.2 mM |

Cell number was determined using a Neubauer hemocytometer. For this, 10 µl of cell suspension were diluted 1:10 in trypan blue, a dye that only stains dead cells. 10 µl of this mixture where then loaded onto the cell counting chamber and the number of cells in 4 quadrants was determined. The number of cells per ml was calculated as mean of the 4 quadrants multiplied by the dilution factor 10 and the dilution factor of the chamber itself $10^4$.

For long term storage of cells, aliquots were frozen stepwise in cryotubes first at – 80 °C and then in liquid nitrogen. For this, cells were trypsinized, centrifuged and resuspended in 900 µL medium per cryotube. Cells where then mixed with 10 % DMSO, transferred to a cryotube and immediately placed on ice. AGS and MKN45 cells were frozen at a density of $1*10^6$ and $1.5*10^6$ cells per ml, respectively. For thawing the cells, they were diluted in 5 ml prewarmed medium and centrifuged at 1000 rpm for 5 minutes. Cells were transferred to a culture flask and incubated at 37 °C and 5 % $CO_2$. After 24 h, medium was changed in order to remove remaining DMSO and dead cells from the culture.

### 4.2.2 Lentiviral knock down of RNF43

Lentiviral vectors were used to integrate DNA coding for short hairpin (sh) RNA into the genome of gastric cancer cells. This shRNA was either nonsense sequence not binding to any target in the cells or specific for RNF43 mRNA. This shRNA could then bind RNF43 mRNA and thereby target it for degradation. In this thesis, cells from two different knock down approaches were used. The first lentiviral knock down was performed in AGS and MKN45 cells during my Master thesis and these cells were then used in this study for chemotherapy and xenograft experiments. The second lentiviral knock down was performed in MKN45 cells only, since this cell line was not suitable for CRISPR/Cas9 editing.

**Table 2: DNA sequences of short hairpin RNA used for a lentiviral knock down of RNF43.**

| **Oligo** | ***forward*** | ***reverse*** |
|---|---|---|
| shRNF43 | TTCTTGGTAAGATCGAGAG | CTCTCGATCTTACCAAGAA |
| shRNF43 (Sirion) | ATGAATCTCCCTCTGTGATTT | AAATCACAGAGGGAGATTCAT |
| shctrl | GTACAGCCGCCTCAATTCT | AGAATTGAGGCGGCTGTAC |
| shctrl (Sirion) | GCAACTTCAGCTATATCATTT | AAATGATATAGCTGAAGTTGC |

To perform the knock down, lentiviral particles were purchased from Sirion Biotech and stored at – 80 °C. shRNA sequences are listed in **Table 2**. MKN45 cells were seeded in 6 well plates at a density of $3*10^5$ cells per well and allowed to attach overnight. A multiplicity of infection (MOI) of 10 virus

particles was diluted in 1 ml of Opti-MEM and hexadimethrine bromide was added to a final concentration of 8 µg/ml. 1 ml of viral suspension was added to each well and incubated for 2 hours at 37 °C 5 % $CO_2$ with occasional swirling. 4 ml of complete culture medium were then added, and cells were incubated for 24 hours. After this, medium was exchanged to normal complete culture medium and cells were expanded. 7 days post transduction, cells were selected for successful integration of the viral construct by adding 200 µg/ml puromycin to the culture for 1 week. RNA was extracted from the cells and RNF43 expression was assessed.

### 4.2.3 Proliferation assay

Cell proliferation was measured using cell counting kit 8 (CCK-8, Sigma), which contains a tetrazolium salt that is reduced to a yellow colored formazan dye in the presence of active dehydrogenases in viable cells. To this end, 2500 and 5000 AGS or MKN45 cells were seeded in quadruplicates in a 96 well plate and allowed to attach overnight. Cells were synchronized by 24 hours of serum starvation, released into cell cycle by addition of complete medium and allowed to proliferate for 48 hours. Cell viability was measured by adding 10 µl of CCK-8 per well and incubating the plate at 37 °C 5 % $CO_2$ for 1 hour. Absorption was measured in a microplate reader (Tecan) at the wavelength of 450 nm and 600 nm (reference).

### 4.2.4 Invasion assay

Boyden chamber invasion assay was used to determine the invasive capacity of the gastric cancer cell line MKN45. In this assay, the cells have to digest an extracellular matrix structure in order to migrate through 8 µm pores of a transwell along a serum gradient.

For this assay, $4*10^5$ MKN45 shctrl or shRNF43 cells were seeded in a 6 well plate and were serum starved 24 hours. The inside of the transwell was coated with 10 µg/ml Matrigel (VWR), an extracellular matrix-like component, while the lower site of the transwell was coated with 10 µg rat collagen I (Gibco) diluted in 0.01 M acetic acid. Transwells were washed 3 times with PBS and placed in a 24 well plate containing 750 µl medium with FCS. Cells were counted and $1*10^5$ MKN45 cells

diluted in 500 µl serum free medium were placed inside the transwell and allowed to migrate for 24 hours. After this incubation time, the inside of the transwells was cleaned with PBS and cotton buds in order to remove non-migrated cells. The lower part of the transwell with attached migrated cells was washed in PBS and fixed with 4 % formaldehyde for 15 minutes. Transwells were then washed again twice with PBS and stained with DAPI diluted in PBS (1:6000) for 10 minutes at room temperature. After washing with PBS, transwells were dried and migrated cells were counted using a fluorescence microscope.

### 4.2.5 Colony formation assay

Single cell colonies were grown in soft agar assay in order to monitor anchorage independent growth *in vitro*. Number of colonies was then measured by 3-(4,5-dimethylthiazol-2-yl)-2,5-diphenyltetrazolium bromide (MTT) and colony size was determined by microscopy.

For this assay, 2% Difco noble agar (Oxoid) diluted in Iscove's Modified Dulbecco's Medium (IMDM, Gibco) was melted at 100 °C and kept liquid at 42 °C while shaking. To prevent cells from attaching to the bottom of the 96 well plate, highly concentrated bottom agar (0.6 %) was added to the wells and allowed to solidify. 500, 1000 or 1500 cells per well where diluted in less concentrated top agar (0.3 % in IMDM 10 % FCS) and seeded on top of the bottom agar. A feeding layer with IMDM 10 % FCS was added to the wells and single cell colonies were allowed to grow for 2 weeks. Pictures of colonies were taken using a Nikon microscope at 10 x magnification. Viable cells were measured by adding 40 µl MTT (5 mg/ml) to the wells and measuring absorption at 570 nm.

### 4.2.6 Chemotherapy treatment

In order to assess whether RNF43 loss could confer resistance to chemotherapy, AGS and MKN45 cells expressing or lacking RNF43 were treated with 5-fluorouracil (5-FU) or cisplatin, two commonly used chemotherapeutic agents in gastric cancer therapy.

First, $LD_{50}$ was determined for AGS and MKN45 cells. To this end, 7500 cells per well were seeded in triplicates into a 96 well plate and 5-FU and Cisplatin were added at different concentrations (1, 2, 5,

10 µg/ml). Cells were allowed to grow for 48 hours and cell viability was measured using CCK-8 as described above. $LD_{50}$ was determined as 2 µg/ml for 5-FU and 10 µg/ml for cisplatin and assays were performed with these concentrations.

### 4.2.7 Irradiation experiments

In order to determine the cells' sensitivity to ionizing radiation, wild type and RNF43 depleted AGS and MKN45 cells were trypsinized, resuspended in medium and treated with 10 or 20 Gγ in a $Cs^{137}$ radiation source (Buchler, Germany). Cells were subsequently seeded for proliferation assays or lysed in order to harvest protein or RNA.

### 4.2.8 Clonogenicity assays

Clonogenicity assays were used to determine the capacity of AGS and MKN45 cells expressing or lacking RNF43 to expand clonally after treatment with irradiation.

To this end, cells were treated with 2.5 or 5 Gγ and 1000 cells were seeded into 6 mm tissue culture dishes. Colonies were allowed to grow for 2 weeks until they were well visible by eye. Medium was then removed, and wells were washed in PBS. For fixing and staining the colonies, crystal violet was diluted in a 6 % glutaraldehyde solution. Cells were incubated for 30 minutes at room temperature. Staining solution was discarded, and wells were washed carefully with tap water, allowed to dry and colonies were counted.

### 4.2.9 Flow cytometric analysis of apoptosis

Annexin V/ Propidium iodide (PI) stainings were performed to analyze cell apoptosis after ionizing radiation. When cells go into apoptosis, the phospholipid phosphatidylserine is translocated to the outer cell membrane where it can be stained with Annexin V. In late apoptosis, PI can enter the cell through the leaky cell membrane. Therefore, cells in early apoptosis will stain as Annexin V positive and PI negative, whereas cells in late apoptosis are double positive.

The optimal time point to measure apoptosis after irradiation was determined by monitoring the cells microscopically and analyzing apoptosis at several time points. Apoptosis was visible 4 days after irradiation in AGS cells and 6 days after irradiation in MKN45 cells. After irradiation, cells were plated in a 6 well plate and allowed to recover. Then, cells were trypsinized, washed twice with PBS and resuspended in 500 µl annexin-binding buffer (Invitrogen). 200 µl of the cell suspension were stained with 5 µl Pacific blue conjugated Annexin V (Invitrogen) and 10 µl PI (Sigma Aldrich, 50 µg/ml) for 15 minutes at room temperature. Negative as well as single color controls were included by mixing irradiated and untreated cells. Stained cells were then analyzed using a CyAn ADP flow cytometer (Beckmann Coulter) and analyzed with FloJo. Gates for positive and negative cells were set according to the negative and single color controls and applied to the samples. The spectra of stained colors did not overlap as experimentally confirmed by the single color staining.

### 4.2.10 Infection with Helicobacter pylori *in vitro*

Frozen aliquots of *H. pylori* strain PMSS1 [60] were thawed and plated on Wilkins Chalgren (WC) agar plates containing *Helicobacter pylori* selective supplement DENT (Oxoid) (**Table 3**). After 3 days of culture, bacteria were split onto new agar plates and allowed to grow for another 48 hours prior to infection.

**Table 3: Composition of Helicobacter pylori selective supplement DENT (Oxoid).**

| Antibiotic | Final concentration |
|---|---|
| Vancomycin | 10 mg/l |
| Trimethoprim | 5 mg/l |
| Amphothericin B | 5 mg/l |
| Cefsulodin | 5 mg/l |

AGS and MKN45 cells were seeded on 24 well plates for protein analysis or 6 well plates for RNA isolation 48 hours prior to infection. Cell number was determined and medium was exchanged to

antibiotics free medium containing FCS. Bacteria were collected in 1 ml of BHI containing 20 % FCS and resuspended. $OD_{600nm}$ was measured in a Biophotometer (Eppendorf) and number of bacteria was calculated as follows:

$$OD_{600\,nm}\,1 = 2 * 10^8\ bacteria/ml$$

Cells were infected at a multiplicity of infection (MOI) of 50 and 100 for 24 hours. After infection, medium was removed, and cells were washed with PBS. Cells were then either lysed in 75 µl SDS sample buffer or 300 µl RNA lysis buffer and further processed.

## 4.3 Protein biochemical methods

### 4.3.1 Immunoprecipitation

In order to determine whether RNF43 interacts with H2AX upon DNA damage, immunoprecipitation experiments were performed after treatment with irradiation. For precipitation of RNF43, the protein was overexpressed together with an HA tag. For ubiquitination assays, γH2AX was precipitated and its posttranslational modifications were observed under endogenous RNF43 expression.

Transfection by lipofectamine

For immunoprecipitation of RNF43, pcDNA4To (Addgene) vector containing *RNF43* cDNA with a HA tag at the C-terminus was transfected into AGS and MKN45 cells. For this, $5*10^6$ cells were seeded in a 10 cm tissue culture dish and transfected with 5 µg plasmid in a final volume of 3 ml Opti-MEM containing Lipofectamine 2000 (1:100). After incubation of the cells with DNA complexes for 3 – 4 hours, 7 ml of complete medium were added, and cells were allowed to grow for 36 hours prior to irradiation.

Immunoprecipitation

Cells were irradiated at 20 Gγ, washed with PBS and resuspended in 1 ml RIPA buffer (**Table 4**) and incubated on ice for 10 minutes. Cells were lysed by sonicating three times for 15 seconds and

centrifuged for 10 minutes at 10,000 x g at 4 °C. The supernatant was transferred to a new tube and precleared using 1 µg of the control IgG (e.g. rabbit IgG for IP antibodies produced in rabbit) and 20 µl of protein A agarose beads (Roche). Samples were incubated with rotation for 30 minutes at 4 °C. To remove all unspecifically bound proteins in the lysate, samples were centrifuged at 3,000 rpm for 1 minute at 4 °C. 10 % of the supernatant was kept as input sample, mixed with 3 x SDS buffer and boiled for 5 minutes at 95 °C. The remaining sample was divided and either incubated with 1 µg of control IgG or with the specific antibody (α-HA or α-γH2AX, **Table 11**) overnight with rotation at 4 °C. To precipitate bound antibodies, 20 µl agarose beads were added to the samples and again incubated with rotation at 4 °C for 4 hours. Beads were collected by centrifugation at 3,000 rpm for 1 minute at 4 °C and washed five times by adding 1 ml PBS and repeating the centrifugation step. Beads were resuspended in 50 µl SDS buffer and boiled at 95 °C for 5 minutes. Protein lysates were then subjected to sodium dodecyl sulfate polyacrylamide gel electrophoresis (SDS-PAGE) and Western Blot.

**Table 4: Composition of RIPA buffer.**

| Component | Final concentration |
|---|---|
| TRIS-HCl pH 7.4 | 50 mM |
| Nonidet P-40 | 1 % |
| NaCl | 150 mM |
| Sodium deoxycholate (DOC) | 0.25 % |
| EGTA | 1 mM |

### 4.3.2 Western Blot

SDS-PAGE and Western Blot were used to analyze activation of DNA damage response after treatment of cells with irradiation, immunoprecipitation or infection with *H. pylori*.

Cells were lysed in SDS sample buffer (**Table 5**), sonicated in a water bath for 10 minutes, boiled at 95 °C for 5 minutes and allowed to cool down.

**Table 5: Composition of SDS sample buffer.**

| Component | Final concentration |
|---|---|
| TRIS pH 6.8 | 62.5 mM |
| SDS | 2 % |
| Glycerol | 10 % |
| Bromophenol blue | 0.01 % |
| Dithiothreitol (DTT) | 50 mM |

8 % and 10 % polyacrylamide gels were used to separate protein lysates according to molecular weight. Separating gel components were mixed according to **Table 6** and casted into Novex gel cassettes (Thermo Fisher). Isopropanol was layered on top of the gel to prevent drying. Separating gels were allowed to solidify for 30 – 60 minutes. Isopropanol was then removed, stacking gel was casted (**Table 7**) and 15 well combs were inserted into the stacking gel.

**Table 6: Composition of a separating SDS-PAGE gel.**

| Component | Volume/gel |
|---|---|
| TRIS (1.5 M, pH 8.8), 0.4 % SDS | 7.5 ml |
| 40 % acrylamide | 1.2 ml (8 %) / 1.5 ml (10 %) |
| 10 % ammonium persulfate | 30 µl |
| Tetramethylethylenediamine (TEMED) | 6 µl |
| $dH_2O$ | To a final volume of 6 ml |

For gelelectrophoresis, gels were placed into an SDS-PAGE tank (Invitrogen) and filled up with SDS running buffer (**Table 8**). Combs were removed and 6 – 10 µl of sample were loaded into the pockets. 8 µl of dual color protein ladder (Biorad) were loaded to identify molecular weight. Electrophoresis was performed at 150 V for 1 hour.

**Table 7: Composition of a stacking SDS-PAGE gel.**

| Component | Volume/gel |
|---|---|
| TRIS (0.5 M, pH 6.5), 0.4 % SDS | 0.5 ml |
| 40 % acrylamide | 0.2 ml |
| 10 % ammonium persulfate | 10 µl |
| Tetramethylethylenediamine (TEMED) | 2 µl |
| $dH_2O$ | To a final volume of 2 ml |

**Table 8: Composition of SDS running buffer.**

| Component | Final concentration |
|---|---|
| TRIS | 25 mM |
| Glycin | 0.2 M |
| SDS | 0.1 % |

**Table 9: Composition of Semi-dry blotting buffer.**

| Component | Final concentration |
|---|---|
| TRIS | 48 mM |
| Glycin | 39 mM |
| SDS | 0.037 % |
| Methanol | 20 % |

Proteins were then blotted from the gel to a nitrocellulose membrane (GE healthcare) by semi-dry blotting. A blotting chamber (Biorad) was moistened with semi-dry blotting buffer (**Table 9**) and 4 layers of whatman paper and the membrane soaked in blotting buffer were placed into the chamber. The gel was then removed from the cassette, placed on top of the membrane and covered with 4

layers of soaked whatman paper. Proteins were blotted on to the membrane at 90 mA per membrane for 1 hour and 40 minutes. Successful blotting was confirmed by staining the membrane with Ponceau solution (0.5 % in 1 % acetic acid). The membrane was blocked for 1 hour in 5 % non-fat dry milk solved in TBS-T (**Table 10**) at room temperature. Then, the membrane was briefly washed in TBS-T and incubated overnight in primary antibody diluted in 5 % BSA/TBS-T. To remove excess antibody, the membrane was washed three times in TBS-T for 10 minutes while shaking. Then, HRP-coupled secondary antibody diluted in blocking buffer was added for 1 hour. The membrane was then washed 6 times for 10 minutes with TBS-T to remove unbound secondary antibody. For detection, Clarity Western Peroxide Reagent and Western Luminol/Enhancer Reagent (Biorad) were mixed 1:1, added to the membrane and incubated for 5 minutes in the dark. Excess detection solution was removed from the membrane and chemiluminescence was detected using a Chemostar ECL imager (Intas Science Imaging). Intensity of protein bands was quantified using LabImage 1D program (Kapelan). A list of the antibodies used can be found in **Table 11**.

**Table 10: Composition of TBS-T buffer.**

| Component | Final concentration |
|---|---|
| TRIS | 50 mM |
| NaCl | 150 mM |
| Tween20 | 0.1 % |
| pH | 7.6 |

**Table 11: List of antibodies used in Western Blot and Immunoprecipitation.**

| Target | Clone | Company | Reactivity | Dilution |
|---|---|---|---|---|
| **Primary Antibodies for Western Blot** | | | | |
| CHK2 | 1C12 | Cell Signaling | H | 1:1000 |
| GAPDH | 14C10 | Cell Signaling | H, M | 1:1000 |
| HA | H6908 | Sigma | - | 1:1000 |
| p-CHK2 (Thr68) | C13C1 | Cell Signaling | H | 1:1000 |
| γH2AX | ab81299 | Abcam | H, M | 1:10000 |
| **Secondary Antibodies for Western Blot** | | | | |
| Rabbit IgG | W4011 | Promega | - | 1:3000 |
| Mouse IgG | W4021 | Promega | - | 1:3000 |
| **Antibodies for Immunoprecipitation** | | | | |
| HA | H6908 | Sigma | - | 1:100 |
| γH2AX | 5438 | Cell Signaling | H, M | 1:50 |

## 4.4 CRISPR/Cas9 cell editing

### 4.4.1 CRISPR/Cas9 design

CRISPR/Cas9 technology was used to introduce base pair deletions or specific mutations into the genomic sequence of RNF43 in AGS cells. Cas9 is a bacterial endonuclease that recognizes a specific stem loop RNA structure. This RNA structure is designed to contain a complementary sequence to the genomic target, the guide RNA that allows the ribonucleoprotein (RNP) complex to bind to the DNA. A protospacer adjacent motif (PAM) consisting of the bases NGG is required next to the binding site for Cas9 to execute its endonuclease function. Cas9 thereby induces a double strand break in the DNA that is either repaired by non-homologous end joining (NHEJ) leading to random insertions or deletions, or by homology directed repair (HDR). The latter can be used to introduce specific

mutations into the genome. For this, a DNA oligo has to be provided containing the desired alteration of the genome flanked by homology arms with a size of 30 – 60 bp at each side. However, HDR is a rather rare event and is very often restricted to S/G2 phase of the cell cycle [233]. To improve efficiency, several inhibitors of NHEJ and enhancers of HDR can be used along CRISPR/Cas9 editing.

**Table 12: Sequences of guide RNAs and repair oligo for CRISPR/Cas9 mediated editing of RNF43.**

| Mutations | Sequence |
|---|---|
| **Guide RNAs** | |
| $AGS^{D196fs}$ | TCAAGCTGGAGAGTCCTCGA |
| $AGS^{R132X}$ | GATGTCAAAGAGGACAGCAC |
| $AGS^{R584fs}$ | AAACCGGAGTCCCCCAGTCC |
| **Repair oligo** | |
| $AGS^{R132X}$ | TGCCTCTGCAGGCTCGGATGGCGGGTGAGTGAGGAGCAAGTGCTGTCCTCTTTGACATCA |
| $AGS^{R584fs}$ | CAGAAACCGGAGTCCCCCAGTCCAGACCTCCTATTCCTCGACACAGCCCCAGCCAGAGCCAC CTTCTCCT |

In this work, several published online tools have been used to design CRISPR/Cas9 approaches to introduce mutations in RNF43. Guide RNA for generation of $AGS^{D196fs}$ cells was designed with tools.genome-engineering.org. Adequate guide RNA was chosen considering a high on-target score and low off-target score. Furthermore, off-targets were ranked after relevance in gastric cancer cell lines, e.g. location in introns or exons or expression in gastric tissue. For specific mutations, guide RNAs as well as templates for HDR were designed using Benchling (www.benchling.com) and the online tool from Integrated DNA Technologies (IDT). Guide RNA scores were compared in both tools and the most suitable was chosen. HDR template suitable for the guide RNA was chosen in Benchling. Sequences of guide RNAs and repair oligos are listed in **Table 12**.

### 4.4.2 CRISPR/Cas9 cloning strategy

Cloning

The guide RNA for generation of $AGS^{D196fs}$ cells was ordered as DNA oligomers in forward and reverse orientation. DNA oligomers were then annealed by mixing 1 µl of each oligomer (100 µM) with 1 µl ATP, T4 ligation buffer and $dH_2O$ to a final volume of 10 µl. Oligomers were then allowed to anneal at 37 °C for 30 minutes followed by 5 minutes incubation at 95 °C and a stepwise decrease of the temperature down to 25 °C with a drop of 1.5 °C per minute. In parallel, pX330 vector (Addgene) was digested using BbsI (NEB) restriction enzyme. 1 µg of plasmid was mixed with 1 µl BbsI, 10 x buffer 2.1 (NEB) and $dH_2O$ to a final volume of 20 µl and incubated at 37 °C for 1 hour. The digested plasmid was then isolated by using Wizard SV Gel and PCR Clean Up Kit (Promega). Guide RNAs were ligated into the plasmid by mixing 1 µl of cleaned up plasmid with 1 µl T4 Ligase (Promega), T4 Ligation buffer, 1 µl of ATP and 6 µl of annealed oligomers and incubating at room temperature for 2 – 3 hours.

Bacterial transformation

Ligated plasmid was then transformed into DH5α competent *E. coli* by adding 2 µl of plasmid to bacteria solution and incubating on ice for 5 minutes. Heat-shock for 42 seconds at 42 °C was used to deliver plasmids to the bacteria followed by incubating them on ice for 10 minutes. 900 µl of LB medium without antibiotics were then added to the bacteria and they were incubated at 37 °C while shaking for 30 minutes. Bacteria were then centrifuged at 4,500 rpm for 5 minutes to remove excess LB medium and plated on LB Ampicillin (100 µg/ml) plates overnight.

Bacterial colony screening

Grown bacterial colonies were screened for successful integration of guide RNA oligomers by PCR. A master mix (**Table 13**) was prepared and a U6 forward primer and the reverse oligomer of the insert were used for screening. Colonies were picked with a pipet tip and dipped into the PCR Master mix. PCR program is described in **Table 14**. PCR samples were loaded on an agarose gel and positive colonies were sent for Sanger sequencing (Eurofins) to confirm successful cloning. Confirmed colonies

were then inoculated into 5 ml of LB-Amp (100 µg/ml) and incubated overnight at 37 °C while shaking. Plasmid was then isolated from bacterial culture using PureYield Plasmid Miniprep System (Promega) according to manufacturer's instructions. An aliquot of the bacterial culture was saved to cryopreserve bacteria containing the plasmid. Thus, bacteria were centrifuged and resuspended in 500 µl of fresh LB medium. Bacteria suspension was then mixed with 500 µl of glycerol, transferred into a cryotube and frozen at – 80 °C. For higher yield of plasmid, bacteria were inoculated in 100 ml LB-Amp medium and incubated overnight at 37 °C while shaking. Bacterial culture was then centrifuged, and plasmids were isolated using PureYield Plasmid Midiprep System (Promega) according to manufacturer's instructions.

**Table 13: Composition of PCR mastermix for bacterial colony screening.**

| Reagent | Volume |
|---|---|
| Go Taq Green Mastermix (2X) (Promega) | 12.5 µl |
| Primers forward/reverse (10 µM) | 1 µl each |
| $dH_2O$ | To a final volume of 25 µl |

**Table 14: PCR program for bacterial colony screening.**

| PCR step | Temperature | Time | |
|---|---|---|---|
| Initial denaturation | 95 °C | 5 min | |
| Denaturation | 95 °C | 30 s | 36 cycles |
| Annealing | 56 °C | 30 s | |
| Elongation | 72 °C | 2 min | |
| Final enlongation | 72 °C | 5 min | |
| Final hold | 12 °C | ∞ | |

Agarose gel electrophoresis

Agarose gel electrophoresis was used to determine presence and size of DNA fragments obtained from PCR. Dependent on the expected fragment size, agarose was diluted to a concentration of 1 – 2 % in TAE buffer (**Table 15**) and heated in a microwave until the agarose was dissolved completely. 5 µl of Roti-Gelstain (Roth) per 100 ml were added and the gel was casted into a tray and allowed to solidify. PCR samples were then loaded onto the gel and 90 to 110 V of voltage were applied for 30 to 50 minutes dependent on gel size and agarose percentage. DNA bands were visualized using UV light in a Gel Doc XR+ Gel documentation system (Biorad).

**Table 15: Composition of TAE buffer.**

| Component | Final volume |
|---|---|
| TRIS | 40 mM |
| Acetic acid | 20 mM |
| EDTA | 1 mM |

### 4.4.3 Delivery of CRISPR/Cas9 constructs

Transfection with lipofectamine

The CRISPR/Cas9 plasmid pX330 (Addgene) was used to generate a random Indel in *RNF43*. This plasmid carried the sequenced for the guide RNA cloned in 4.4.2 as well as for the Cas9 protein which were expressed in gastric cancer cells upon transfection.

Transfection with Lipofectamine 2000 (Invitrogen) was used to deliver plasmid DNA to AGS cells. For transfection of pX330, $3*10^6$ cells were seeded in a 6 well plate. Lipofectamine 2000 was diluted 1:50 in 200 µl Opti-MEM (Gibco) and incubated for 5 minutes at room temperature. 1 µg plasmid diluted in 200 µl Opti-MEM was mixed with Lipofectamine 2000 and incubated for 20 min at room temperature. 400 µl of DNA complex solution was added to each well and incubated at 37 °C 5 % $CO_2$

for 2 – 3 hours. 2 ml of Opti-MEM were added for another 3 – 4 hours before 2 ml complete medium were added to the cells until further selection.

Single cell selection

Since pX330 plasmid harbored the coding sequence for GFP, cells were sorted 48 h after transfection. For this, cells were trypsinized and washed with PBS. Cells were then resuspended in 500 µl PBS and kept on ice. An Aria III cell sorter (Becket Dickinson) was used to sort GFP positive cells. Sorted cells diluted in FCS were then plated in an appropriate volume and allowed to recover.

**Table 16: Sequences of PCR primers for amplification of RNF43 exons.**

| **Exon** | **Annealing temperature [°C]** | ***Forward*** | ***Reverse*** |
|---|---|---|---|
| Exon 2 | 61 | TATGTATGGTTGAAGTGCATTGCT | ATTTCAAACAGATGGAAAGTGAAATATA |
| Exon 3 | 68 | AAGCCTCCCTAACCCAAGTC | AGCACAGGGTCTTCTCACAG |
| Exon 4 | 58 | CCTCAGCCCAACCTCTACTG | ACAGGGCTGCTGTGACTTCT |
| Exon 5 | 60 | GTGGGCACTTTCCCCCTG | GGCAAGGTCTGGAGGTCTA |
| Exon 6 | 60 | ACCCTTTCCCTCTCTGCTC | GCCGCCAAAGACCCCAC |
| Exon 7 | 62 | CCCCAATCTGAGCCCCATT | GGTCATGGAGGTGAACCACA |
| Exon 8 | 63 | CTACAGAAGCCTTTGGTTTGGA | AGAGGGGAGTCCTTGGCC |
| Exon 9 | 65 | AGCCATGTCTTTCTGAATGCA | CACACCCACTTCCCTCTGAA |

For single cell selection, cells were seeded in low density on 15 cm tissue culture dishes and colonies were allowed to grow for 1 – 2 weeks. For picking the colonies, medium was removed from the plate and cells were covered with 10 ml PBS. Using a pipette, colonies were scratched off the plate, taken up in the pipette with a volume of 20 µl and transferred into a 48 well plate with 100 µl PBS. Cells

were then incubated with 50 µl of trypsin for 10 minutes at 37 °C 5 % $CO_2$ and 500 µl complete medium were added. Cells were allowed to attach overnight and medium was exchanged to remove residual trypsin.

**Table 17: Composition of the PCR mastermix for Exon amplification.**

| Reagent | Volume |
|---|---|
| Q5 High-Fidelity mastermix (2X) (NEB) | 12.5 µl |
| Primers forward/reverse (10 µM) | 1.25 µl each |
| Template DNA | 5 µl |
| $dH_2O$ | To a final volume of 25 µl |

For screening for successful alteration of the genome, cells were expanded and DNA was isolated from at least $3*10^5$ cells using Quick-DNA Microprep Kit (Zymoresearch) according to manufacturer's instructions in an elution volume of 30 µl. DNA content was measured using a Nanodrop (Thermo Fisher) and the exon of interest was amplified using polymerase chain reaction (PCR). In these exon PCRs, Q5 high fidelity polymerase (New England Biolabs) was used in order to reduce error rates during amplification. The primers used for exon PCRs are listed in **Table 16** and PCR master mix and conditions are described in **Table 17** and **Table 18**. Successful amplification was monitored by loading part of the sample on an agarose gel with Roti-Gel stain (Roth) and PCR samples were cleaned up using Wizard SV Gel and PCR Clean Up Kit (Promega) according to manufacturer's instructions. 12 µl of the PCR product were mixed with 3 µl exon primer (10 µM) and send for Sanger sequencing to Eurofins. Sequence analysis was performed using CLC Main Workbench 7 (Qiagen).

**Table 18: PCR program for amplification of RNF43 exons.**

| PCR step | Temperature | Time | |
|---|---|---|---|
| Initial denaturation | 98 °C | 5 min | |
| Denaturation | 98 °C | 10 s | 40 cycles |
| Annealing | See **Table 16** | 30 s | |
| Elongation | 72 °C | 20 – 30 s/kb | |
| Final enlongation | 72 °C | 2 min | |
| Final hold | 12 °C | ∞ | |

AGS$^{D196fs}$ cells were screened for potential alterations in CRISPR/Cas9 off targets. Thus, PCR for off target sequences was performed as described above with the primers listed in **Table 19**.

**Table 19: Sequences of PCR primers for off target amplification.**

| Primer | *Forward* | *Reverse* |
|---|---|---|
| *LTK* | GTACCCAGAATCAGGACCCC | TGAGTCTTGAAGCGTGGGTA |
| *WW2C* | TGCAGGCAAGTCTTCCAAAA | AGTGGATGGGTAACTTGGCA |
| *SLX4* | CAGGTGTGAACTACTGCGTC | CTGTGAAGATGGAGGTTGGC |

RNP electroporation

CRISPR/Cas9 Ribonucleincomplexes (RNP) were used to introduce targeted point mutations into AGS cells. In these complexes, guide RNAs are first aligned with tracer RNA and then brought into a complex with recombinant Cas9 protein. These complexes were then transferred into AGS cells via electroporation together with a homology repair (HR) template.

5 µl of guide RNA (100 µM) and 5 µl of tracer RNA (100 µM) were mixed and incubated for 5 minutes at 95 °C and were cooled to room temperature. 6.6 µl of Cas9 (final amount 412.5 pmol) were added and incubated for 15 minutes at room temperature.

$5*10^5$ AGS cells were suspended in 82 µl Nucleofector Solution and 18 µl Supplement (SF Cell Line 4D Nucleofector Kit X, Lonza). 16.6 µl of the RNP complexes were added to the cells as well as 4 µl of the single stranded HR template (10 µM). Cells were transferred to an electroporation cuvette and electroporation was done in a 4D Nucleofector (Lonza) with the recommended pulse program DS-135. Electroporated cells were transferred to a 6 well plate. NHEJ inhibitor Nu7026 (final concentration 20 µM) and HR enhancer TrichostatinA (final concentration 0.1 µM) were added to the cells 30 minutes after electroporation. Cells were sorted for successful transfection 24 hours post electroporation by the ATTO550 labeled tracer RNA on an Aria III cell sorter (Becton Dickinson). Sorted cells were seeded for single cell selection and screened as described above.

## 4.5 Molecular biological methods

### 4.5.1 RNA isolation from cell culture and murine and human gastric tissue

RNA was isolated from cells or murine gastric tissue pieces to analyze gene expression of RNF43 as well as target genes of different signaling pathways.

For RNA isolation from cells, the GenElute Mammalian Total RNA Miniprep Kit (Sigma) was used according to manufacturer's instructions. Remaining DNA was digested using DNA-free DNA removal kit (Invitrogen) and RNA concentration was measured using a Nanodrop (Thermo Fisher).

For RNA isolation from gastric tissue, pieces had to be homogenized first. Thus, tissue pieces were transferred to a precellys tube containing ceramic beads. Homogenization solution from Maxwell LEV simply RNA Kit (Promega) or lysis buffer from GenElute Mammalian Total RNA Miniprep Kit (Sigma) were added, tubes were placed into a precellys homogenizer (Bertin Instruments) and were shaken twice for 15 seconds at 5000 rpm. Samples were then centrifuged, and supernatant was transferred

to a new tube. RNA isolation with Maxwell LEV simply RNA Kit (Promega) was conducted as described in manufacturer's instructions, and RNA was eluted in 60 µl $dH_2O$. For isolation with the Sigma Kit, DNA digestion was performed on column. For this, only half of the recommended wash buffer 1 was passed through the column. Then, DNAse I (Qiagen) was applied to the column according to manufacturer's instructions. After this, the Sigma isolation protocol was continued with the second half of wash buffer 1, a washing step with wash buffer 2 and elution of the RNA in 30 µl of nuclease-free $H_2O$. RNA concentration was measured with a Nanodrop.

### 4.5.2 Reverse Transcription

Reverse transcription from RNA into coding DNA (cDNA) was performed by using Moloney Murine Leukemia Virus (M-MLV) reverse transcriptase (Promega). For this, 1 µg RNA, 150 ng of random primers and nuclease free $H_2O$ were mixed to a final volume of 14 µl and incubated at 70 °C for 5 minutes, and on ice for another 5 minutes. A master mix was prepared containing 5 µl reverse transcription buffer, 1 µl M-MLV reverse transcriptase (200 units), 1.25 µl of dNTP mix (10 mM) and nuclease free $H_2O$ to a final volume of 25 µl. 11 µl of master mix were added to each sample and incubated for 10 minutes at room temperature, 50 minutes at 50 °C and 15 minutes at 70 °C. cDNA was then stored at – 20 °C. To determine the amount of contaminating DNA in the RNA sample, a negative control without reverse transcriptase was included in the experiment.

### 4.5.3 Quantitative real time (RT) PCR

Expression of genes was analyzed by measuring abundance of corresponding cDNA by quantitative RT PCR. GoTaq qPCR master mix (Promega) contains the dye SYBR Green I, which binds double stranded DNA. These complexes then emit fluorescent light that can be detected in a qPCR machine. When sufficient amount of cDNA is amplified, fluorescent light passes a detection threshold. The PCR cycle, at which this occurs, is determined as $C_t$ value.

For RT-qPCR, cDNA samples were diluted 1:10 (RNA derived from cell culture) or 1:5 (RNA derived from tissue) in nuclease-free $H_2O$, and 4 µl were loaded in each well of a 384 well plate (white wells,

black frame, 4titude). A mastermix was prepared containing 5 µl of GoTaq qPCR master mix (Promega) and 0.5 µl of specific primers (10 µM, **Table 20** and **Table 21**) per sample and added to the wells. The plate was sealed with an optically clear adhesive film (4titude) to avoid evaporation and centrifuged briefly to collect PCR reaction mix at the bottom of the wells. Samples were then placed into a Realtime Cycler CFX384 (Biorad) and the qPCR program was started (**Table 22**).

For analysis, Bio-Rad CFX Manager program was used. Gene expression was normalized to the house keeping gene *GAPDH* and $\Delta C_t$ value was calculated as follows:

$$\Delta C_T = 2^{(-1)*(C_{T\ gene\ of\ interest} - C_{T\ GAPDH})}$$

Furthermore, melting curves were checked to ensure specificity of the PCR reaction.

**Table 20: Murine primer sequences for RT-qPCR.**

| **Primer** | ***Forward*** | ***Reverse*** |
|---|---|---|
| *Axin2* | CAGGAGGATGCTGAAGGCTCAAAGC | CTCAAAAACTGCTCCGCAGGCAAAT |
| *Cxcl1* | TGCACCCAAACCGAAGTCAT | TTGTCAGAAGCCAGCGTTCAC |
| *Cxcl10* | AAGTGCTGCCGTCATTTTCT | CCTATGGCCCTCATTCTCAC |
| *Cxcl13* | ATATGTGTGAATCCTCGTGCCA | GGGAGTTGAAGACAGACTTTTGC |
| *Gapdh* | GCCTTCTCCATGGTGGTGAA | GCACAGTCAAGGCCGAGAA |
| *Ifnγ* | TCAAGTGGCATAGATGTGGAAGAA | TGGCTCTGCAGGATTTTCATG |
| *Il-17* | GCTCCAGAAGGCCCTCAGA | AGCTTTCCCTCCGCATTGA |
| *Lgr5* | GGGAGCGTTCACGGGCCTTC | GGTTGGCATCTAGGCGCAGGG |
| *Rnf43* | GGGGCAAACTATGACGTG | CTGCTGAAGAGGATCCGGTC |
| *Sox2* | CATGGGCTCTGTGGTCAAGT | CGGGGAGGTACATGCTGATC |
| *Tnfa* | CGAATGGGTTGTACCTTGTC | CGGACTCCGCAAAGTCTAAG |

**Table 21: Human primer sequences for RT-qPCR.**

| Primer | *Forward* | *Reverse* |
|---|---|---|
| *GAPDH* | GAAGGTGAAGGTCGGAGT | GAAGATGGTGATGGGATTTC |
| *RNF43* | GAGTGTGCTCCAGATGTGTT | AGTCCTCTTCCAGTCCTT |

**Table 22: PCR program for RT-qPCR.**

| qPCR step | Temperature [°C] | duration [mm:ss] |
|---|---|---|
| Pre-Incubation | 95 | 05:00 |
| Amplification<br><br>40 cycles | 95 | 00:10 |
| | 60 | 00:30 |
| | Plate read | |
| Melting curve | 60 | 00:31 |
| Melting curves 70 cycles | 60<br><br>+ 0.5 °C/ cycle<br><br>Ramp 0.5 °C /s | 00:05 |
| | Plate read | |
| Hold | 12 | ∞ |

### 4.5.4 DNA extraction from human gastric tissue

DNA was isolated from human gastric biopsies obtained for organoid culture to screen for mutations and *RNF43* single nucleotide polymorphisms (SNPs). For DNA isolation, QuickDNA Miniprep Plus Kit

(Zymoresearch) was used according to manufacturer's instructions. The DNA was eluted in 50 µl nuclease-free $H_2O$. DNA concentration was measured using a Nanodrop and 2.5 µl of DNA were used to perform exon PCRs (described in 4.4.3). PCR products were cleaned up as described before and sent for Sanger sequencing to Eurofins. Sequence analysis was performed using CLC Main Workbench program.

### 4.5.5 DNA extraction from FFPE embedded tissue

In order to analyze *RNF43* mutations in human gastric biopsies, DNA was extracted for next-generation sequencing.

For this, hematoxylin-eosin (H&E) stainings were analyzed to locate the region containing the lesion of interest. 10 µm tissue sections were cut with a rotary microtome (Leica) and samples were picked up with forceps and placed into a 1.5 ml reaction tube. Dependent on the size of the tissue, 5 – 20 tissue sections were collected for DNA extraction. DNA extraction was performed with a GeneRead DNA FFPE Kit (Qiagen) according to manufacturer's instructions and DNA was eluted in 50 µl nuclease-free $H_2O$. Next-generation sequencing was performed at the Institute of Pathology (Technical University Munich). Mutations found in the samples were confirmed by Sanger sequencing. For this, PCR of the corresponding exon was performed (see 4.4.3). PCR products were cleaned up and sent to Eurofins.

## 4.6 Immunofluorescence

Immunofluorescence stainings were used to analyze RNF43 expression and localization as well as co-localization with γH2AX in gastric cancer cell lines.

$1.5*10^5$ cells were seeded on a cover slip in a 12 well plate and allowed to attach overnight. For co-localization experiments, cells were treated with irradiation prior to seeding. For staining, medium was removed, and cells were placed on ice and washed with PBS. Cells were fixed with cold methanol/acetone (1:1) for 15 minutes on ice. Wells were then washed three times with PBS at room temperature and cells were permeabilized using IF blocking buffer (3 % BSA, 1 % Triton X-100, 1 %

Saponine in PBS) for 15 minutes at room temperature. Cover slips were washed three times in IF wash solution 1 (3 % BSA, 1 % Saponine in PBS) and incubated overnight in primary antibody diluted in IF wash solution 1 at 4 °C in a humidified chamber. To remove antibody excess, cover slips were again washed with IF wash solution 1 and incubated with secondary antibody for 1 hour at room temperature. Three wash steps in wash solution 2 (1 % Saponine in PBS) were applied and cover slips were dried and mounted on to a microscopic slide using 1 drop of Vectashield containing DAPI (Vectorlabs). Staining was analyzed by confocal microscopy using an Olympus Fluoview FV10i microscope.

## 4.7 Histological methods

### 4.7.1 Embedding of tissue pieces

Tissue pieces were placed into embedding cassettes and incubated in 3.5 - 3.7 % formaldehyde for 24 to 48 hours at 4 °C. After fixation, cassettes were washed with PBS and afterwards dehydrated and embedded in paraffin in the Institute of Pathology (TUM). 4 µm tissue sections were cut using a rotary microtome (Leica) and mounted on Superfrost adhesion slides (Thermo Scientific).

### 4.7.2 Hematoxylin eosin staining

In order to analyze epithelial architecture, tissue sections were stained with hematoxylin and eosin. For deparaffinization and rehydration, slides were placed in a hybridization oven for 20 minutes at 60 °C and subsequently incubated in Roticlear (Roth) three times for 10 minutes, twice 10 minutes in absolute ethanol and 5 minutes each in 90 %, 70 % and 50 % ethanol. After a short incubation in $dH_2O$, slides were stained with hematoxylin solution (Roth) for 6 minutes. pH switch and thereby color change was induced by rinsing the slides in tap water. Next, tissue sections were incubated in 1 % eosin solution (Morphisto) for 6 minutes and again washed in tap water. For dehydration, samples were incubated 5 minutes each in 50 %, 70 %, 90 %, twice in absolute ethanol and finally 3 times for 10 minutes in Roticlear. Slides were mounted with Roti-Mount (Roth) and allowed to dry overnight.

### 4.7.3 Periodic acid Schiff (PAS) staining

Mucus-producing cells were identified by PAS staining. Samples were deparaffinized and rehydrated as described in 4.7.2. Next, slides were oxidized in 1 % periodic acid for 5 minutes. After rinsing with $dH_2O$, slides were incubated in Schiff reagent for 15 minutes. Samples were then washed in lukewarm tap water for 5 minutes, counterstained with hematoxylin for 1 minute and washed again in tap water. Slides were dehydrated and mounted as described in 4.7.2.

### 4.7.4 Immunohistochemistry

Murine and human gastric tissue samples were stained with different markers in order to analyze inflammation, proliferation and DNA damage response. A list of the antibodies used can be found in **Table 23**. Slides were deparaffinized and rehydrated as described before. After washing in $dH_2O$, heat induced antigen retrieval was performed using 10 mM sodium citrate (pH 6) or 1 mM EDTA (pH 8 for pSTAT3 staining). Slides were boiled in a pressure cooker for 10 minutes and allowed to cool down for 30 minutes. Tissue intrinsic peroxidase was blocked by incubating the slides with 3 % $H_2O_2$ for 10 minutes. Next, slides were washed with $dH_2O$ and TBS-T and blocked with 5 % goat serum diluted in TBS-T in order to reduce background. Primary antibodies were diluted in Signal Stain Antibody diluent (Cell Signaling) and incubated over night at 4 °C or 1 hour at room temperature for Mucin 2.

Slides were then washed four times with TBS-T and incubated with HRP-labeled secondary antibody for 1 hour at room temperature. Next, slides were again washed four times with TBS-T and bound antibodies were detected using diaminobenzidine (DAB). For this, slides were incubated with Signal Stain DAB Substrate Kit (Cell signaling) for 7 minutes at room temperature. Samples were then washed with $dH_2O$ and counterstained with hematoxylin for 5 minutes. Dehydration was performed as described in 4.7.2 and slides were mounted with Roti-Mount.

**Table 23: Antibodies used for immunohistochemistry.**

| Target | Clone | Company | Reactivity | Dilution |
|---|---|---|---|---|
| ALDH1 | D9Q8E | Cell Signaling | H | 1:200 |
| Non-phospho β-catenin (Ser45) | D2U8Y | Cell Signaling | H, M | 1:1000 |
| CD3 | SP7 | Thermo Fisher | H, M | 1:150 |
| CD44 | E7K2Y | Cell Signaling | H, M | 1:150 |
| Cleaved caspase 3 (Asp175) | 9661 | Cell Signaling | H, M | 1:300 |
| Ki67 | D3B5 | Cell Signaling | M | 1:400 |
| Ki67 | D2H10 | Cell Signaling | H | 1:400 |
| MUC2 | Lum 2.3 | (Carlstedt 1995) | M | 1:3000 |
| p-STAT3 (Tyr705) | D3A7 | Cell Signaling | H, M | 1:200 |
| p65 | D14E12 | Cell Signaling | H, M | 1:800 |
| RNF43 | HPA008079 | Invitrogen (ATLAS) | H | 1:1000 |
| SOX2 | C70B1 | Cell Signaling | M | 1:250 |
| SOX2 | D6D9 | Cell Signaling | H | 1:300 |
| Vimentin | D21H3 | Cell Signaling | H, M | 1:100 |
| γH2AX | ab81299 | Abcam | H, M | 1:5000 |

### 4.7.1 Staining analysis

Stained slides were scanned with a Virtual Slide Microscope (Olympus) and analyzed with VS-Desktop (Olympus) software. For each sample, 5 high power fields were counted, and the area of the analyzed field was determined. For Vimentin a score was established as follows: 0 indicates less than 10 %

positive cells per HPF, 1 less than 25 % positive cells, 2 less than 50 % and 3 more than 50 % positive cells. The score for SOX2, CD44 and ALDH1 was determined similarly: 0 equals less than 25 % positive cells per HPF, 1 less than 50 %, 2 less than 75 % and 3 more than 75 % positive cells.

## 4.8 Xenografts

A xenograft tumor model was used to investigate the impact of RNF43 on the tumorigenic potential of gastric cells *in vivo*. To allow the human gastric cancer cells to grow in a murine environment and to prevent tumor rejection, homozygous athymic nude mice (Crl:NU(NCr)-*Foxn1*$^{nu}$ mice, Charles River) were used in these experiments. These mice lack a thymus and therefore cannot develop functional T cells. Additional treatment with full body irradiation prior to injection, which temporarily abolishes the remaining immune system, allows the gastric cancer cells to grow to xenograft tumors in this model.

### 4.8.1 Establishment and analysis of xenograft tumors

Female athymic nude mice were irradiated with 4.5 Gγ 24 hours prior to cell injection. AGS and MKN45 shctrl and shRNF43 cells were expanded and 5*10$^6$ cells were injected per mouse per cell line. To facilitate anchorage of the cells, Cultrex Basement Membrane Extract (Trevigen) was added to the cells resuspended in Opti-MEM to a final concentration of 7 mg/ml in a final injection volume of 200 µl per mouse. Cells were placed on ice and injected subcutaneously into the flanks of the mice using a Sub Q injection needle (26 G, Becton Dickinson). To reduce mouse numbers and to be able to directly compare tumor growth, control and RNF43 knock down cells were simultaneously injected into the right and left flank, respectively. Tumor growth was monitored weekly and experiments were terminated when mice had reached end point criteria such as low body score index or tumor size above a diameter of 1.5 cm. Tumors were then resected completely and weighed. Part of the tumor was snap frozen in liquid nitrogen for DNA or RNA analysis and the rest was placed into an embedding cassette, fixed in formaldehyde and embedded as described in 3.6.1. Tissue sections (4 µm) were cut

and samples were stained with HE and by immunohistochemistry to analyze expression of gastric stem cell markers and proliferation. A list of the antibodies used can be found in **Table 23**.

### 4.8.2 Chemotherapeutic treatment

To assess the influence of RNF43 on resistance to chemotherapy in vivo, we used the established xenograft model in combination with chemotherapeutic treatment. Since recovery rate of tumors derived from MKN45 cells was very high and tumors grew rapidly, this cell line was chosen for chemotherapy experiments.

For these experiments, MKN45 shctrl and shRNF43 cells were injected as described above. Tumor growth was observed, measured with a caliper and tumor volume was calculated as follows:

$$\text{Volume} = (\text{length} * \text{width} * \text{height})/2$$

When tumors had reached a size of 40 – 70 $mm^3$, chemotherapeutic treatment was started. Mice were injected intraperitoneal with 10 mg/kg cisplatin or 50 mg/kg 5-fluorouracil twice a week and tumor volume was determined over time. The experiment was finished when tumors reached a volume of 600 $mm^3$ or when mice scored end point criteria such as low body score index. Tumors were resected, weighed and prepared for RNA isolation and paraffin embedding as described above.

## 4.9 Rnf43 loss of function mouse models

Two mouse lines were used in this study. In *Rnf43*$^{\Delta Exon8}$ mice, Rnf43 loss of function was induced by a deletion of 57 bp inside Exon 8 of the genomic DNA which completely abrogates the functional domain. In Rnf43$^{H292R/H295R}$ mice, the structure of the zinc finger domain is disrupted by two point mutations.

### 4.9.1 Genotyping

*Rnf43*$^{\Delta Exon8}$ and Rnf43$^{H292R/H295R}$ mice were bred homozygously in an FVB/N background under SPF conditions. For genotyping, ears of the mice were punched, and ear pieces were collected in 250 µl tail lysis buffer (**Table 24**) and 5 µl proteinase K. Tubes were incubated overnight at 56 °C while shaking

and proteinase K was subsequently heat inactivated at 95 °C for 10 minutes. For higher purity of the DNA, it was precipitated by adding 700 µl of isopropanol and centrifugation for 10 minutes at 13,000 rpm. Supernatant was discarded and DNA was washed with 500 µl of 70 % ethanol and centrifuged for 5 minutes at 13,000 rpm. Supernatant was discarded and tubes were dried for 30 – 60 minutes. DNA was resuspended in 200 µl nuclease-free $H_2O$ and allowed to completely dissolve overnight at 4 °C. Genotyping was performed by amplifying a 318 bp sequence containing Exon 8. Primers for this PCR are listed in **Table 25**, master mix composition and PCR cycler program can be found in **Table 26** and **Table 27**, respectively. For *Rnf43*$^{\Delta Exon8}$ mice, the PCR product was directly loaded on a 2 % agarose gel, since the 57 bp deletion could directly be observed by gel electrophoresis. Rnf43$^{H292R/H295R}$ mice carried a third but silent mutation that allowed cleavage of the PCR product by the restriction enzyme BsmAI (NEB). Following PCR, 0.5 µl (5 units) of restriction enzyme were added to the sample and incubated at 55 °C for 2 hours. Samples were then loaded on an agarose gel and cleavage of the PCR product into two sequences of 130 bp and 188 bp, respectively was observed.

**Table 24: Composition of tail lysis buffer.**

| Component | Final concentration |
|---|---|
| KCl | 50 mM |
| TRIS pH 8.3 | 10 mM |
| Igepal | 0.45 % |
| Tween20 | 0.45 % |

**Table 25: Genotyping primer sequence for Exon 8 of murine Rnf43.**

| Primer | *Forward* | *Reverse* |
|---|---|---|
| *Rnf43* | CCAAACTTGCCCAGAGTCAG | CATCCATCTGTACGCACACAG |

**Table 26: Composition of the mastermix for genotyping of Rnf43 mouse models.**

| Reagent | Volume |
|---|---|
| Go Taq Green mastermix (2X) (Promega) | 12.5 µl |
| Primers forward/reverse (10 µM) | 1.25 µl each |
| Template DNA | 2.5 µl |
| $dH_2O$ | To a final volume of 25 µl |

**Table 27: PCR program for mouse genotyping.**

| PCR step | Temperature | Time | |
|---|---|---|---|
| Initial denaturation | 95 °C | 3 min | |
| Denaturation | 95 °C | 30 s | 35 cycles |
| Annealing | 56 °C | 30 s | |
| Elongation | 72 °C | 30 s | |
| Final enlongation | 72 °C | 5 min | |
| Final hold | 12 °C | ∞ | |

### 4.9.2 Infection with *H. pylori*

*H. pylori* was cultured as in 4.2.10. For infection, bacteria were collected in BHI, optical density was measured and number of bacteria per ml was calculated. Mice were infected twice with $2*10^8$ bacteria diluted in 200 µl BHI by oral gavage. Mice were scored weekly and experiment was terminated after 3 months or 6 months of infection.

### 4.9.3 Analysis of gastric tissue

Mice were sacrificed by cervical dislocation and organs were collected for analysis. The stomach was separated from esophagus, intestine and forestomach and opened along the greater curvature.

Lateral areas were snap frozen in liquid nitrogen for RNA isolation or collected in BHI containing 20 % FCS for determination of bacterial load. The central area of the lesser curvature was used for paraffin embedding. Thus, tissue was placed on a little wooden piece to prevent shrinking during dehydration and fixed in formaldehyde.

### 4.9.4 Determination of bacterial load

To determine bacterial load after *H. pylori* infection, a stomach piece was weighed and placed into 1 ml of BHI 20 % FCS. Tissue was minced using a homogenizer (T10 Ultra-Turrax, IKA). Serial dilutions (1:10, 1:100, and 1:1000) were plated on WC plates containing DENT supplement (Oxoid) (**Table 3**) and additional antibiotics (**Table 28**) and incubated at 37 °C, 10 % $CO_2$ 5 % $O_2$ for 4 – 5 days. *H. pylori* colonies were counted and number of bacteria per mg stomach was calculated.

**Table 28: List of additional antibiotics for determination of bacterial load.**

| Component | Final concentration |
|---|---|
| Bacitracin | 200 µg/mL |
| Nalidixicacid | 10 µg/mL |
| Polymyxin B | 3 µg/mL |

## 4.10 Organoid culture

Organoid culture is a recently developed 3D culture technique that allows long term culture of primary cells. Crypts containing stem cells can be isolated from various tissues and grown to mini-organs in growth factor enriched medium and an extracellular matrix like structure. In this project, gastric glands were isolated from human gastric biopsies as well as murine stomach and grown into organoids following a protocol recently published [234].

### 4.10.1 Establishment of gastric organoids from murine and human gastric tissue

For isolation of gastric glands, tissue was cut into small pieces and washed with cold chelation buffer (**Table 29**, pH 7.0) 5 times by pipetting up and down. Tissue was then digested by adding EDTA to a final concentration of 10 mM and incubated at 4 °C for 30 minutes for murine tissue and 10 minutes at room temperature for human tissue while shaking. Chelation buffer and EDTA were removed and tissue was transferred to a 10 cm petri dish. Glands were released from the tissue by applying physical force with a glass slide, taken up in basal medium (Advanced DMEM/F12 supplemented with 1X HEPES, 1X Glutamax and 1 % Penicillin/Streptomycin), and transferred to a 15 ml tube. Large tissue pieces were allowed to settle and supernatant containing the glands was transferred to a new tube. Number of glands was determined, and glands were collected by centrifugation for 5 minutes at 200 g and 4 °C. Then, glands were taken up in 50 µl Matrigel, a basement membrane-like matrix, per well and seeded at a density of around 500 glands per well in a 24 well plate. Matrigel drops were allowed to solidify in the incubator for 10 minutes and 500 µl organoid medium (**Table 30**) supplemented with Rho kinase inhibitor Y27632 (10 µM) were added per well. Medium was exchanged twice a week. Remaining tissue pieces were snap frozen for isolation of RNA and DNA.

**Table 29: Composition of chelation buffer.**

| Component | Final concentration |
|---|---|
| $Na_2HPO_4$ | 5.6 mM |
| $KH_2PO_4$ | 8.0 mM |
| NaCl | 96.2 mM |
| KCl | 1.6 mM |
| Sucrose | 43.4 mM |
| D-sorbitol | 54.9 mM |
| DTT | 0.5 mM |

**Table 30: Composition of culture medium for human and murine gastric organoids.**

| Component | Final concentration |
|---|---|
| Advanced DMEM/F12 | 50 % |
| Wnt-, R-Spondin- and Noggin conditioned medium (L-WRN) | 50 % |
| HEPES (Gibco) | 1X |
| Glutamax (Gibco) | 1X |
| Penicillin/Streptomycin (Gibco) | 1X |
| B27 Supplement | 1X |
| N2 Supplement | 1X |
| Nicotinamide | 20 mM |
| N-acetyl-cysteine | 2 mM |
| P38 inhibitor | 20 µM |
| FGF-10 | 200 ng/ml |
| TGFβ inhibitor | 2 µM |
| Gastrin | 1 nM |
| EGF | 50 ng/ml |

### 4.10.2 Treatment with chemotherapy

In order to assess sensitivity to chemotherapy, organoids were treated with cisplatin or 5-fluorouracil. 200 – 300 isolated gastric glands were seeded in 25 µl Matrigel in a 48 well plate and allowed to grow to organoids for 4 – 5 days. Cisplatin (10 µg/ml) or 5-FU (2 µg/ml) were added to the organoids and incubated for 5 days. Organoid viability was measured using Cell Titer Glo 3D (Promega), which contains a luciferase that induces luminescence upon the presence of ATP. This assay therefore directly measures viable cells in 3D culture. For measurement, medium was removed from the

organoids and basal medium and Cell Titer Glo reagent were added 1:1 to the culture. The plate was then incubated for 10 minutes at room temperature while shaking and without agitation for another 20 minutes. 20 µl of the supernatant were transferred into a 96 well plate (black walls, clear bottom, Corning) and luminescence was measured in a SpectraMax plate reader (Molecular Devices). Signal from treated organoids was normalized to untreated controls.

### 4.11 Statistical analysis

Results are presented as mean ± SD of three independent experiments for *in vitro* experiments and as dot plots with medians for *in vivo* experiments, unless indicated otherwise. Statistical analysis of normally distributed data was performed using t test or One-way ANOVA with Dunnett's multiple comparison test. If data was not normally distributed, Mann-Whitney *U*-Test was used. Statistical significance was established when $p \leq 0.05$.

# 5 Results

## 5.1 Depletion of RNF43 in gastric cancer cell lines

In this project, gastric cancer cell lines AGS and MKN45 were used to analyze the impact of RNF43 on their tumorigenic potential and its role during DDR. According to COSMIC database, no mutations were reported in *RNF43* in those cell lines (Cosmic ID COSS906790 and COSS925340, respectively). To confirm this in the cell lines used in house, DNA was extracted from AGS and MKN45 cells and exons 2 – 9 were amplified. NGS was performed and analyzed at the Department of Internal Medicine II (Technical University Munich). MKN45 cells did not show any mutations or SNPs in *RNF43*. In AGS cells, two point mutations, I47V and R343H were detected. These mutations have been described to be SNPs that commonly occur. Therefore, AGS cells also express wild type RNF43 as previously published.

### 5.1.1 Lentiviral RNF43 knock down in MKN45 cells

To assess the endogenous function of RNF43, lentiviral knock down was performed in MKN45 cells. RT-qPCR was used to analyze to what degree RNF43 expression was reduced in these cells. Lentiviral transduction of MKN45 cells led to a 60 % reduction of RNF43 expression (**Figure 7A**).

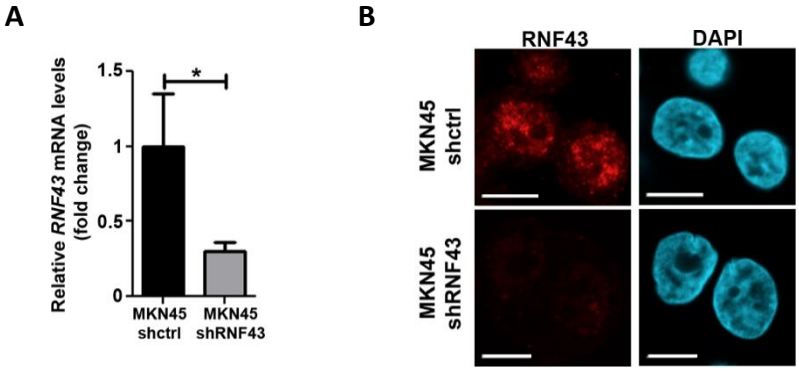


**Figure 7: RNF43 was successfully knocked down in MKN45 cells.** A) *RNF43* mRNA levels after lentiviral knock down measured by qRT-PCR and normalized to shcontrol (shctrl) cells. Bars represent mean ± SD from three independent experiments. Student's t-test. *P<0.05. B) Confocal immunofluorescence imaging of MKN45 cells showing RNF43 (red) and nuclei (blue). Scale bars indicate 10 µm. Adapted and reprinted from [235] with permission from Elsevier Inc.

Reduction of RNF43 was confirmed on protein level by immunofluorescence staining and confocal microscopy. While RNF43 was detected in the nucleus of MKN45 shcontrol (shctrl) cells, it could barely

be detected in shRNF43 cells (**Figure 7B**), indicating that RNF43 was successfully depleted from MKN45 cells.

### 5.1.2 RNF43 knock out in AGS cells via CRISPR/Cas9 technology

CRISPR/Cas9 system was used to induce a deletion in the genomic sequence of RNF43 and therefore deplete RNF43 function. Two out of 10 screened colonies showed a homozygous 4 bp deletion inside exon 6 leading to a changed amino acid sequence at Asp196 and a premature stop codon (D196fs*5) (**Figure 8A**). To verify loss of the wild type protein, confocal immunofluorescence was performed. RNF43 could be detected in the nucleus of wild type AGS cells, whereas no protein was detected in AGS$^{D196fs}$ cells (**Figure 8B**).

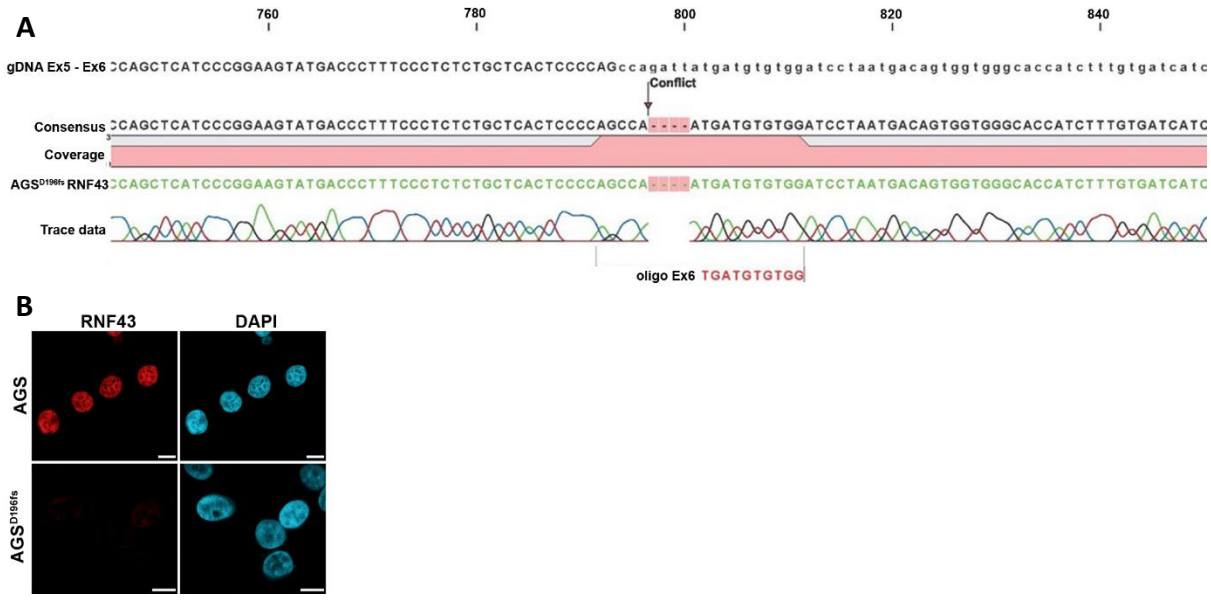


**Figure 8: RNF43 was knocked out in AGS cells via CRISPR/Cas9.** A) Sanger sequencing of *RNF43* exon 6 amplified from genomic DNA from AGS$^{D196fs}$ cells aligned to *RNF43* wild type sequence. B) Confocal immunofluorescence imaging of AGS cells. Nuclei are depicted in blue, RNF43 in red. Scale bars indicate 10 µm. Adapted and reprinted from [235] with permission from Elsevier Inc.

Since CRIPSR/Cas9 delivery by plasmid could lead to prolonged presence of the protein inside the cells, the risk of targeting other sites in the genome is increased. Therefore, off targets had to be analyzed for their genomic integrity in order to exclude effects of additionally induced mutations. To select relevant off target sites for further analysis, several parameters were considered. First, only sites

inside coding sequences were selected for further investigation. Furthermore, genes that were either located on the Y chromosome or not expressed in the adult stomach were excluded from analysis. This way, three potential off targets were selected for further investigation (**Table 31**), all of which have been reported to be expressed in the adult stomach.

**Table 31: List of potential off targets of the approach selected for verification**

| Gene | Location | Off target score | Expressed in the stomach |
|---|---|---|---|
| SLX4 structure-specific endonuclease subunit (*SLX4*) | chr16:+3650931 | 0.2 | Yes (GTEx Portal) |
| Homo sapiens WW and C2 domain containing 2 (*WWC2*) | chr4:-184236855 | 0.1 | Yes (GTEx Portal) |
| Homo sapiens leukocyte receptor tyrosine kinase (*LTK*), transcript variant 2 | chr15:+41799772 | 0.0 | Yes (GTEx Portal) |

To analyze whether these genes were altered, off target sites were amplified and sequenced. Sanger sequencing showed that no mutations were induced in the selected off targets (**Figure 9**). Taken together, CRISPR/Cas9 technique was successfully used to specifically induce a deletion in the genomic sequence of RNF43 in AGS cells thereby leading to a loss of the RING domain.

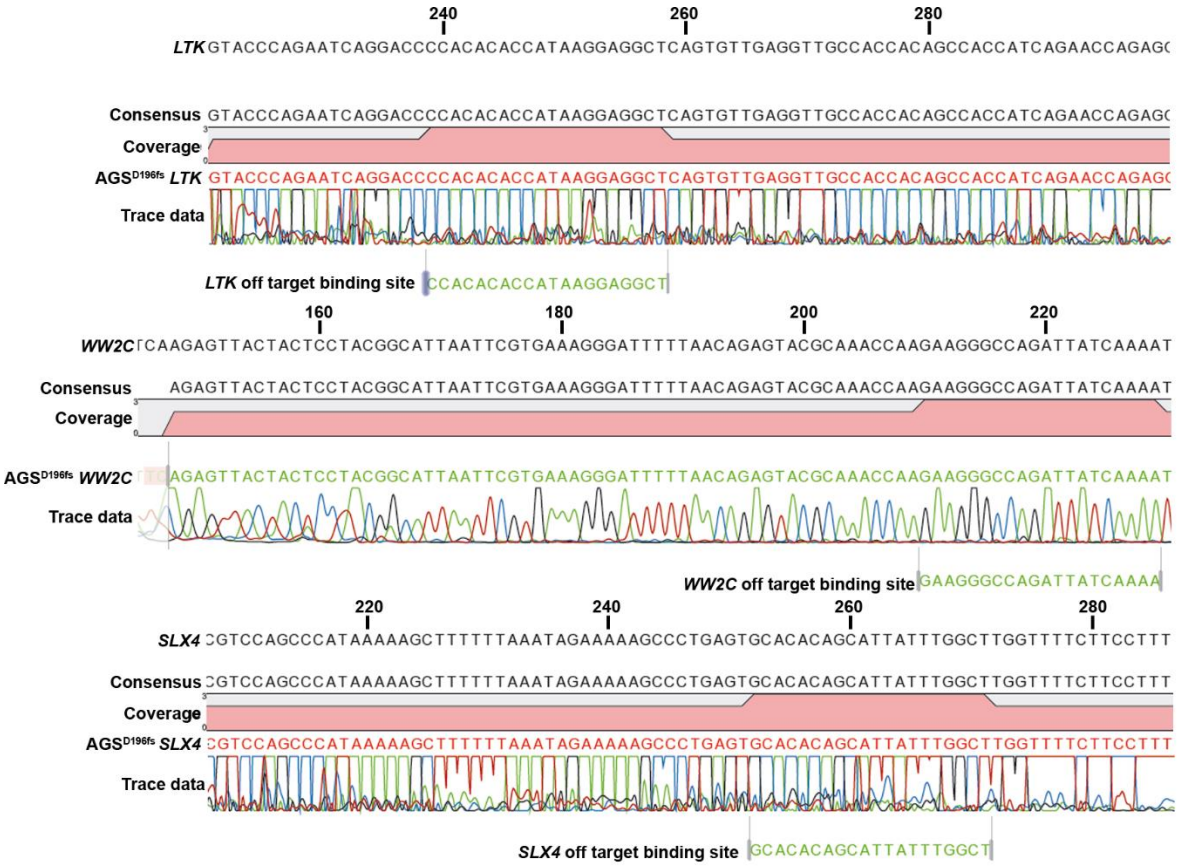


**Figure 9: Potential off targets of the CRISPR/Cas9 approach were not altered in AGS$^{D196fs}$ cells.** Sanger sequencing of the off target binding sites of *LTK*, *WW2C* and *SLX4* amplified from genomic DNA isolated from AGS$^{D196fs}$ cells.

## 5.2 Endogenous function of RNF43 in the stomach

### 5.2.1 RNF43 reduces the tumorigenic potential of gastric cancer cells *in vitro*

The proliferative and invasive capacity of gastric cancer cells were investigated to determine whether RNF43 altered their tumorigenic potential *in vitro*. Proliferation assays showed that depletion of RNF43 in MKN45 shRNF43 cells as well as in AGS$^{D196fs}$ cells increased their proliferative capacity (**Figure 10A, B**). This was further confirmed in MKN45 shRNF43 cells by soft agar assays. Single cell colonies grown independently of anchorage were bigger in RNF43 depleted cells compared to control cells, as observed by microscopy and MTT measurement (**Figure 10C**). Additionally, cell invasion through an extracellular matrix like structure along an FCS gradient was investigated in MKN45 cells. The number of invaded cells was enhanced in MKN45 shRNF43 cells compared to shctrl cells, indicating that RNF43 negatively regulates the invasive capacity of gastric cancer cells (**Figure 10D**). These findings confirmed

the results obtained using AGS and MKN45 cells, where the expression of RNF43 was knocked down using another lentivirus [236].

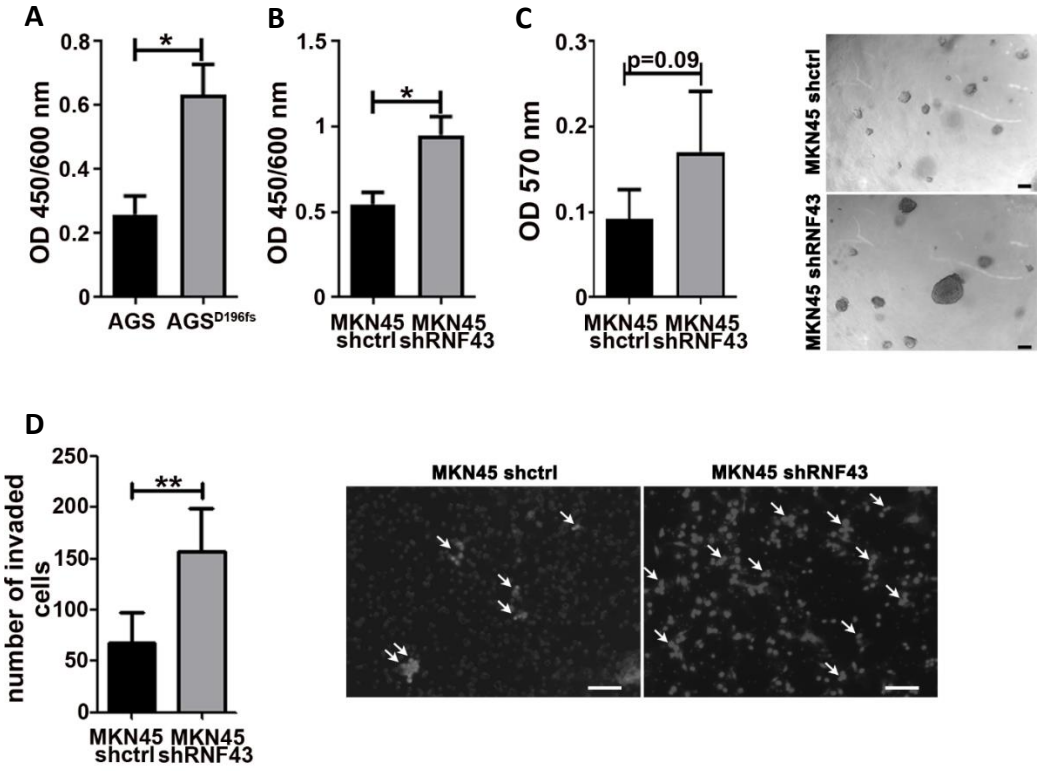


**Figure 10: RNF43 depletion increases the tumorigenic potential of gastric cancer cells *in vitro*.** A, B) 2500 AGS and AGS$^{D196fs}$ (A) or MKN45 shctrl and shRNF43 (B) cells per well were seeded in quadruplicates and allowed to proliferate for 5 days. Cell viability was determined by adding CCK-8 (Sigma) to the cells and measuring OD 450/600 nm with a photometer. C) 1000 MKN45 shctrl and shRNF43 cells were seeded in triplicates in 0.3 % soft agar and allowed to grow for 14 days. Cell viability was measured by adding MTT and assessing OD 570 nm in a photometer. Pictures were taken at 10 x magnification. Scale bars indicate 100 µm. D) $10^5$ MKN45 shctrl and shRNF43 cells were seeded in transwells in duplicates and allowed to migrate along an FCS gradient through matrigel and collagen for 24 h. Cells were fixed, stained with DAPI and invaded cells were counted. Arrows indicate invaded cells. Scale bars indicate 100 µm. Bars represent mean ± SD from three (A, B, D) or four (C) independent experiments. Student's t-test. *P<0.05, **P<0.01. Adapted and reprinted from [237] with permission from Oxford academic.

### 5.2.2 RNF43 depletion increases tumor growth in a xenograft model

Since increased tumorigenic potential was observed for AGS shRNF43 and MKN45 shRNF43 cells *in vitro*, we further investigated the tumorigenic capacity of these cells in a xenograft model. For these experiments, lentiviral knock down cells generated during my Master thesis were injected into immunocompromised *Foxn1$^{nu}$ mice*. When mice were sacrificed, it could be observed macroscopically that MKN45 shRNF43 cells grew to bigger tumors compared to shctrl cells. Furthermore, tumor weight

was significantly increased in RNF43 depleted tumors (**Figure 11A**). A similar trend could be observed for RNF43 depleted AGS cells. However, due to low overall recovery rate of tumors, this was not significant (**Figure 11B**). Taken together, these results indicate that loss of RNF43 increases the tumorigenic potential of gastric cancer cells *in vivo*.

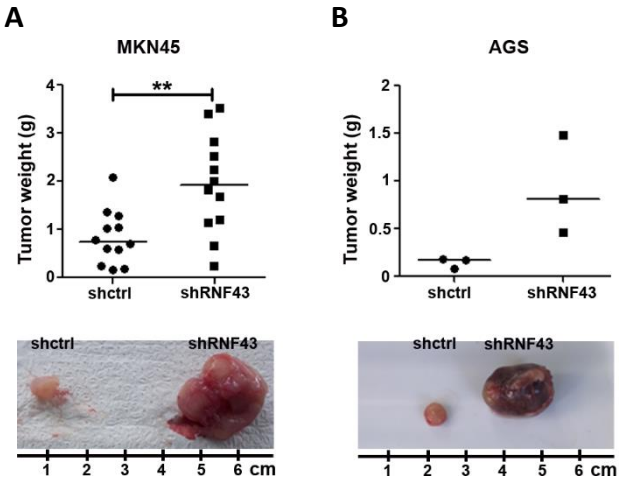


**Figure 11: RNF43 depletion increases tumor growth in a xenograft model.** $5*10^6$ MKN45 (A) or AGS (B) cells were injected subcutaneously into the flanks of Foxn1$^{nu}$ mice. Tumors were allowed to grow for 2 - 6 weeks, resected and weighed. Each dot represents a tumor; horizontal lines represent medians. Mann-Whitney U-Test. **P<0.01. Adapted and reprinted from [237] with permission from Oxford academic.

### 5.2.3 RNF43 negatively regulates the expression of stem cell markers in xenograft tumors

Recently, RNF43 has been described to negatively regulate stemness in gastric cells. Overexpression of the protein was shown to reduce Wnt activity as well as tumorigenic potential of these cells. To characterize whether RNF43 loss had a similar effect in our xenograft model, expression of gastric stem cell markers as well as EMT markers and Wnt signaling activity were analyzed in MKN45 cells. Loss of RNF43 expression led to a significantly higher expression of the gastric stem cell marker SOX2 as well as of the gastric cancer stem cell markers CD44 and ALDH1 (**Figure 12A**, **B** and **C**, respectively). Furthermore, expression of the EMT marker Vimentin was increased in MKN45 shRNF43 cells compared to shctrl cells (**Figure 12D**). Interestingly, no differences in Wnt signaling activity, as detected by nuclear β-catenin staining, were observed in these cells (**Figure 12E**). These findings indicate that loss of RNF43 increases the stemness of gastric cancer cell lines and induces EMT independently of Wnt signaling.

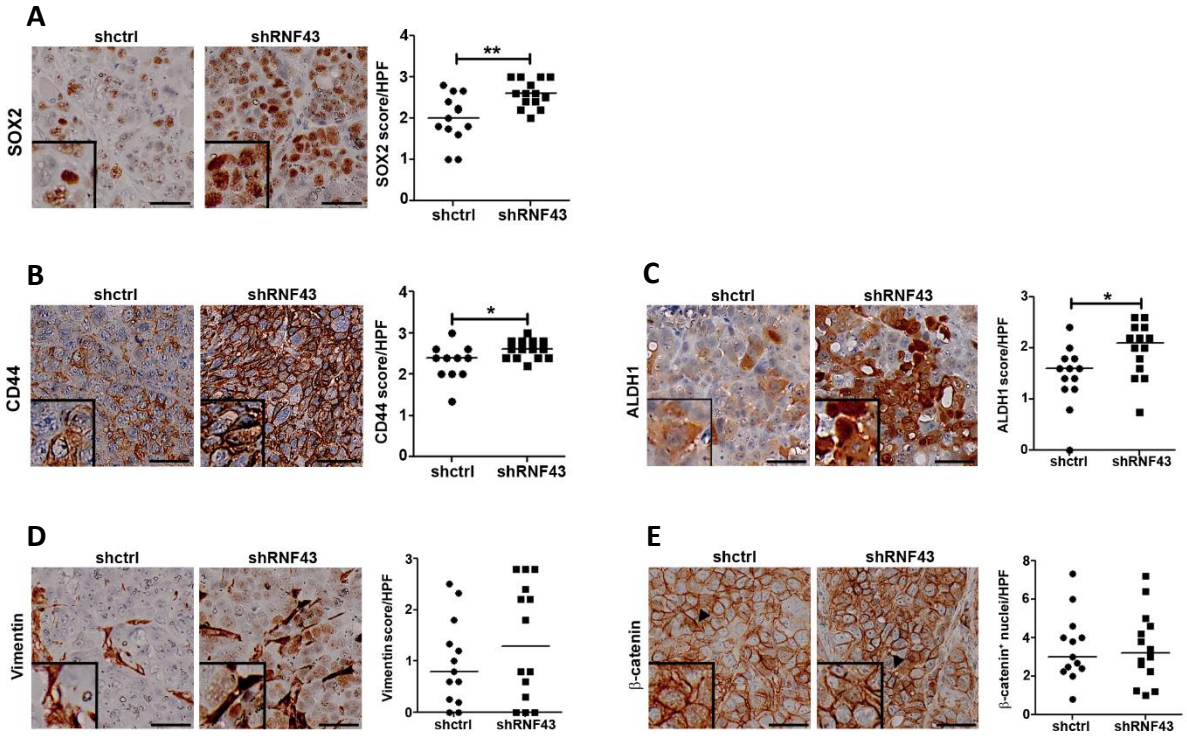


**Figure 12: RNF43 negatively regulates stemness in gastric cancer cells MKN45 *in vivo*.** Representative images and quantification of MKN45 xenograft tumors stained by immunohistochemistry for SOX2 (A), CD44 (B), ALDH1 (C), Vimentin (D) and β-catenin (E). Arrowheads indicate positive cells. Scale bars indicate 50 µm. Horizontal bars represent the median; each dot represents one tumor. Mann-Whitney U-Test. *P<0.05, **P<0.01. Adapted and reprinted from [237] with permission from Oxford academic.

### 5.2.4 Loss of RNF43 function increases the proliferation of murine gastric organoids

To confirm the tumor suppressor activity of RNF43 *ex vivo* and *in vivo*, two mouse lines were generated bearing loss of function alterations in the RING domain of the protein. *Rnf43*$^{\Delta Exon8}$ mice carry a deletion of 57 bp inside Exon 8 of the genomic DNA which completely abrogates the functional domain. Rnf43$^{H292R/H295R}$ mice harbor two point mutations that disrupt the structure of the zinc finger domain. Gastric organoids from these mice were used as a primary cell culture model. Organoids from *Rnf43*$^{\Delta Exon8}$ and Rnf43$^{H292R/H2925R}$ mice as well as FVB/N mice were seeded at equal density and grown for 17 days. Loss of RNF43 function increased the growth of murine gastric organoids supporting the findings observed in gastric cancer cell lines (**Figure 13**).

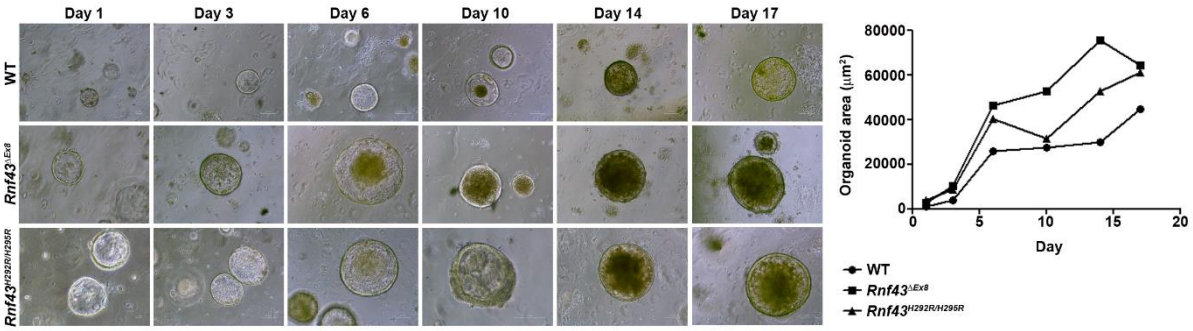


**Figure 13: Depletion of RNF43 increases the growth capacity of murine gastric organoids.** Representative images of murine gastric organoids grown from FVB/N wild type, *Rnf43*$^{\Delta Exon8}$ and Rnf43$^{H292R/H2925R}$ mice at different days. Quantification represents organoid sizes from one out of three independent experiments. Adapted and reprinted from [237] with permission from Oxford academic.

### 5.2.5 Loss of functional RNF43 alters gastric homeostasis *in vivo*

*Rnf43*$^{\Delta Exon8}$ and Rnf43$^{H292R/H2925R}$ mice were sacrificed at different time points to investigate the role of Rnf43 in gastric tissue homeostasis *in vivo*. Tissue architecture was analyzed in sections stained with H&E. From 16 weeks on, *Rnf43*$^{\Delta Exon8}$ mice developed multifocal hyperplasia of the glandular stomach, which progressed to marked hyperplasia at later time points. Staining of Ki67 showed that proliferation spread to the lumen at 24 weeks of age. Thickening of the gastric mucosa was also observed. Rnf43$^{H292R/H2925R}$ mice displayed similar changes of the gastric epithelium, but this phenotype could be observed already 4 weeks after birth in some mice. At later time points, mice showed hyperplasia with cellular atypia and a thickening of the gastric mucosa (**Figure 14**).

To characterize changes in expression of the stem cell marker Sox2, mRNA levels of *Sox2* were analyzed at 12, 24 and 40 weeks after birth. *Sox2* expression was slightly increased in *Rnf43*$^{\Delta Exon8}$ mice at 12 and 24 weeks. However, there were no changes observed at 40 weeks. In Rnf43$^{H292R/H2925R}$ mice, no changes were observed at 12 weeks, but an increase of *Sox2* expression was observed at 24 and 40 weeks (**Figure 15A**). Taken together, loss of RNF43 function only slightly increased expression of the stem cell marker *Sox2* indicating that expansion of this stem cell compartment might not or only partially contribute to the pathologic changes observed in mutant mice.

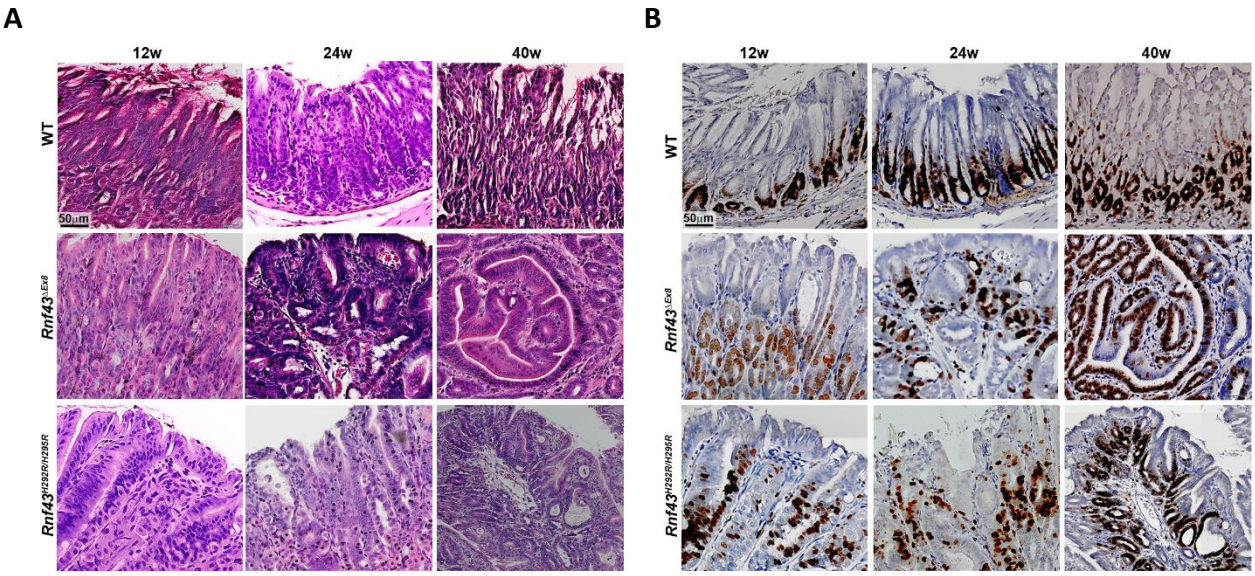


**Figure 14: Loss of Rnf43 function induces pathologic changes in the gastric mucosa of mutant mice.** Representative images of hematoxylin-eosin staining (A) and Ki67 immunohistochemistry staining (B) of 12, 24 and 40 weeks old Rnf43 wild type, *Rnf43*$^{\Delta Exon8}$ and Rnf43$^{H292R/H295R}$ mice. Scale bar indicates 50 µm. Adapted and reprinted from [237] with permission from Oxford academic.

To investigate whether the epithelial changes were due to increased activation of the Wnt signaling pathway, we analyzed mRNA expression of the Wnt target genes *Axin2* and *Lgr5* in the stomach of 12, 24 and 40 weeks old mice. Interestingly, Wnt target genes were downregulated in *Rnf43*$^{\Delta Exon8}$ and Rnf43$^{H292R/H2925R}$ mice compared to wild type mice at 12 weeks after birth. At 24 weeks, no significant differences were detected for *Lgr5* expression, whereas *Axin2* expression was significantly reduced in Rnf43$^{H292R/H2925R}$ mice. At the later time point, no changes in Wnt target gene expression were observed in *Rnf43*$^{\Delta Exon8}$ mice. In Rnf43$^{H292R/H2925R}$ mice, *Axin2* was significantly upregulated at 40 weeks (**Figure 15B** and **C**). Taken together, these data indicate that changes observed in the stomach of *Rnf43*$^{\Delta Exon8}$ and Rnf43$^{H292R/H2925R}$ mice were not induced by increased Wnt activity after loss of Rnf43 function.

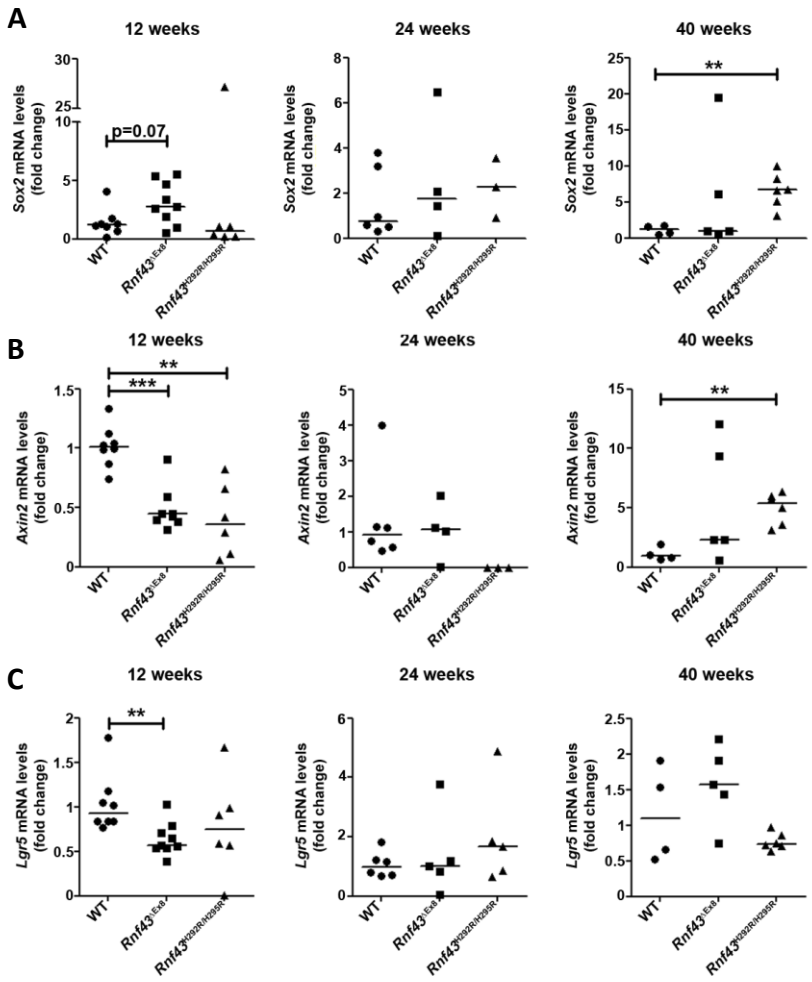


**Figure 15: Wnt signaling is not elevated upon loss of Rnf43 function.** *Sox2* (A), *Lgr5* (B) or *Axin2* (C) expression in the stomach analyzed by qRT-PCR. mRNA levels were normalized to *Gapdh* and are depicted as fold change to wild type mice. Horizontal bars represent medians; each dot represents one mouse. Mann-Whitney U-Test. **P<0.01, ***P<0.001. Adapted and reprinted from [237] with permission from Oxford academic.

## 5.3 The role of RNF43 in DNA damage response

### 5.3.1 RNF43 is involved in the DDR in gastric cancer cells

Previously published data hinted towards a role of RNF43 in DDR in the pancreas [232]; however, whether and by which mechanism RNF43 could be involved in this pathway in the stomach has never been investigated. To elucidate this, gastric cancer cells were treated with ionizing radiation to induce DNA damage. Analysis of mRNA expression showed, that *RNF43* was upregulated upon treatment of AGS and MKN45 cells with 10 and 20 Gγ (**Figure 16A**). When co-staining RNF43 and the DDR marker γH2AX in AGS cells after treatment with 20 Gγ, co-localization of RNF43 and γH2AX in DDR foci was

observed. Additionally, upregulation of RNF43 in the cells after irradiation could also be detected in these immunofluorescence stainings when comparing treatment with 0 or 20 Gγ (**Figure 16B**).

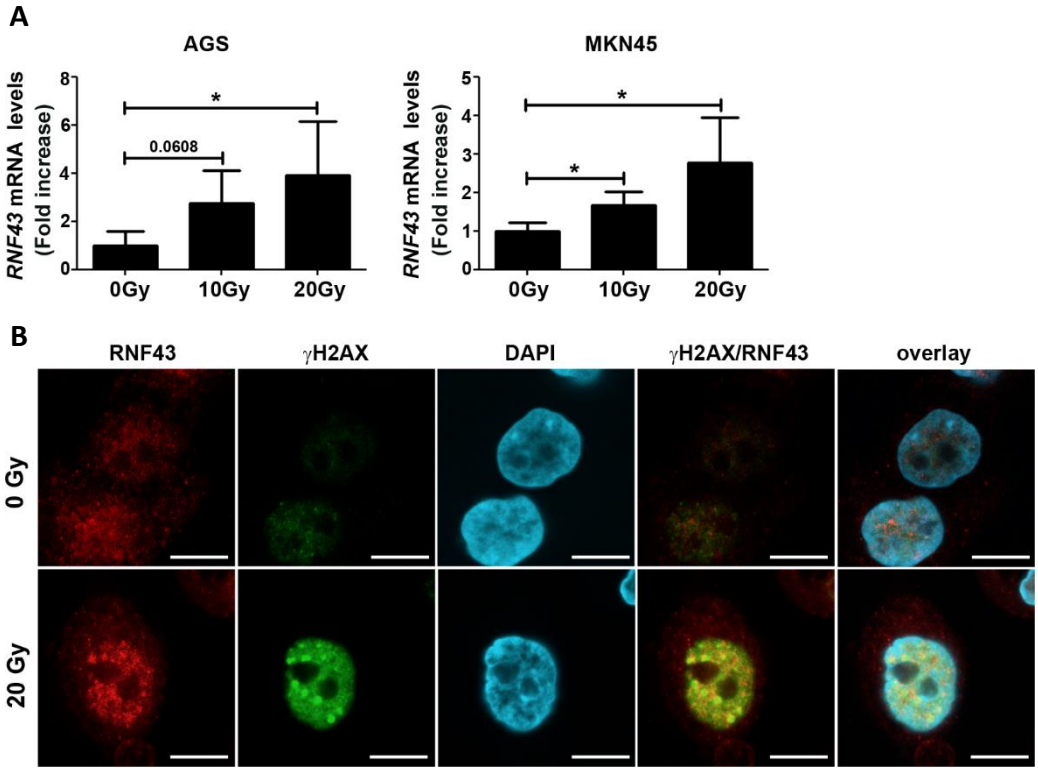


**Figure 16: RNF43 is upregulated upon DNA damage and colocalizes with γH2AX.** A) *RNF43* mRNA levels in AGS and MKN45 cells analyzed by qRT-PCR, normalized to *GAPDH* and depicted as fold change to untreated control. Bars indicate mean ± SD from four independent experiments. *P<0.05. B) Confocal immunofluorescence staining of RNF43 (red) and γH2Ax (green). Nuclei are depicted in blue. Scale bars indicate 10 µm. Adapted and reprinted from [235] with permission from Elsevier Inc.

To confirm that the observed co-localization was due to interaction between RNF43 and γH2AX, we overexpressed HA tagged RNF43 in AGS cells and performed immunoprecipitation. Western Blot analysis showed that γH2AX could be precipitated together with RNF43, indicating that the two proteins interact (**Figure 17A**). Since several E3 ubiquitin ligases had been described to mono-ubiquitinate γH2AX, and it had been shown that this was an important step during DDR activation, we investigated whether ubiquitination levels of γH2AX would change upon depletion of RNF43. For this, γH2AX was immunoprecipitated and ubiquitination was observed by Western Blot. RNF43 depleted AGS and MKN45 cells showed reduced levels of ubiquitin at γH2AX residues lysine 48 and lysine 63 compared to control cells, indicating that RNF43 is involved in ubiquitination of γH2AX (**Figure 17B** and **C**). These data hinted towards a role of RNF43 in DDR. Therefore, DDR activation

was further investigated by Western Blot. Treatment of AGS wild type and MKN45 shctrl cells with 10 and 20 Gγ led to induction of DDR as detected by phosphorylation of H2AX and Chk2. In RNF43 depleted AGS$^{D196fs}$ and MKN45 shRNF43 cells, DDR activation was reduced (**Figure 17D** and **E**). Taken together, these results imply that RNF43 is involved in DDR activation by mediating ubiquitination of γH2AX.

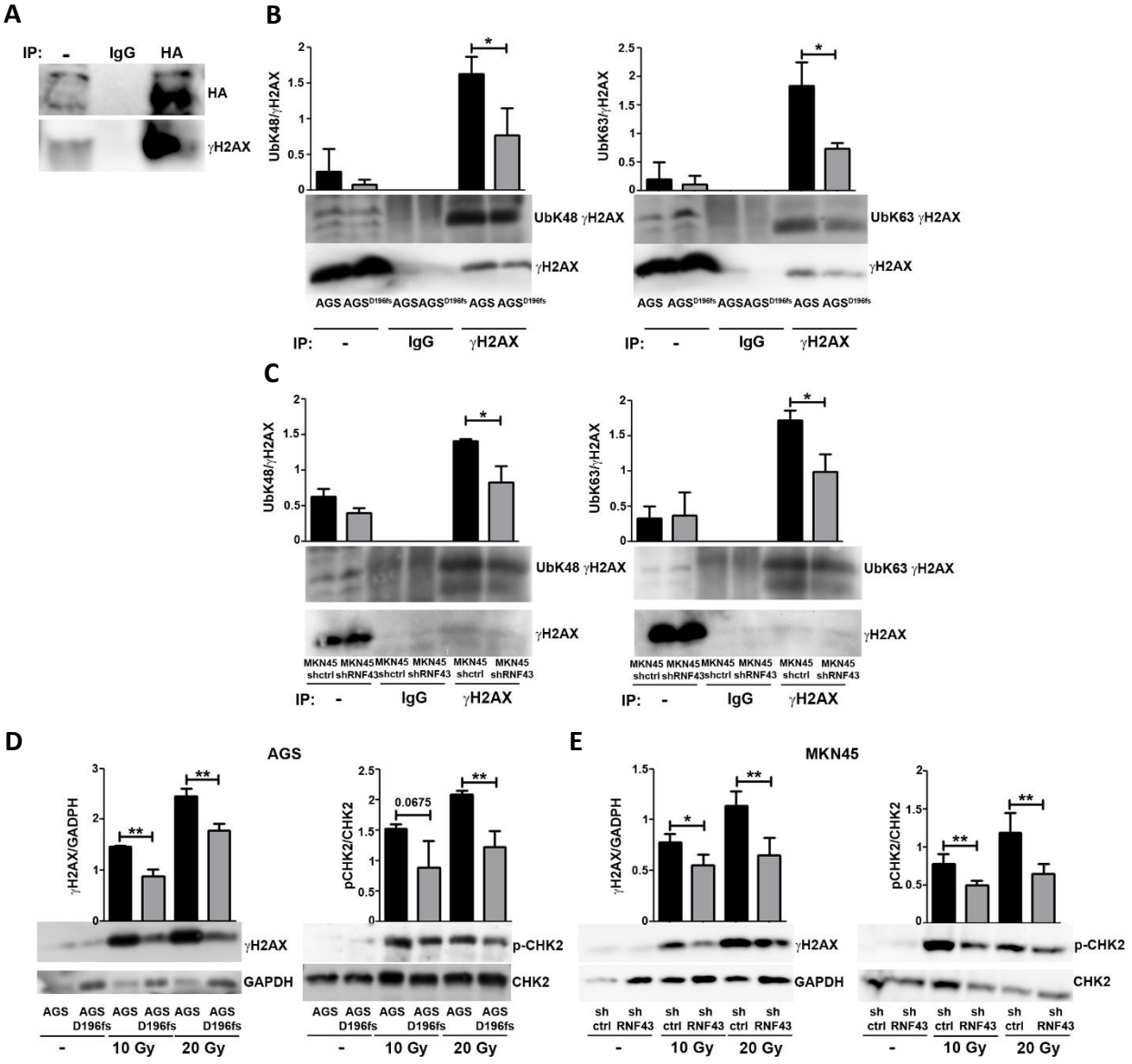


**Figure 17: RNF43 is involved in DDR activation in vitro.** A) Immunoprecipitation of HA-tagged RNF43 overexpressed in AGS cells. Representative image of three independent experiments. B), C) Ubiquitination levels after immunoprecipitation of γH2AX in AGS (B) or MKN45 (C) cells. Representative Western Blot images and quantification from three independent experiments, bars indicate mean ± SD. D), E) Protein levels of DDR activation markers in D) AGS or E) MKN45 cells after treatment with γ-irradiation. Representative Western Blot images and quantification, bars indicate mean ± SD from three independent experiments. *P<0.05, **P<0.01. Adapted and reprinted from [235] with permission from Elsevier Inc.

### 5.3.2 Loss of RNF43 confers resistance to irradiation induced apoptosis

When DDR is activated, the cell will first try to repair the DNA damage, however, if damage burden is too high, the cell undergoes apoptosis. To investigate how loss of RNF43 and thereby reduced DDR activation would change cellular behavior upon DNA damage, we analyzed cell survival upon treatment with ionizing radiation. Proliferation assays showed that number of viable cells was reduced in MKN45 shctrl and AGS wild type cells. However, depletion of RNF43 enhanced the survival of MKN45 shRNF43 and AGS$^{D196fs}$ cells upon irradiation (**Figure 18A**). To further investigate the capacity of these cells to clonally expand after irradiation, they were treated with 2.5 or 5 Gγ and seeded in low density to analyze growth of single cell colonies. Loss of RNF43 led to an increased number of single cell colonies, indicating that this conferred resistance to irradiation (**Figure 18B**). Furthermore, induction of apoptosis was analyzed to determine whether the increased number of viable cells upon RNF43 depletion was due to reduction of apoptosis. Upon treatment with 10 and 20 Gγ, AGS wild type and MKN45 shctrl cells underwent apoptosis, as observed by AnnexinV/PI staining. However, the number of AnnexinV single positive and double positive cells was reduced for AGS$^{D196fs}$ and MKN45 shRNF43 cells compared to controls (**Figure 18C** and **D**). These data strongly suggest that loss of RNF43 enhances cell survival by conferring resistance to DNA damage induced apoptosis.

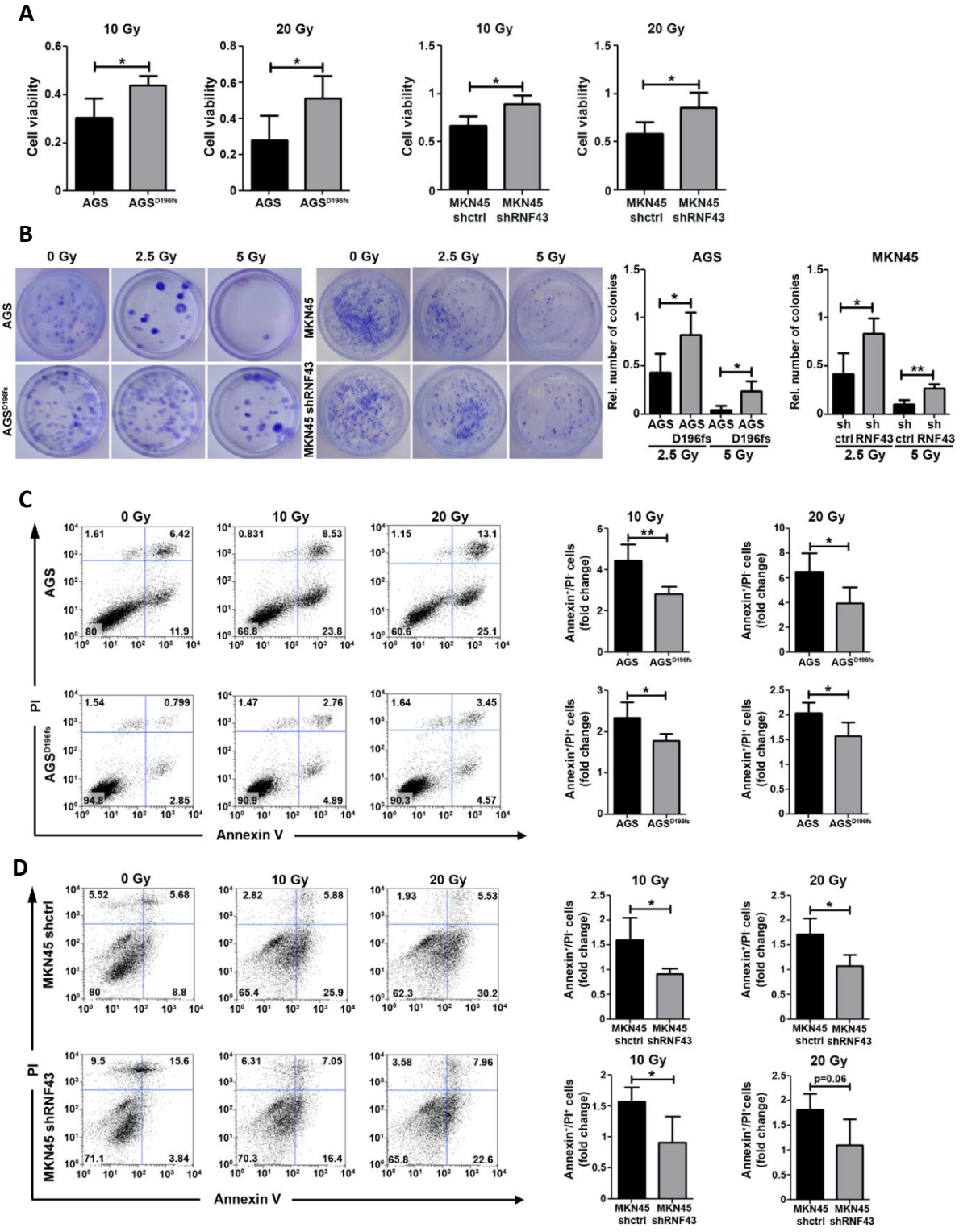


**Figure 18: RNF43 depletion in gastric cancer cell lines confers resistance to γ-irradiation.** A) Cell viability of AGS and MKN45 cells after treatment with 10 or 20 Gγ. OD 450/600 nm was measured after addition of CCK-8 with a photometer and normalized to untreated control. B) Single cell colonies were allowed to grow for 14 days and stained with crystal violet after treatment with γ-irradiation. Colonies were counted and normalized to untreated control. C), D) Representative dot plots and quantification of AnnexinV/PI staining and subsequent FACS analysis. Cell numbers were normalized to untreated control. Bars indicate mean ± SD from four independent experiments. *P<0.05, **P<0.01. Adapted and reprinted from [235] with permission from Elsevier Inc.

### 5.3.3 RNF43 depletion reduces susceptibility to chemotherapy *in vitro* and *ex vivo*

Chemotherapy is the most important neoadjuvant therapy for gastric cancer patients. Since the commonly used therapeutics cisplatin and 5-FU act by inducing DNA damage [177, 224-226], we investigated the role of RNF43 in chemotherapy resistance. Treatment of control cells with $LD_{50}$ of both agents led to a decreased number of viable cells, whereas RNF43 depleted gastric cancer cells were more resistant to chemotherapeutic treatment (**Figure 19A**). To confirm this in a different model, murine organoids derived from wild type and *Rnf43*$^{\Delta Exon8}$ mice were treated with chemotherapeutics for 5 days. Analysis of organoid viability showed that organoids derived from Rnf43 mutant mice were more resistant to 5-FU and cisplatin compared to control organoids (**Figure 19B**).

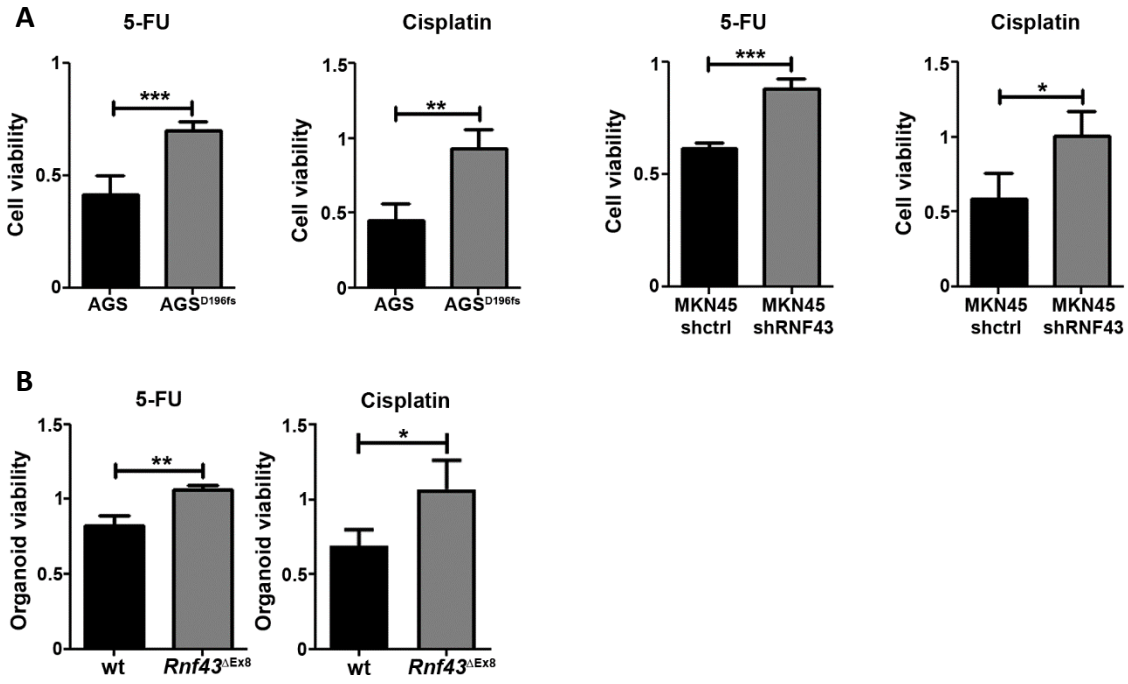


**Figure 19: Loss of RNF43 confers resistance to chemotherapy *in vitro*.** A) Cell viability of AGS and MKN45 cells measured by OD 450/600 nm after treatment with 5-FU or cisplatin for 48 h and normalized to untreated control. B) Organoid viability measured by Cell titer glo 3D luminescence and normalized to untreated control. Bars indicate mean ± SD from three independent experiments. Student's t-test. *P<0.05, **P<0.01, P<0.001. Adapted and reprinted from [235] with permission from Elsevier Inc.

### 5.3.4 Loss of RNF43 confers resistance to DNA damage inducing chemotherapy *in vivo*

Depletion of RNF43 led to an increased resistance to chemotherapy in gastric cancer cells *in vitro*. To confirm these findings *in vivo*, we used the established xenograft model and treated the mice with cisplatin or 5-FU. Since tumor recovery rate from MKN45 cells was nearly 100 % (**Figure 11**), these cells were selected for further experiments. When tumors had established, mice were treated with 50 mg/kg 5-FU or 10 mg/kg cisplatin twice a week. Tumors derived from MKN45 shctrl cells stopped growing upon treatment with chemotherapy while tumors derived from RNF43 depleted cells continuously grew despite being treated with cisplatin or 5-FU (**Figure 20**). These results showed that RNF43 conferred resistance to DNA damage inducing chemotherapeutics in a xenograft model.

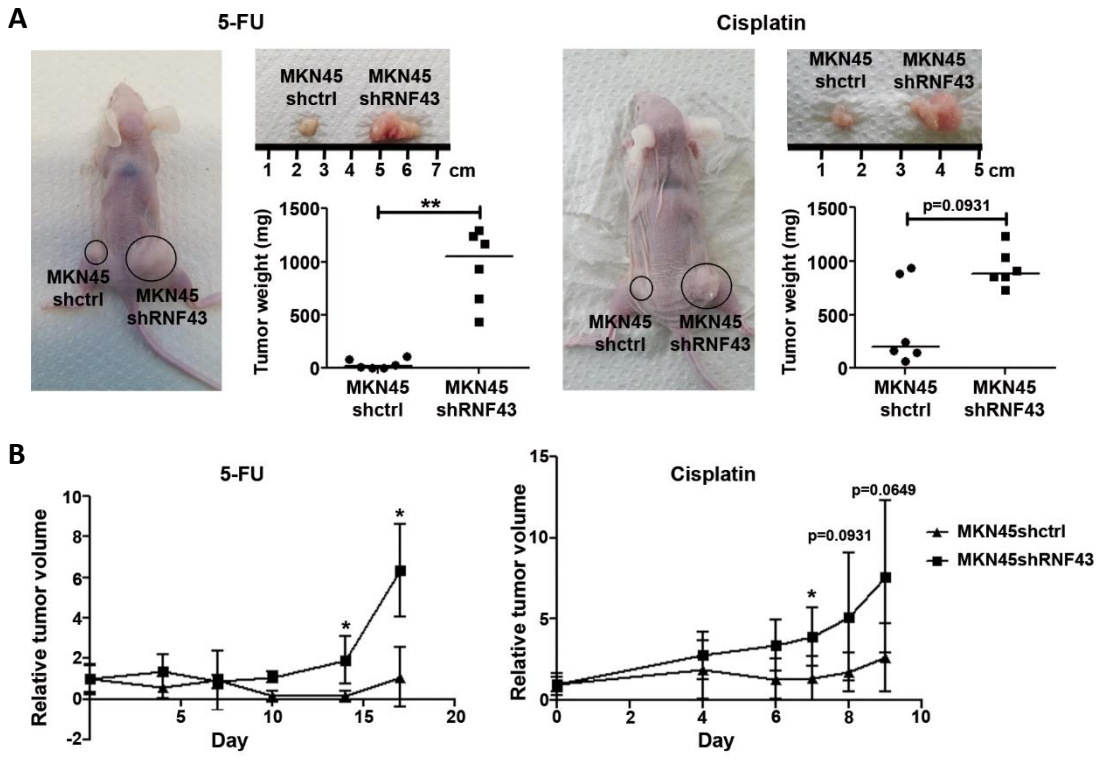


**Figure 20: RNF43 depletion confers resistance to chemotherapy in a xenograft model.** A) Representative images from *Foxn1$^{nu}$* mice and resected tumors. Tumors were weighed after resection. Each dot represents one tumor; horizontal bars represent medians. B) Tumor sizes measured using a caliper and calculated as V=length*width*height/2 mm$^3$. Values were normalized to respective tumor sizes at day 0. Dots with error bars represent mean ± SD from all tumors. Mann-Whitney U-Test. *P<0.05, **P<0.01. Adapted and reprinted from [235] with permission from Elsevier Inc.

To further analyze DDR activation and proliferation upon treatment of the tumors with chemotherapy, immunohistochemistry was performed. Tumors derived from MKN45 shctrl cells showed strong

activation of DDR as detected by γH2AX staining, while RNF43 depleted tumors showed reduced DDR activation. Furthermore, tumors derived from MKN45 shRNF43 cells showed less induction of apoptosis as detected by levels of cleaved caspase 3 compared to their control counterparts. In line with this, moderate proliferation was detected by Ki67 staining in control tumors while tumors derived from RNF43 depleted cells showed high proliferation rate (**Figure 21**). Taken together, these data showed that chemotherapeutic treatment of xenograft tumors activated DDR and induced apoptosis in tumors originated from shctrl cells, whereas those originated from RNF43 depleted cells were still able to proliferate. Therefore, these results strongly suggest that RNF43 depletion confers resistance to chemotherapy by preventing the DNA damage mediated induction of apoptosis and allows the tumors to continuously proliferate.

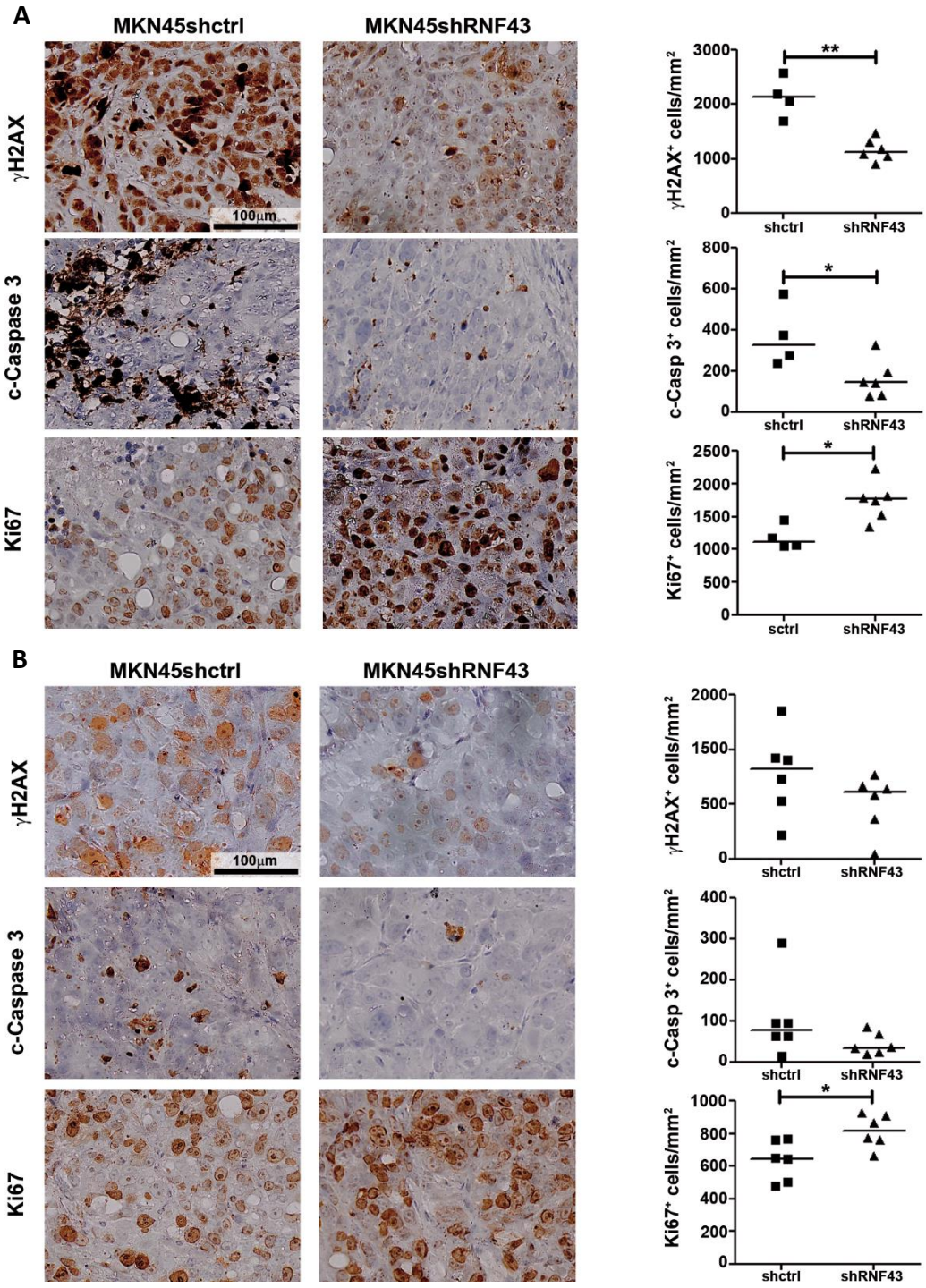


**Figure 21: RNF43 depletion decreases DDR activation in xenograft tumors upon chemotherapeutic treatment.** Representative images of MKN45 tumors treated with 5-FU (A) or cisplatin (B) stained for γH2AX, cleaved caspase 3 and Ki67 by immunohistochemistry. Quantifications were obtained from 5 high power fields. Each dot represents one tumor; horizontal bars represent medians. Scale bars indicate 100 µm. Mann-Whitney U-Test. *P<0.05, **P<0.01. Adapted and reprinted from [235] with permission from Elsevier Inc.

### 5.3.5 RNF43 expression correlates with susceptibility to chemotherapy in human gastric organoids

Human organoids were established from gastric biopsies to confirm a role of RNF43 in response to chemotherapy. Organoid cultures were treated with 5-FU or cisplatin for 5 days and organoid viability was analyzed. Organoids from different patients responded quite variously to chemotherapy. Thus, organoid viability after treatment with chemotherapy was normalized to untreated control organoids. An organoid viability normalized to control above 95 % was defined as non-responder and treated organoids with a viability of less than 95 % were defined as responders. To analyze, whether SNPs or mutations could have an effect on responsiveness to chemotherapy, exons of RNF43 were amplified and sequenced. Patients in this cohort mostly presented with healthy stomach or gastritis, however, *RNF43* mutations have been described to often occur in the transition from adenoma to carcinoma. As expected for this cohort, no *RNF43* mutations were found. The SNPs I47V, R117H, R343H, L418M and P686R were found in 23, 9, 6, 18 and 7 out of 40 patients, respectively. Comparison with chemotherapy data showed, that none of these SNPs could be correlated with susceptibility to cisplatin or 5-FU (**Figure 22**).

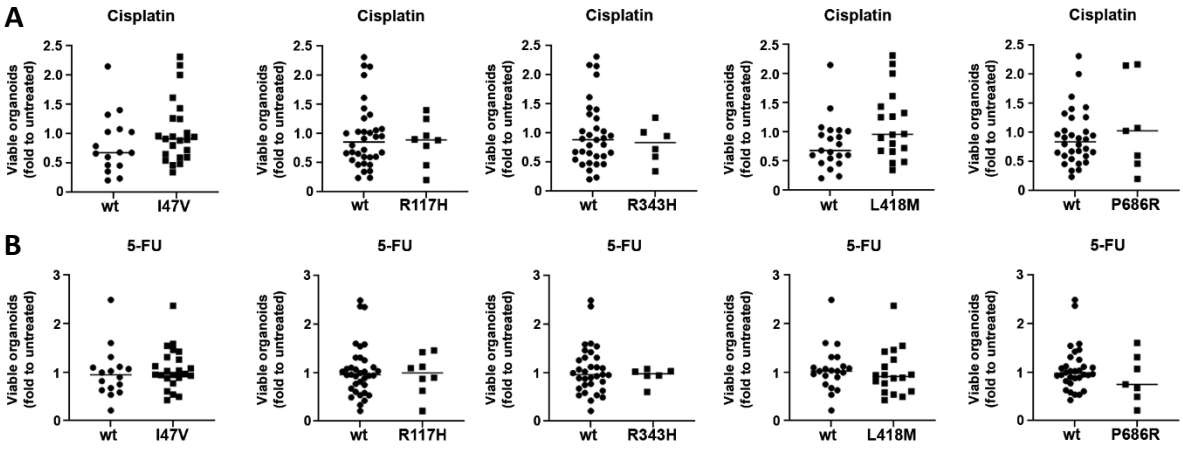


**Figure 22: SNPs of RNF43 in human gastric organoids do not alter their susceptibility to chemotherapy.** Organoid viability after treatment with cisplatin (A) or 5-FU (B) measured by Cell titer glo 3D luminescence and normalized to untreated control. Each dot represents a patient sample; horizontal bars represent medians. Adapted and reprinted from [235] with permission from Elsevier Inc.

Furthermore, *RNF43* expression in these samples was analyzed by RT-qPCR. *RNF43* expression could be negatively correlated with organoid viability upon treatment with 5-FU and a similar trend could be observed for cisplatin, however this was not significant. When grouping the samples in responders or non-responders to chemotherapy, it could be observed that for both agents, responders had significantly higher expression of *RNF43* compared to non-responders (**Figure 23**). These data confirmed the findings from gastric cancer cells and murine organoids and indicated that RNF43 is involved in response to chemotherapy in human gastric organoids.

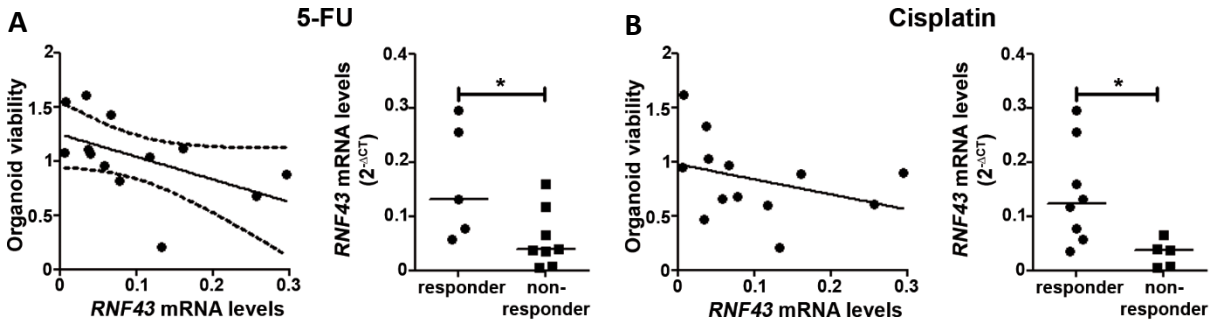


**Figure 23: *RNF43* expression correlates with response to chemotherapy in human gastric organoids.** Human organoids were treated with 5-FU (A) or Cisplatin (B) for 5 days and organoid viability was measured using Cell titer glo 3D luminescence and normalized to untreated controls. *RNF43* mRNA levels were measured by RT-qPCR and values were normalized to *GAPDH*. Each dot represents one patient sample; horizontal bars represent medians. Dashed lines indicate 95 % confidence interval. Mann-Whitney U-Test. *P<0.05. Adapted and reprinted from [235] with permission from Elsevier Inc.

### 5.3.6 RNF43 is involved in DDR activation upon *H. pylori* infection *in vitro*

*H. pylori* has been described to directly induce DSBs in host cells [112]. Therefore, we investigated whether RNF43 would also be involved in DDR activation upon infection. When AGS and MKN45 cells were infected with *H. pylori* at MOI 50 or 100 for 24 hours, DDR was activated in control cells upon infection with *H. pylori* while DDR activation was reduced in RNF43 depleted AGS and MKN45 cells (**Figure 24A** and **B**). Furthermore, RNF43 was upregulated compared to uninfected controls (**Figure 24C**). These data suggest that RNF43 is also involved in DDR activation upon infection with *H. pylori*.

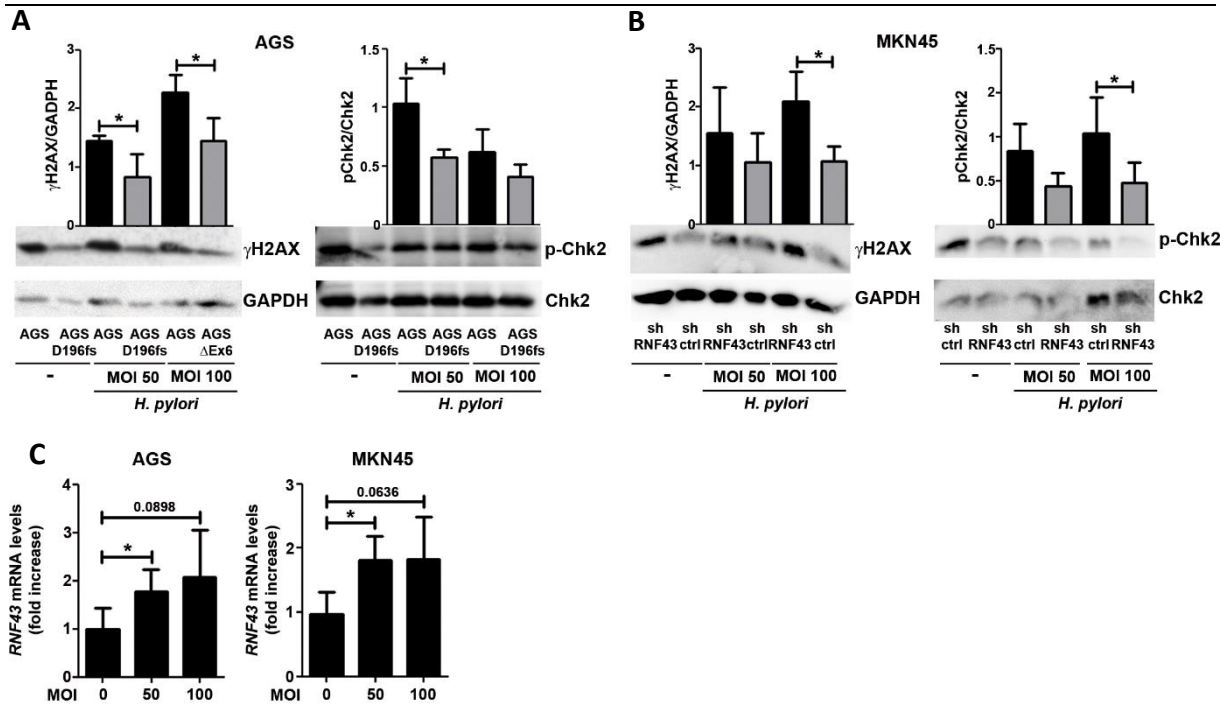


**Figure 24: RNF43 is involved in DDR activation upon *H. pylori* infection *in vitro*.** Representative Western Blot images and quantification for γH2Ax and p-Chk2 levels from AGS (A) and MKN45 (B) cells infected with *H. pylori* PMSS1 for 24 h. C) *RNF43* mRNA levels from AGS and MKN45 cells infected with H. pylori for 24 h. Values were normalized to *GAPDH* and are depicted as fold increase to uninfected controls. Bars indicate mean ± SD from four independent experiments. Student's t- test. *P<0.05. Adapted and reprinted from [235] with permission from Elsevier Inc.

### 5.3.7 RNF43 depletion leads to reduced DDR activation upon *H. pylori* infection *in vivo*

To confirm the role of RNF43 in DDR activation after infection *in vivo*, wild type and *Rnf43*$^{\Delta Exon8}$ mice were infected with *H. pylori* for 3 months and gastric tissue was stained for DDR activation and apoptosis. In FVB/N mice, infection upregulated *Rnf43* expression (**Figure 25A**) and induced DDR and apoptosis as detected by γH2AX and cleaved caspase 3 staining. In contrast, DDR was not significantly activated in *Rnf43*$^{\Delta Exon8}$ mice upon *H. pylori* infection. Furthermore, *Rnf43*$^{\Delta Exon8}$ mice did not show increased cleaved caspase 3 levels during *H. pylori* infection (**Figure 25B**). Taken together, these results indicate that RNF43 depletion in mice leads to a reduced activation of DDR upon *H. pylori* infection thereby preventing induction of apoptosis.

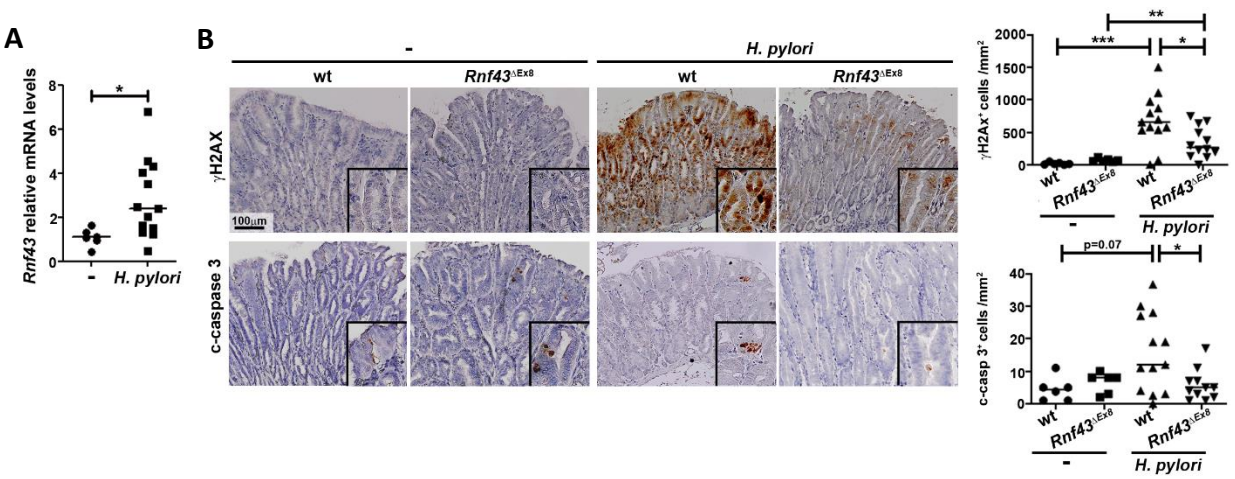


**Figure 25: RNF43 is involved in DDR activation upon *H. pylori* infection *in vivo*.** A) *Rnf43* mRNA levels measured in the stomach of FVB/N mice after infection with *H. pylori* PMSS1 for three months. Values were normalized to *Gapdh* and are depicted as fold change to uninfected wild type mice. B) Representative images of immunohistochemical staining of γH2AX and cleaved caspase 3. Each dot represents one mouse; horizontal lines indicate medians. Scale bars indicate 100 µm. Mann-Whitney U-Test. *P<0.05, ***P<0.001. Adapted and reprinted from [235] with permission from Elsevier Inc.

## 5.4 The role of RNF43 during *H. pylori* infection

### 5.4.1 Rnf43 loss of function increases inflammation during *H. pylori* infection

To further characterize the role of RNF43 during *H. pylori* infection, infected *Rnf43*$^{\Delta Exon8}$ mice were analyzed for bacterial load and inflammation. After 3 months of infection, *Rnf43*$^{\Delta Exon8}$ mice showed a decreased bacterial load as compared to wild type mice (**Figure 26A**). Furthermore, infiltration of neutrophils and mast cells as well as T cells was increased in *Rnf43*$^{\Delta Exon8}$ mice leading to a higher inflammation score (according to the updated Sydney system for gastritis classification) compared to FVB/N mice (**Figure 26B** and **C**). Additionally, expression of the cytokines *Ifng* and *Tnfα* and the chemokine *Cxcl1* (murine IL-8 homologue) was increased in *Rnf43*$^{\Delta Exon8}$ mice compared to wild type mice **(Figure 26D**). *Cxcl1* is a direct target gene of canonical NF-KB signaling indicating increased activation of this pathway in these mice while higher expression of *Ifng* and *Tnfα* could be explained by the increased infiltration of different immune cells observed in these mice (**Figure 26C**).

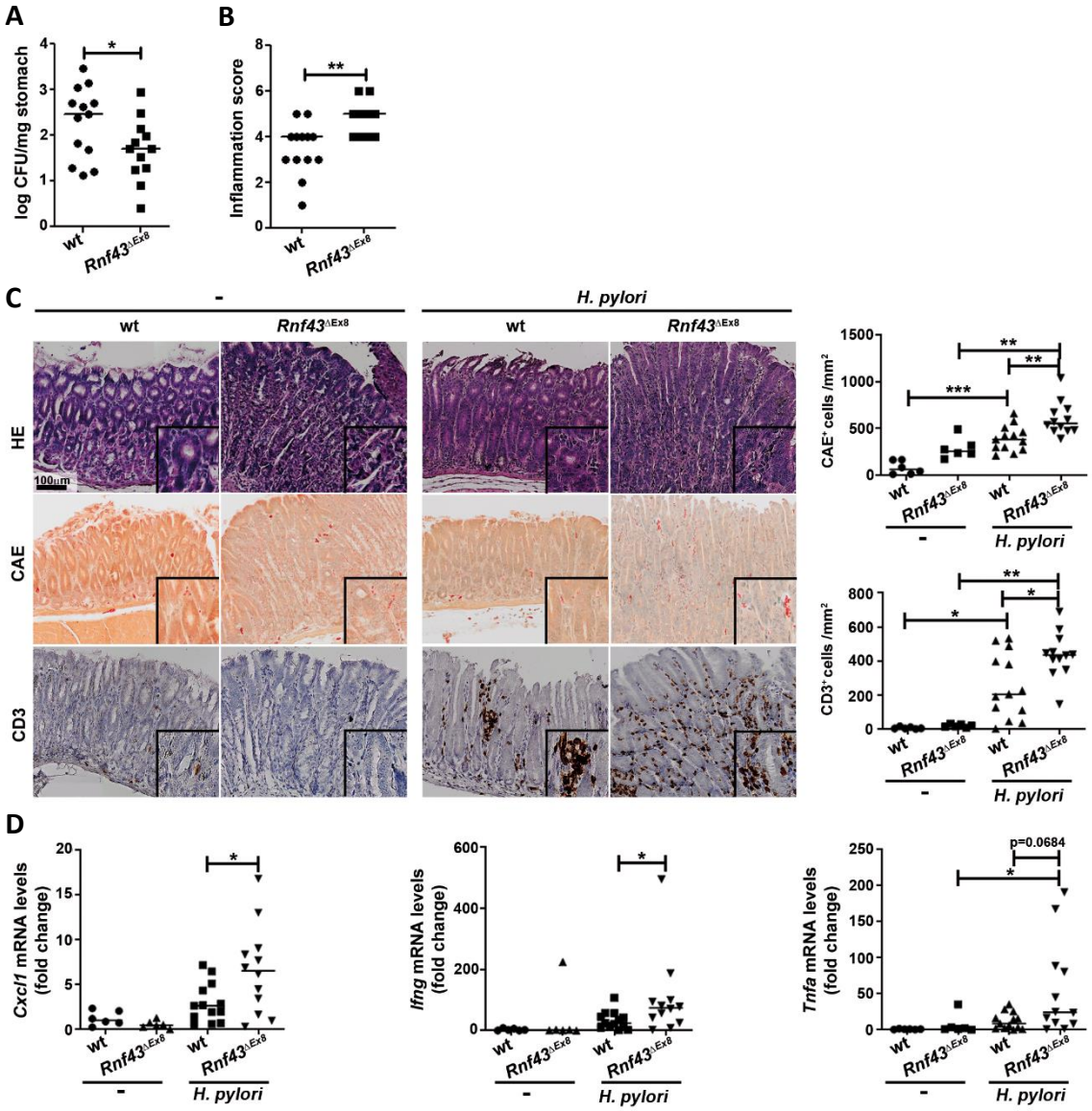


**Figure 26: *Rnf43$^{\Delta Exon8}$* mice display high inflammation upon infection with *H. pylori*.** A) Bacterial load in the stomach of FVB/N and *Rnf43$^{\Delta Exon8}$* mice after three months of *H. pylori* PMSS1 infection. B) Inflammation score of the gastric tissue upon infection. C) Representative images and quantification of hematoxylin-eosin and chloracetate esterase (CAE) staining as well as immunohistochemistry for CD3 of the gastric mucosa of FVB/N and *Rnf43$^{\Delta Exon8}$* mice upon infection. D) mRNA levels of *Cxcl1*, *Ifng* and *Tnfa* in the stomach of infected mice. Values were normalized to *Gapdh* and are depicted as fold increase compared to uninfected wild type animals. Each dot represents one mouse; horizontal bars indicate medians. Mann-Whitney U-Test. *P<0.05, **P<0.01, ***P<0001. Adapted and reprinted from [235] with permission from Elsevier Inc.

Since *H. pylori* was shown to activate Wnt and STAT3 signaling, which have been linked to gastric carcinogenesis, we analyzed whether these pathways were altered in *Rnf43$^{\Delta Exon8}$* mice under basal conditions and during *H. pylori* infection. We could observe no differences in Wnt activity as detected by nuclear β-catenin between FVB/N and *Rnf43$^{\Delta Exon}$* mice under basal conditions. Upon infection, Wnt

signaling was activated in the stomach of these mice to a similar extent, indicating that Rnf43 loss of function did not have an impact on Wnt signaling. In contrast, STAT3 activity was slightly increased in *Rnf43*$^{\Delta Exon}$ mice compared to wild type mice. *H. pylori* infection lead to a strong activation of STAT3 signaling in *Rnf43*$^{\Delta Exon}$ mice and this was significantly higher than in FVB/N mice (**Figure 27**). Taken together, this data indicated that Rnf43 loss of function increases inflammation in the stomach upon *H. pylori* infection and this leads to higher activation of inflammation-related pathways such as NF-κB and STAT3 signaling, while Wnt is not altered.

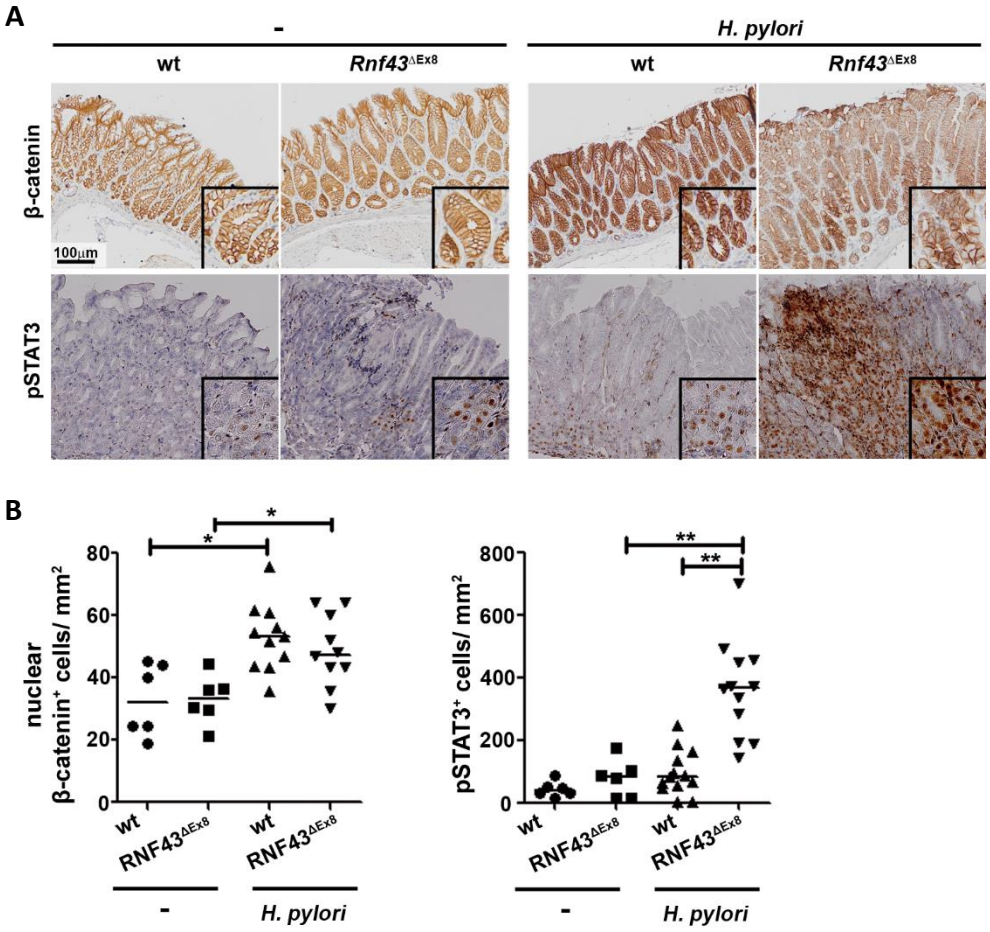


**Figure 27: Loss of function of Rnf43 alters carcinogenic pathways activated upon *H. pylori* infection.** A) Representative pictures of tissue section stained for β-catenin and pSTAT3 by immunohistochemistry obtained from *H. pylori* infected mice. Scale bar indicates 100 µm. B) Quantification of gastric tissue stained for β-catenin and pSTAT3 after 3 months of infection. Each dot represents one mouse; horizontal bars indicate medians. Mann Whitney U-Test. *P<0.05, **P<0.01. Adapted and reprinted from [235] with permission from Elsevier Inc.

### 5.4.2 *Rnf43* mutations increase inflammation during *H. pylori* infection

Since we could observe higher inflammation in *Rnf43*$^{\Delta Exon8}$ mice, we analyzed whether infection of Rnf43$^{H292R/H295R}$ mice leads to a similar phenotype. Indeed, we could observe a slightly decreased bacterial load in Rnf43$^{H292R/H295R}$ mice compared to wild type mice upon infection with *H. pylori* for 3 months (**Figure 28A**). Furthermore, infiltration of the stomach with T cells was increased in Rnf43 mutant mice (**Figure 28B** and **C**) and this was accompanied by enhanced expression of *Cxcl1* and *Ifng* (**Figure 28D**). Thus, similar to *Rnf43*$^{\Delta Exon8}$ mice, Rnf43$^{H292R/H295R}$ mice showed higher inflammation upon *H. pylori* infection.

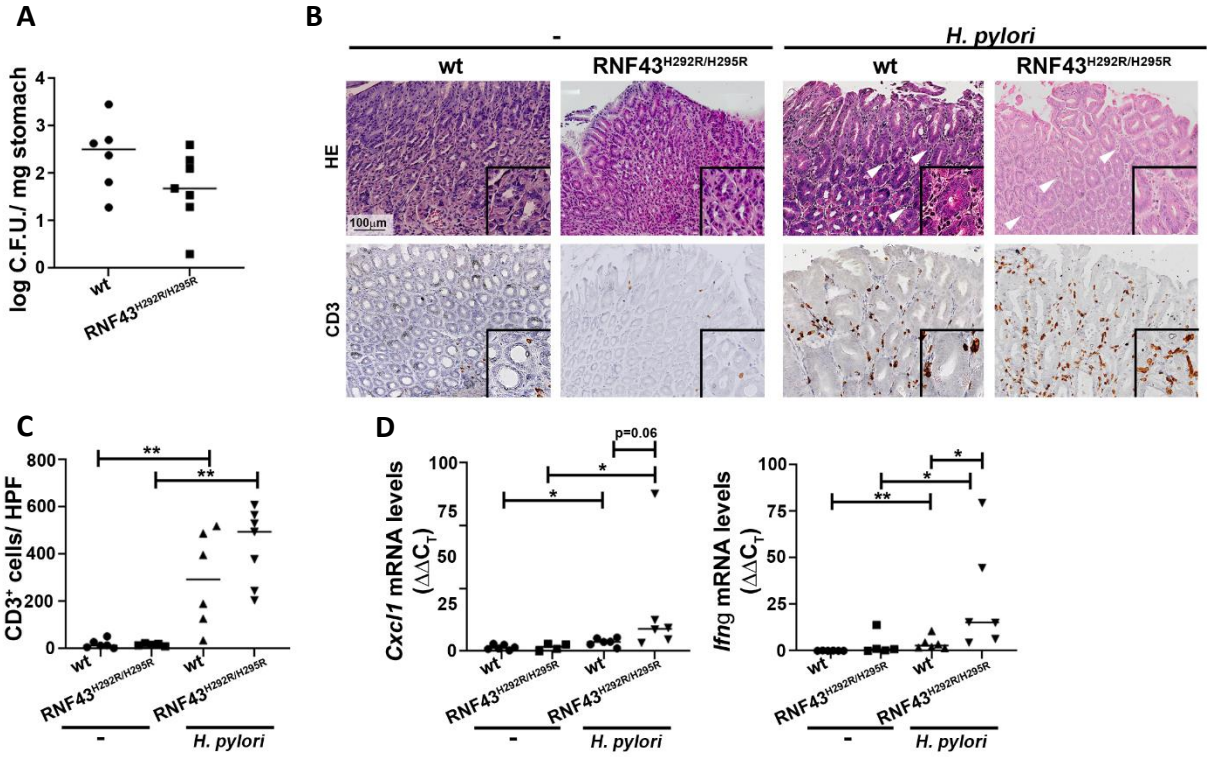


**Figure 28: Rnf43$^{H292R/H295R}$ mice display high inflammation upon infection with *H. pylori*.** A) Bacterial load in the stomach of FVB/N and Rnf43$^{H292R/H295R}$ mice after three months of *H. pylori* PMSS1 infection. B) Representative images of hematoxylin-eosin staining and immunohistochemistry for CD3 of the gastric mucosa of FVB/N and Rnf43$^{H292R/H295R}$ mice upon infection. C) Quantification of infiltrating CD3$^+$ cells upon H. pylori infection. D) mRNA levels of *Cxcl1* and *Ifng* in the stomach of infected mice. Values were normalized to *Gapdh* and are depicted as fold increase compared to uninfected wild type animals. Each dot represents one mouse; horizontal bars indicate medians. Mann-Whitney U-Test. *P<0.05, **P<0.01.

### 5.4.3 Rnf43 mutations aggravate *H. pylori*-induced gastric pathology

In Rnf43 mutated mice, we could observe gastric hyperplasia and thickening of the gastric mucosa, however, these mice did not develop neoplasia under basal conditions. Thus, we performed long-term

*H. pylori* infection for 6 months to analyze whether ongoing inflammation could induce neoplasia. Since Rnf43$^{H292R/H295R}$ mice developed hyperplastic changes in the gastric mucosa earlier and more frequently than *Rnf43$^{\Delta Exon8}$* mice, we chose those for long-term infection.

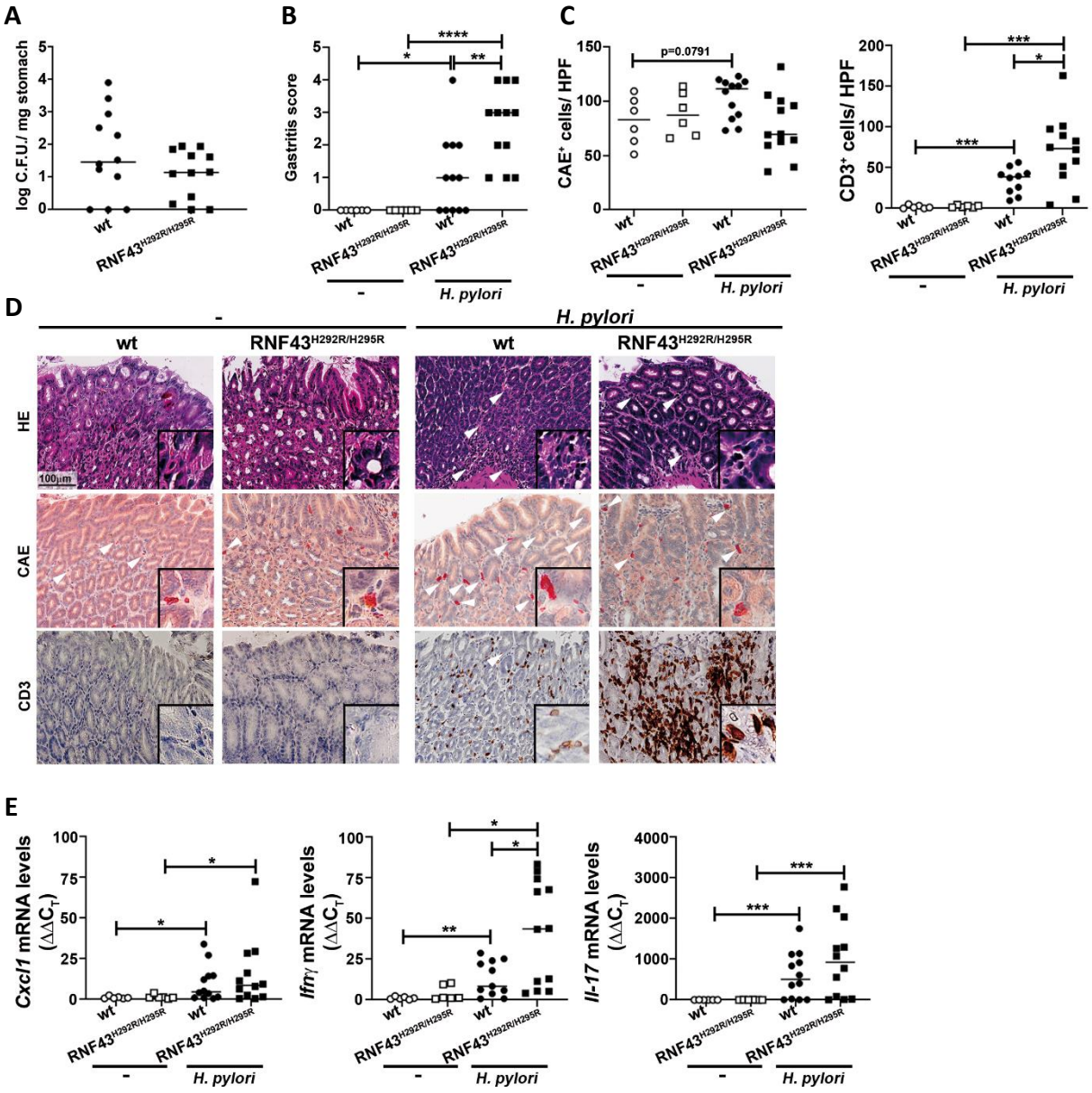


**Figure 29: Mutations in *Rnf43* lead to high inflammation in *H. pylori* infected mice.** A) Bacterial load per mg stomach of mice infected for 6 months with *H. pylori* strain PMSS1. B) Gastritis score of infected animals determined by chronicity and activity of inflammation in corpus and antrum according to the updated Sydney system for gastritis classification. C) Quantification of chloracetate esterase (CAE) and CD3 positive cells obtained from 5 different high power fields. D) Representative images from immunohistochemically stained gastric tissue sections. Scale bars indicate 100 µm. E) mRNA levels of *Cxcl1*, *Ifng* and *Il-17* in the stomach of control and PMSS1 infected animals. Values are normalized to *Gapdh*. Each dot represents one mouse; horizontal bars depict medians. Mann-Whitney U-Test. *P<0.05, **P<0.01, ***P<0.001. Adapted and reprinted from [238] with permission from MDPI.

Upon infection of Rnf43$^{H292R/H295R}$ mice with *H. pylori* for 6 months, bacterial load was not different from wild type mice (**Figure 29A**). Furthermore, we could not detect differences in neutrophil and mast cell infiltration. However, T cell infiltration was increased in Rnf43 mutant mice compared to wild type mice leading to a higher gastritis score when evaluated according to the updated Sydney system for gastritis classification (**Figure 29B**,**C** and **D**). No differences were detected in the expression of *Cxcl1*, whereas *Il-17* levels were slightly increased and *Ifng* levels were significantly higher in Rnf43$^{H292R/H295R}$ mice (**Figure 29E**). Taken together, these results show that RNF43 depletion leads to a higher inflammation in the stomach of *H. pylori* infected mice.

Since *H. pylori* infection is one of the main drivers of gastric carcinogenesis, we assessed how long term infection of Rnf43$^{H292R/H295R}$ mice would alter the gastric tissue. When sacrificing the mice, thickening of the gastric was already detected macroscopically (**Figure 30A**). Infected Rnf43$^{H292R/H295R}$ mice developed hyperplasia, atrophy and metaplasia in the corpus while wild type mice only showed some reactive changes upon infection. We established a pathologic score considering presence and severity of reactive changes, atrophy, hyperplasia and metaplasia observed in the stomach. Rnf43$^{H292R/H295R}$ mice displayed significantly higher pathology in the stomach compared to wild type mice upon *H. pylori* infection **Figure 30B** and **C**). To further characterize whether we could find SPEM or intestinal metaplasia in these mice, the presence of mucus and the intestinal mucin Muc2 were analyzed by PAS staining and immunohistochemistry, respectively (**Figure 30D**). While wild type mice did not express Muc2 in the stomach, metaplastic lesions of Rnf43$^{H292R/H295R}$ mice stained positive for this intestinal mucin, indicating that *H. pylori* induced intestinal metaplasia in these mice. Additionally, we analyzed proliferation in the stomach. While no overall differences could be observed between Rnf43$^{H292R/H295R}$ and wild type mice, lesions in the stomachs of Rnf43$^{H292R/H295R}$ mice were highly proliferative (**Figure 30E**). These results showed that transactivating mutations of RNF43 aggravate pathology induced by *H. pylori* infection.

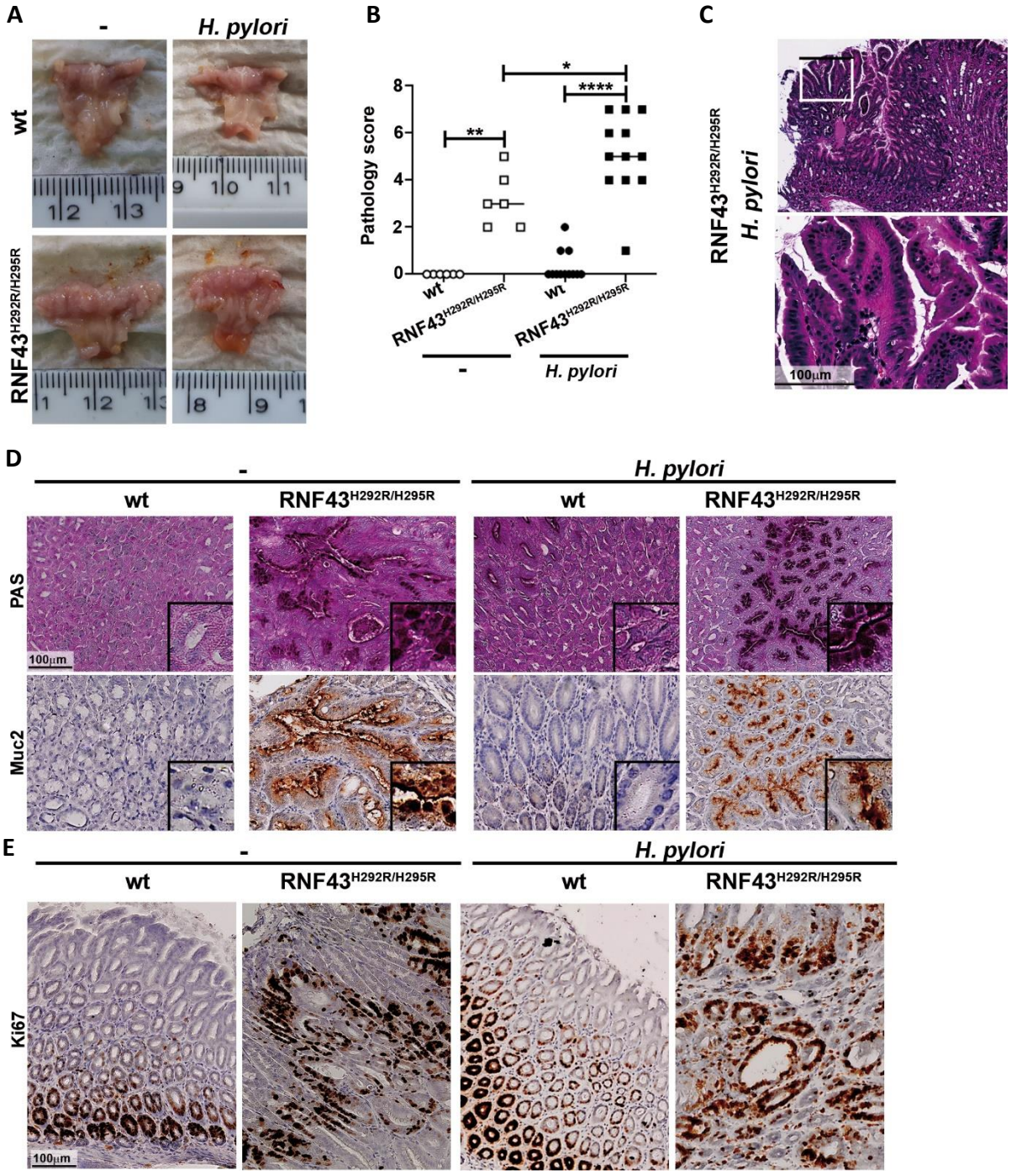


**Figure 30: Mutations in *Rnf43* aggravate gastric pathology upon chronic infection with *H. pylori*.** A) Representative images of murine stomachs resected from mice after infection with *H. pylori* for 6 months. B) Pathologic score of infected animals determined as presence of reactive changes, atrophy, hyperplasia and metaplasia. Each dot represents one mouse; horizontal bars indicate medians. Mann-Whitney U-Test. *P<0.05, **P<0.01, ****P<0.0001. C) Representative image of hyperplasia in mouse stomach after infection. D), E) Representative images of tissue sections stained with D) PAS or immunohistochemistry for Muc2 or for E) Ki67. Scale bars indicate 100 µm. Adapted and reprinted from [238] with permission from MDPI.

As mentioned before, infection with *H. pylori* has been shown to alter several pathways that are associated with the development of gastric cancer. Furthermore, *H. pylori* was reported to influence

the stem cell compartment by driving the expansion of LGR5$^{+}$ and CD44$^{+}$ cells and the downregulation of Sox2.

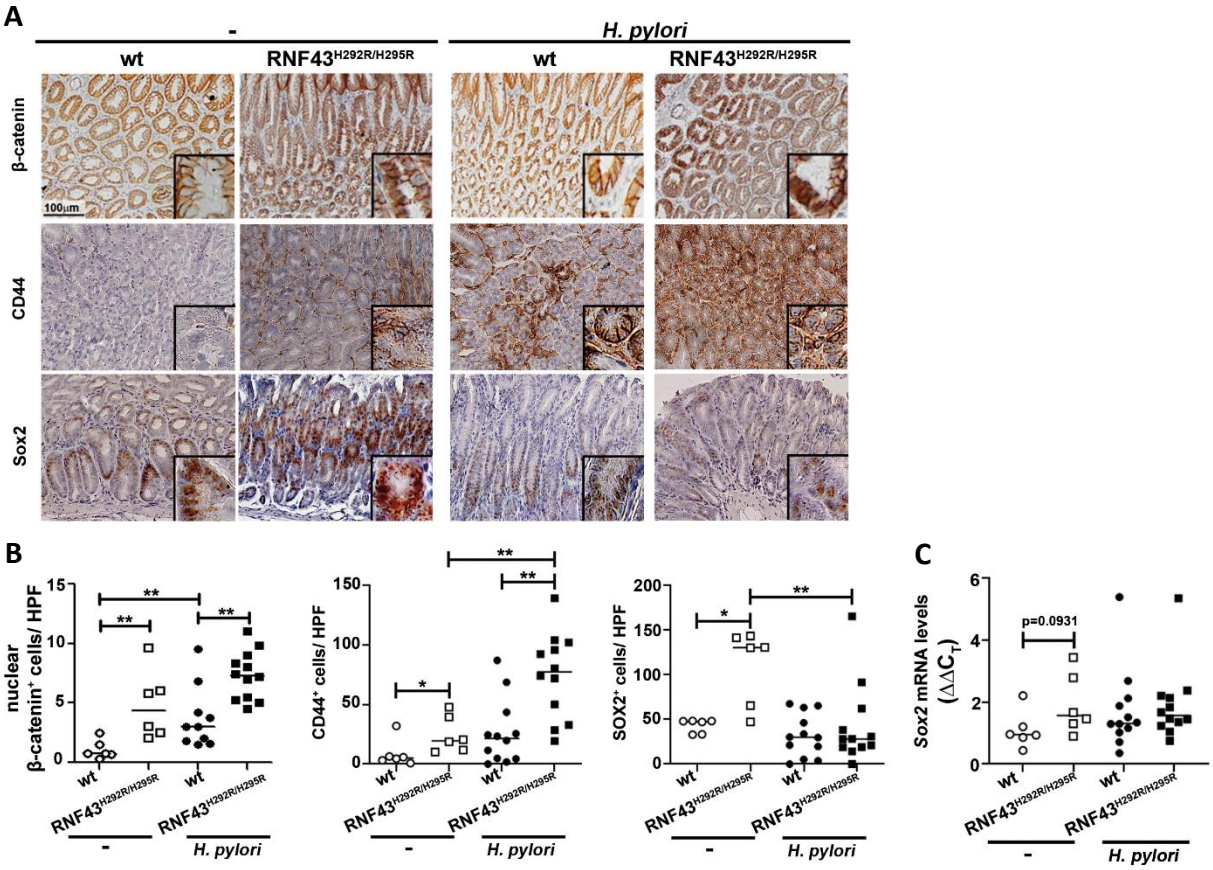


**Figure 31: Mutations in *Rnf43* alter carcinogenic pathways activated upon *H. pylori* infection.** A) Representative pictures of gastric tissue sections stained by immunohistochemistry obtained from *H. pylori* infected FVB/N and Rnf43$^{H292R/H295R}$ mice. Scale bar indicates 100 µm. B) Quantification of β-catenin, CD44 and Sox2 positive cells from five different high power fields of stained gastric tissue after 6 months of *H. pylori* infection. C) *Sox2* mRNA levels in the stomach of animals infected for 6 months. Values are normalized to *Gapdh* and shown as fold change to uninfected wild type mice. Each dot represents one mouse; horizontal bars indicate medians. Mann Whitney U-Test. *P<0.05, **P<0.01. Adapted and reprinted from [238] with permission from MDPI.

To analyze, whether mutation of Rnf43 alters those pathways and whether this adds to the alteration observed during *H. pylori* infection, we analyzed their activation status by immunohistochemistry and RT-qPCR. Staining of nuclear β-catenin showed that Wnt activity was enhanced in Rnf43$^{H292R/H295R}$ mice compared to wild type mice under basal conditions (**Figure 31A** and **B**). Notably, Wnt signaling was further activated upon *H. pylori* infection in both mouse lines. To further analyze the stem cell compartment, expression of Sox2 was examined by immunohistochemistry and RT-qPCR. While Rnf43

mutant mice showed increased Sox2 expression compared to wild type mice under basal conditions, it was downregulated upon *H. pylori* infection in these mice, whereas no changes were observed in wild type mice (**Figure 31**). Additionally, we analyzed the expression of $CD44^{+}$ cells in the gastric tissue. Under basal conditions, $Rnf43^{H292R/H295R}$ mice showed higher expression of CD44 compared to wild type mice. Upon infection, CD44 expression was enhanced in both mouse lines, leading to a higher overall expression in Rnf43 mutant mice compared to wild type mice under inflammatory conditions (**Figure 31A** and **B**). Taken together, these data showed that mutation of *Rnf43* in mice led to higher Wnt activity and an expansion of the Sox2 and CD44 positive stem cell compartment in the gastric tissue and these effects were further enhanced upon *H. pylori* infection.

As described before, enhanced NF-κB activation as detected by expression of the target gene *Cxcl1* was seen during infection of $Rnf43^{\Delta Exon8}$ mice with *H. pylori* for 3 months (**Figure 26**). In line with this, nuclear localization of p65 was increased in $Rnf43^{H292R/H295R}$ mice upon infection compared to wild type mice (**Figure 32A** and **B**). Gene expression analysis of the target genes *Cxcl10* (canonical NF-κB) and *Cxcl13* (non-canonical NF-κB) showed that only canonical NF-κB signaling was enhanced in Rnf43 mutant mice, whereas there were no differences in non-canonical NF-κB signaling between Rnf43 mutant and wild type mice (**Figure 32C**). These data implied that in $Rnf43^{H292R/H295R}$ mice, NF-κB signaling was hyperactivated upon infection with *H. pylori*.

To analyze whether STAT3 signaling would be differentially regulated in Rnf43 mutant mice, we stained tissue sections for phosphorylated STAT3 (pSTAT3). In $Rnf43^{H292R/H295R}$ mice STAT3 signaling was enhanced compared to wild type mice under basal conditions, but levels of pSTAT3 did not increase in Rnf43 mutant mice upon *H. pylori* infection compared to wild type infected mice (**Figure 32A** and **D**). Taken together, these results suggested that alteration of Rnf43 in mice leads to hyperactivation of STAT3 signaling. However, while in $Rnf43^{H292R/H295R}$ mice these changes were already observed under basal conditions, a further inflammatory trigger is necessary to hyperactivate STAT3 signaling in $Rnf43^{\Delta Eonx8}$ mice.

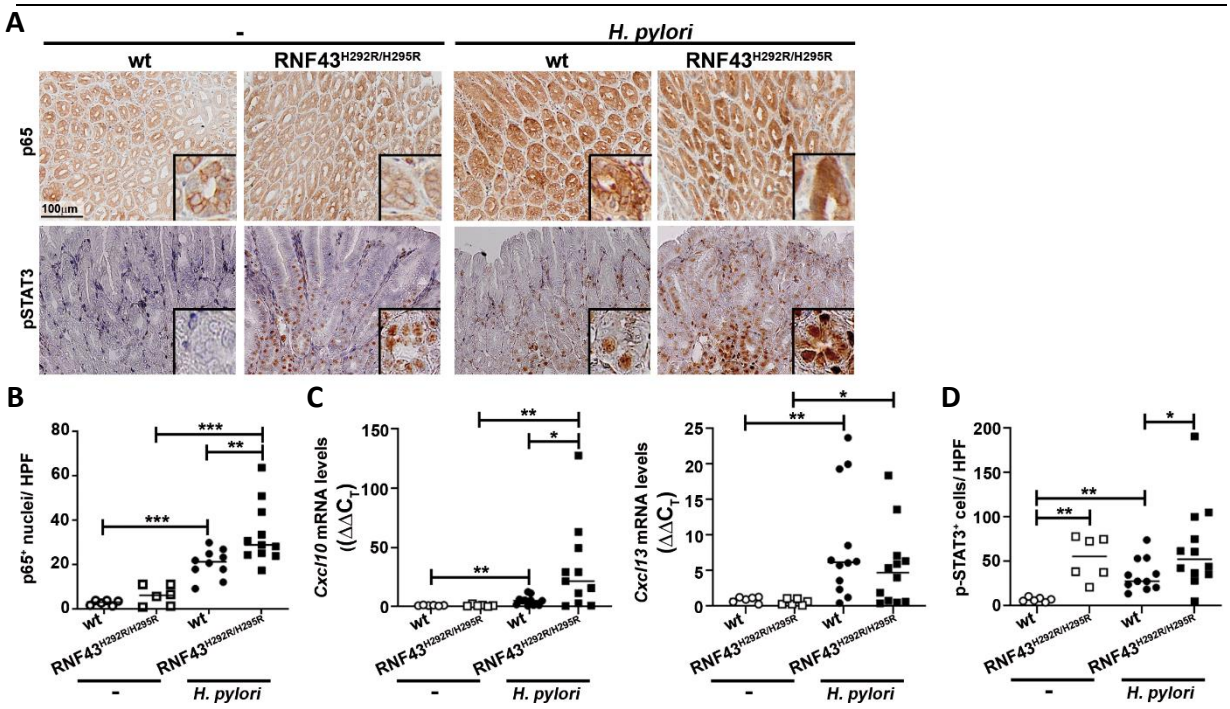


**Figure 32: *Rnf43* mutation alters activation of STAT3 and NF-κB signaling upon *H. pylori* infection.** A) Representative images of gastric tissue sections stained for p65 or pSTAT3 by immunohistochemistry after 6 months of *H. pylori* PMSS1 infection. Scale bar indicates 100 µm. B) Quantification of p65 expressing cells per high power field. C) mRNA levels of *Cxcl10* and *Cxcl13* in the stomach of control and infected mice. Values were normalized to *Gapdh* and are shown as fold change to uninfected wild type mice. D) Quantification of pSTAT3 positive cells per high power field. Each dot represents one mouse; horizontal bars indicate medians. Mann Whitney U-Test. *P<0.05, **P<0.01, ***P<0.001. Adapted and reprinted from [238] with permission from MDPI.

In summary we could show that pathways that are targeted by *H. pylori* were altered when Rnf43 was mutated in mice. Hyperactivation of Wnt, NF-κB and STAT3 signaling, as well as increased levels of gastric stem cell and cancer stem cell markers might be involved in aggravating *H. pylori* induced pathology leading to metaplasia and hyperplasia in Rnf43$^{H292R/H295R}$ mice.

## 5.5 Histopathological analysis of RNF43 in human gastric samples

*In vitro* and in different mouse models *in vivo* we could show that RNF43 was important in gastric tissue homeostasis and that it was involved in DNA damage response. To confirm this in human samples, we obtained a cohort of gastric biopsies from healthy individuals (n=20), patients with different types of gastritis (n=80), intestinal metaplasia (n=27, IM) and intestinal (n=30) as well as diffuse-type (n=25) gastric cancer from the Institute of Pathology (Klinikum Bayreuth). These samples were then analyzed for their RNF43 expression, proliferation and activation of DNA damage response.

Furthermore, several IM and gastric cancer samples were selected for sequencing to determine the mutational status of *RNF43* as well as other genes related to gastric carcinogenesis.

### 5.5.1 RNF43 is upregulated during gastritis

To analyze whether RNF43 is differentially expressed during gastritis, biopsies from patients with *H. pylori* induced gastritis (n=24), *H. pylori* eradicated gastritis (n=26) or C-type gastritis (n=30) were stained by immunohistochemistry.

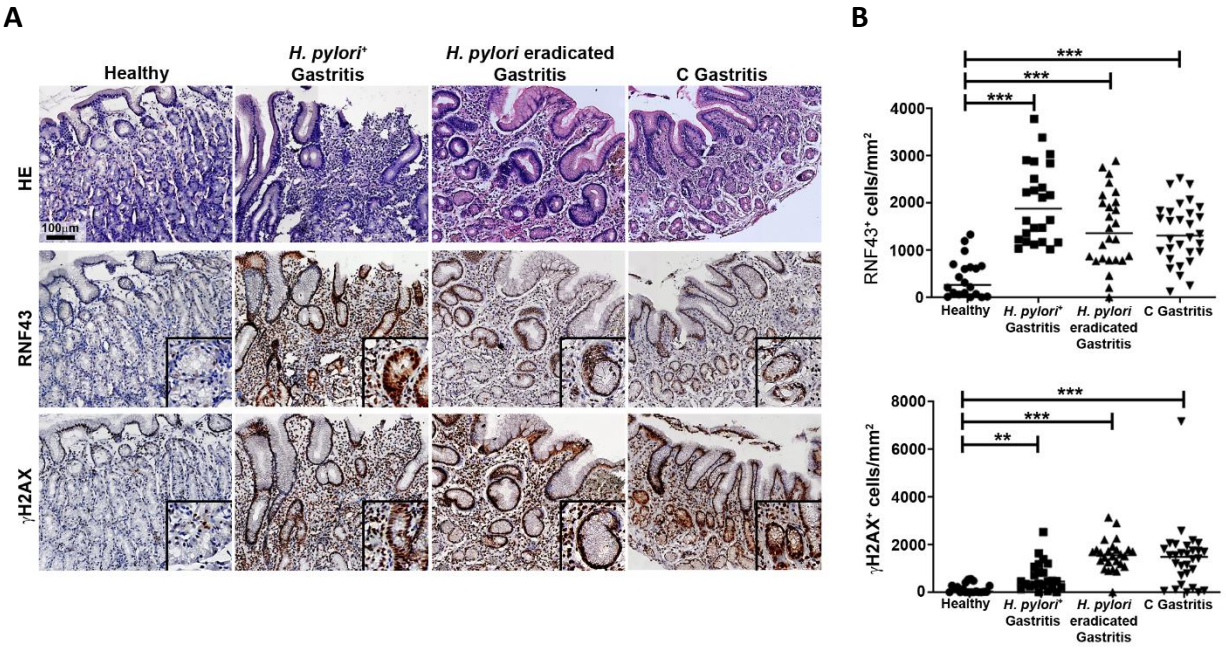


**Figure 33: RNF43 expression is upregulated during gastritis.** A) Representative images of biopsy samples from healthy individuals or gastritis patients stained with hematoxylin-eosin or for RNF43 and γH2AX by immunohistochemistry. Scale bar indicates 100 µm. B) Quantification of RNF43 and γH2AX positive cells in gastric biopsies. Each dot represents one biopsy sample; horizontal bars indicate median. One-way ANOVA followed by Dunn's multiple comparison test. **P<0.01, ***P<0.001. Adapted and reprinted from [235] with permission from Elsevier Inc.

Comparison with biopsies from healthy individuals showed that RNF43 was significantly upregulated in *H. pylori*-driven gastritis. RNF43 levels were also elevated in *H. pylori* eradicated or negative gastritis patients, however, to a lesser extent (**Figure 33**). These data showed that chronic gastritis leads to an upregulation of RNF43 expression in the stomach, confirming the results observed in our mouse models (**Figure 25**). Additionally, activation of DNA damage response was analyzed in these gastritis samples by staining the tissue for γH2AX. Compared to biopsies from healthy individuals, DNA damage response was highly activated in all three gastritis types (**Figure 33**). However, when

directly comparing RNF43 expression levels and phosphorylation of H2AX, we could not find a correlation between these two parameters.

### 5.5.2 RNF43 is upregulated during the course of malignant transformation and correlates with DDR

RNF43 was described to play an important role in tissue homeostasis, however, its expression pattern during the course of malignant transformation has not been investigated. To this end, we stained the obtained biopsy samples for RNF43 and evaluated its expression levels. As described above, RNF43 was upregulated during *H. pylori* driven gastritis. However, during progression to intestinal metaplasia, RNF43 was significantly down regulated compared to gastritis. It has to be noted that two groups could be detected in IM cases that either displayed higher levels of RNF43 than healthy individuals or had completely lost RNF43 expression. In intestinal-type gastric cancer, we detected significantly higher expression of RNF43 compared to healthy individuals. However, RNF43 expression varied strongly among patients. In diffuse-type gastric cancer, RNF43 levels were significantly lower compared to gastritis. Similar to IM, a subgroup of these samples did not express RNF43 at all, while other samples showed very high levels of RNF43 expression (**Figure 34A** and **B**).

Furthermore, we analyzed DDR activation in these samples to correlate it with RNF43 expression. As described above, DDR was highly activated in *H. pylori*-infected gastritis samples. Similar to RNF43 expression, DDR activation varied drastically among samples throughout malignant transformation. In IM as well as intestinal and diffuse-type gastric cancer a subset of patients did not or hardly displayed DDR activation in the malignant tissue indicating that DDR components might have been lost. On the other hand, some patients displayed quite high levels of active DDR signaling (**Figure 34A** and **B**). Additionally, we analyzed whether RNF43 expression could be associated with active DDR in gastric malignancies. Interestingly, we could find a positive correlation between RNF43 expression and γH2AX levels in IM samples as well as in biopsies from diffuse-type gastric cancer (**Figure 34C**). In contrast, no correlation was found in intestinal-type gastric cancer. In summary, these results show

that RNF43 is differentially expressed in different stages of gastric carcinogenesis and this could be positively correlated with active DDR signaling in IM and diffuse-type gastric cancer.

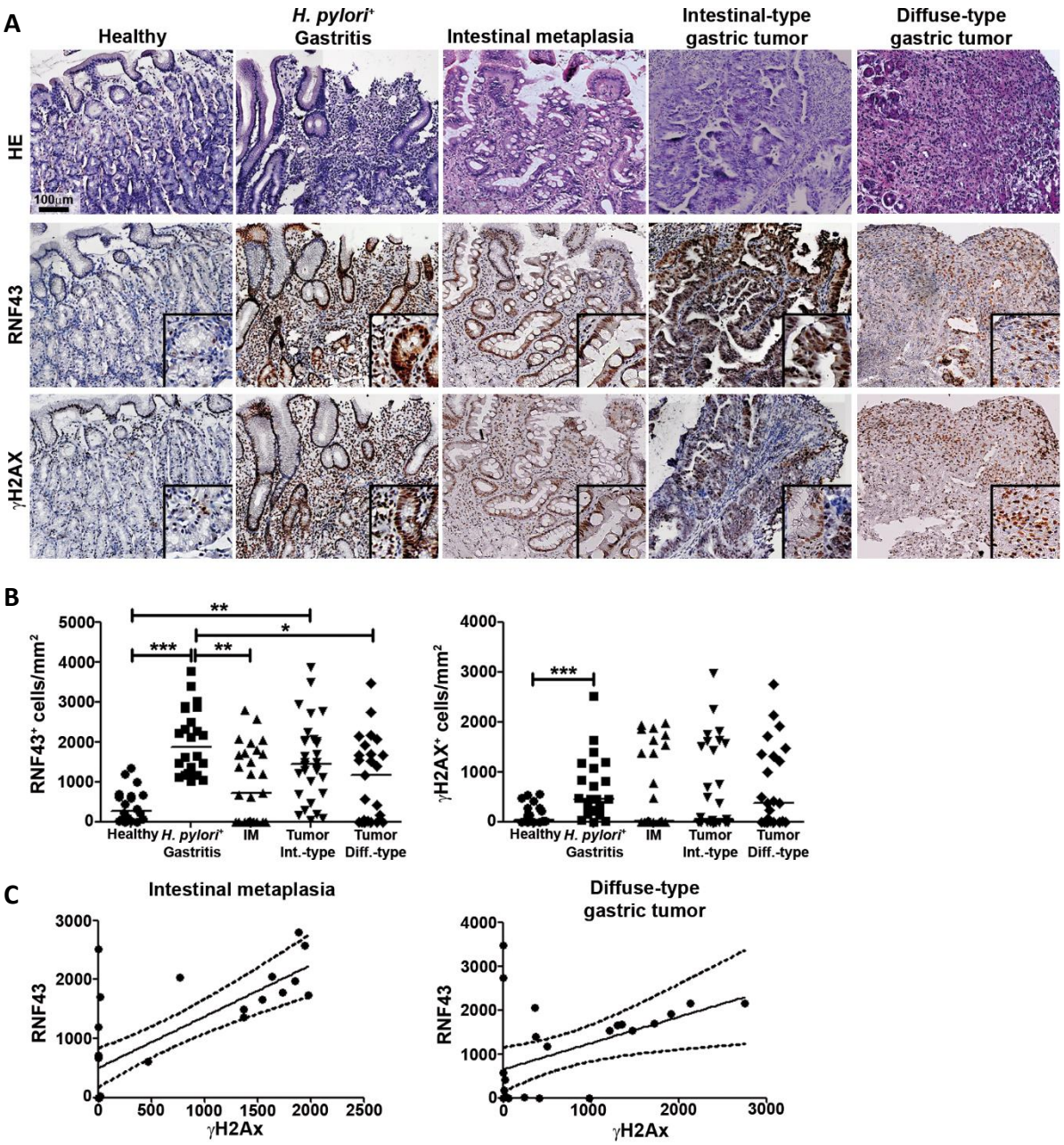


**Figure 34: RNF43 expression is differentially regulated during gastric carcinogenesis and correlates with DDR activation.** A) Representative images of gastric biopsies stained with hematoxylin-eosin or for RNF43 and γH2AX by immunohistochemistry. Scale bar indicates 100 µm. B) Quantification of RNF43 and γH2AX positive cells in stained biopsy samples. Each dot represents one biopsy sample; horizontal bars indicate medians. One-way ANOVA followed by Dunn's multiple comparison test. *P<0.05, **P<0.01, ***P<0.001. C) Linear regression of RNF43 and γH2AX. Each dot represents one biopsy sample, dashed lines indicate 95 % confidence interval. Adapted and reprinted from [235] with permission from Elsevier Inc.

### 5.5.3 *RNF43* is mutated in gastric cancer samples

*RNF43* has been described to be frequently mutated in late stages of gastric tumorigenesis. To verify this, we extracted DNA from intestinal metaplasia (n=12) as well as intestinal (n=15) and diffuse-type gastric cancer (n=13). In collaboration with the Institute of Pathology (TUM), genes related to gastric carcinogenesis were sequenced in these samples using Next-Generation Sequencing and an Ion Torrent system (Thermo Fisher). A summary of the sequencing results is depicted in **Table 32**. We found that SNPs in RNF43 are common in IM and gastric cancer patients. The variant I47V displayed the highest frequency of 57 % (24/42) while R117H, R343H, L418M and P686R were found in 38 % (16/42), 5 % (2/42), 48 % (20/42) and 21 % (9/42), respectively. While none of the IM cases analyzed showed *RNF43* mutations, we found *RNF43* mutations in 2 intestinal-type gastric cancers and in 2 diffuse-type gastric cancers. Sample GCi 14 carried a synonymous R371R mutation and the point mutation D628G (Cosmic mutation ID: COSM3195615) along with a mutation in Cyclin D1 (CCND1). In the second intestinal-type tumor (GCi 15) we found the mutation R132X (COSM981870) leading to a premature stop codon. This tumor also carried mutations in F-Box and WD Repeat Domain Containing 7 (FBXW7), Ras homolog family member A (RHOA) and AT-Rich Interaction Domain 1A (ARID1A). The diffuse-type tumor sample GCd 4 carried the frameshift mutation R584fs, which had not been described before, as well as mutations in *ERBB2* and *CDH1*. In GCd 9, we found the mutation R132X in *RNF43* as well as a mutation in *p53*. None of these tumors had lost RNF43 expression but displayed elevated RNF43 expression levels compared to healthy individuals. It has to be noted that the antibody used for IHC binds to its epitope in the amino acid region C298 – H427 and therefore cannot detect the mutant RNF43 R132X protein. However, RNF43 expression could still be detected in these tumors indicating that the mutation is heterozygous, and the cells still carry one wild type allele or that not all cells carry this mutation due to tumor heterogeneity. Interestingly, the intestinal-type tumors with *RNF43* mutation showed either none or low DDR activation, while the diffuse-type tumors showed elevated DDR activation. In summary, we found *RNF43* mutations in 14.3 % of gastric tumors while no

mutations were found at earlier stages, indicating that alteration of RNF43 is an important step in the transition to carcinoma.

**Table 32: Mutations found in intestinal metaplasia (n=12), intestinal- (n=15) and diffuse-type (n=15) gastric cancer.**

| Sample | RNF43 SNPs | RNF43 mutations | Other mutations |
|---|---|---|---|
| **Intestinal metaplasia** | | | |
| IM 1 | p.I47V<br>p.R117H<br>p.P686R | | APC p.A1471Gfs*14<br>BRAF p.N581S |
| IM 2 | p.I47V<br>p.R117H | | APC p.R1445fs<br>KRAS p.G13D |
| IM 3 | p.R117H<br>p.P686R | | |
| IM 4 | Wt | | ERBB4 p.L713V |
| IM 5 | p.I47V<br>p.R117H<br>p.L418M | | APC p.R1432X |
| IM 6 | p.R117H<br>p.P686R | | |
| IM 7 | p.R117H | | |
| IM 8 | p.I47V<br>p.L418M<br>p.P686R | | |
| IM 9 | p.R117H<br>p.L418M | | |

| | | | |
|---|---|---|---|
| IM 10 | p.I47V | | |
| IM 11 | p.R117H | | |
| IM 12 | p.I47V<br>p.R117H<br>p.L418M | | |
| **Gastric cancer intestinal** | | | |
| GCi 1 | p.I47V<br>p.R117H<br>p.L418M | | PTPRT p.P1075Rfs<br>PIK3CA p.E542K<br>TLR4 p.L10M |
| Gci 2 | p.P686R | | ERBB2 p.V842I |
| Gci 3 | p.R117H<br>p.P760P | | MDM2 amplification |
| Gci 4 | Wt | | Sox2 p.E36G<br>APC p.R1432X<br>PREX2 p.L50V<br>TP53 p.G66R |
| Gci 5 | p.I47V<br>p.R117H<br>p.L418M | | TP53 p.E204X |
| Gci 6 | p.I47V<br>p.L418M<br>p.P686R | | TP53 p.R116Q<br>TP53 p.Y88H<br>CDKN2A p.Q50H |
| Gci 7 | p.I47V<br>p.R117H | | TLR4 p.L298V<br>PTPRT p.E911G |
| Gci 8 | p.I47V<br>p.L418M | | ARID1A p.P1467fs<br>PTEN M134T |

| | | | |
|---|---|---|---|
| | p.P686R | | TP53 R151H |
| Gci 9 | Wt | | |
| Gci 10 | p.I47V<br>p.L418M | | |
| Gci 11 | p.I47V<br>p.R343H<br>p.L418M | | CDKN2A p.Q70X<br>PTEN p.R130X<br>TGFBR2 p.D405N |
| Gci 12 | R117H | | |
| Gci 13 | p.I47V<br>p.L418M | | TP53 p.G134E<br>APC p.R1432X |
| Gci 14 | p.I47V<br>p.R117H | p.R371R<br>p.D628G | CCND1 p.S257P |
| Gci 15 | | p.R132X | FBXW7 p.A508D<br>RHOA p.Y42C<br>ARID1A p.P2095fs |
| **Gastric cancer diffuse** | | | |
| GCd 1 | p.I47V<br>p.L418M | | PREX2 p.R186Q |
| GCd 2 | p.I47V<br>p.R117H<br>p.P686R | | |
| GCd 3 | | p.R584fs | ERBB2 p.R678Q<br>CDH1 p.E429G |
| GCd 4 | p.I47V<br>p.L418M | | |

| | | | |
|---|---|---|---|
| GCd 5 | p.L418M | | CDH1 p.D254H |
| GCd 6 | p.I47V<br>p.L418M | | |
| GCd 7 | | p.R132X | TP53 p.R117M |
| GCd 8 | p.I47V<br>p.R343H<br>p.L418M | | ARID1A p.R2158L<br>CDH1 c.531+1G>T |
| GCd 9 | p.I47V<br>p.L418M | | CDH1 p.E243K |
| GCd 10 | p.I47V<br>p.L418M | | KRAS p.G13D<br>TP53 p.R150W<br>PIK3CA p.N345K<br>PIK3CA p.A1066V<br>MTOR p.R2317I |
| GCd 11 | p.P686R | | |
| GCd 12 | p.I47V<br>p.L418M | | |
| GCd 13 | p.I47V<br>p.L418M | | PIK3CA p.H1047R |

### 5.5.4 N-terminal but not C-terminal mutations in RNF43 confer resistance to radio- or chemotherapy

In AGS$^{D196fs}$ cells, we could show that a truncating mutation conferred resistance to radio- and chemotherapy (**Figure 18** and **Figure 19**). However, this mutation has never been reported in gastric cancer samples. Therefore, we sought to analyze whether the RNF43 mutations R132X and R584fs found in our biopsy cohort could also influence susceptibility to γ-irradiation or chemotherapy. Thus,

we set out to introduce these mutations into AGS cells via CRISPR/Cas9 RNPs. However, when we screened the obtained cells, none of the analyzed clones carried the exact desired mutations. Thus, we selected clones that displayed truncating mutations in close proximity to the R132X (A136fs) or the R584fs (Q577fs) mutations for further screening. When subjecting these cells to γ-irradiation and seeding them in clonogenicity assays, $AGS^{Q577fs}$ cells showed a reduction in single cell expansion similar to wild type AGS cells. In contrast, $AGS^{A136fs}$ cells showed higher proliferative capacity upon irradiation indicating that this mutation conferred resistance to treatment (**Figure 35A** and **B**). Similarly, chemotherapeutic treatment reduced cell viability of $AGS^{Q577fs}$ cells comparable to wild type cells while $AGS^{A136fs}$ cells were more resistant to administration of 5-FU or cisplatin than wild type AGS cells (**Figure 35C**). Taken together, these results showed that an early truncating mutation in RNF43 confers resistance to DNA damage inducing radio- or chemotherapy while late mutations downstream of the functional domain did not change therapy response.

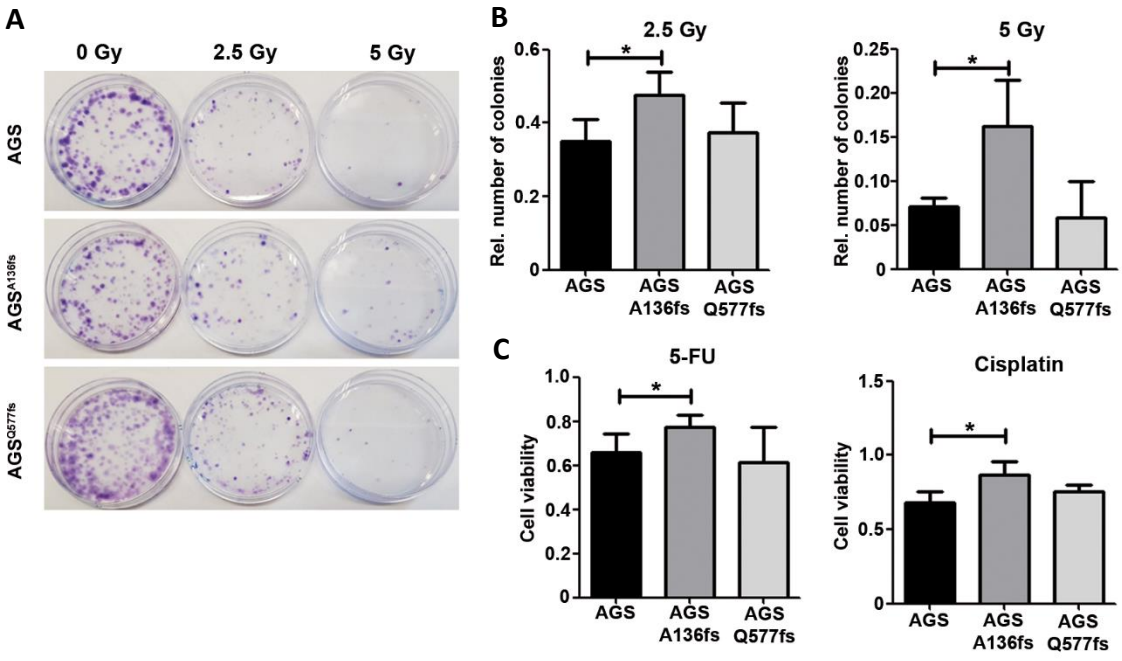


**Figure 35: Early but not late frameshift mutations in RNF43 influence susceptibility to radio- and chemotherapy.** A) Representative images of AGS cells grown in single cell colonies for 2 weeks after γ-irradiation. B) Quantification of single cell colonies normalized to untreated control cells. C) Cell viability measured after treatment with 5-FU or cisplatin for 48 h measured at OD 450/600 nm after addition of CCK-8. Values are normalized to untreated control. Bars indicate mean ± SD from four different experiments. Student's t-test. *P<0.05. Adapted and reprinted from [235] with permission from Elsevier Inc.

# 6 Discussion

## 6.1 RNF43 acts as a tumor suppressor in the stomach

RNF43 has been proposed to function as a tumor suppressor by negatively regulating Wnt signaling in the colon and pancreas. In the stomach, mutations in *RNF43* have been described to be driving mutations in gastric carcinogenesis. This suggested that the protein plays an important role during tissue homeostasis. When first discovered, RNF43 was described to be an oncogene overexpressed in hepatocellular carcinoma [155] as well as colorectal cancer [239]. However, following studies have shown that RNF43 acts as a tumor suppressor, since transient knock down of RNF43 led to increased proliferation of colorectal cancer cell lines [240]. In the stomach, this role was confirmed in two studies where overexpression of RNF43 in gastric cell lines inhibited proliferation *in vitro* as well as in a xenograft mouse model. RNF43 was shown to negatively regulate stem-cell like properties in gastric cells since RNF43 overexpression led to reduced sphere formation and downregulation of the stem cell markers CD44 and CD54 [159, 160]. In line with that, we could show that loss of endogenous RNF43 in the gastric cancer cell lines AGS and MKN45 increased their tumorigenic potential *in vitro*. This tumor suppressive role for endogenous RNF43 in gastric cells was confirmed in a xenograft tumor model, where we observed that RNF43 related to expression of stem cell markers. Thus, xenograft tumors derived from RNF43 *knock down* cells showed increased expression of the stem cell marker SOX2 and the cancer stem cell markers CD44 and ALDH1. This data suggested that RNF43 is important in gastric tissue homeostasis by negatively regulating stemness.

To further explore the role of endogenous RNF43 in gastric homeostasis, we generated two mouse models lacking Rnf43 function. In these mice, we could detect changes in the epithelial architecture of the stomach with increasing age. *Rnf43*$^{\Delta Exon8}$ mice showed thickening of the mucosa, hyperproliferation and multifocal hyperplasia from 16 weeks of age on, while Rnf43$^{H292R/H295R}$ mice showed similar changes from 4 weeks of age on. However, even older mice at 40 weeks of age did not developed neoplasia. Thus, loss of Rnf43 function leads to some changes in tissue architecture but is

not sufficient to induce carcinogenesis. *RNF43* mutations have been reported to be associated with mutations in *BRAF* in colorectal cancers [163, 241] and to emerge during the transition from adenoma to early gastric cancer [151]. These observations suggest that mutations in *RNF43* co-occur with mutations in oncogenes and when neoplastic changes have already established, respectively. This was further confirmed in the pancreas, where loss of Rnf43 in *KRAS* mutated mice did accelerate malignant progression while pathology at the early age was mainly driven by the *KRAS* mutation [242]. Previous studies using Rnf43 *knock out* mice showed that loss of Rnf43 function was not sufficient to induce malignant changes in the intestine. However, these studies solely described the phenotype in intestine and colon of these mice and did not analyze other organs. In these mouse models, only knock out of a second ubiquitin ligase, ZNRF3 [142], or induction of DSS colitis [240] led to hyperproliferation of intestinal cells and larger colorectal tumors, respectively. Thus, a second trigger such as inflammation might be needed to induce neoplastic changes in the gastrointestinal tract of mice with Rnf43 loss of function. To explore this, we infected our mice with *H. pylori*, as this infection is the major risk factor for gastric cancer. *H. pylori* infection is characterized by a chronic inflammation of the gastric epithelium that can activate oncogenic pathways, thereby driving the carcinogenic processes.

*Rnf43* expression was upregulated in wild type mice infected for three months. RNF43 was described to be a direct Wnt target gene [157, 158] and Wnt signaling was shown to be upregulated during *H. pylori* infection [11, 43]. Indeed, we detected increased levels of nuclear β-catenin in wild type mice upon infection. Therefore, upregulation of Rnf43 may be mediated by increased Wnt activity.

Rnf43 loss of function mice showed higher inflammation compared to wild type mice and this was accompanied by decreased bacterial loads after three months of infection. This was in line with previous studies, where an inverse correlation between bacterial colonization and inflammation was described for infection of mice with *H. pylori* [243, 244]. Higher inflammation in Rnf43 loss of function mice was detected by infiltration of inflammatory cells, such as T cells and neutrophils and macrophages. In both mouse lines, we could detect increased levels of *Cxcl1* compared to wild type mice upon infection, indicating increased NF-κB signaling. Furthermore, we detected increased levels

of Wnt activity in Rnf43$^{H292R/H295R}$ mice compared to wild type mice after 6 months of infection. It has been reported for several cell types that Wnt signaling can regulate NF-κB activity. In bronchial epithelial cells, Wnt inhibitors led to decreased expression of NF-κB target genes in an β-catenin-dependent manner [245], while canonical Wnt signaling induced expression of receptors of the TNF receptor family that were shown to induce NF-κB signaling in colorectal cells [246]. Additionally, it was shown that βTRCP, which is a direct target gene of Wnt signaling, could also target IκB, an inhibitor of NF-κB signaling, for degradation, thereby activating this pathway [247]. Thus, increased Wnt activity in Rnf43$^{H292R/H295R}$ mice could contribute to enhanced NF-κB signaling. The resulting increase in *Cxcl1* may lead to increased recruitment of innate and subsequently adaptive immune cells, which account for the elevated expression of the cytokines *Ifng* and *Il-17* upon infection of Rnf43 loss of function mice.

We detected increased activity of STAT3 signaling pathway in Rnf43$^{H292R/H295R}$ and *Rnf43$^{\Delta Exon8}$* mice compared to wild type mice. STAT3 signaling was shown to be upregulated upon infection with *H. pylori* [248] and has been linked to gastric carcinogenesis [249]. This pathway is activated by several cytokines such as IL-6 which are secreted by infiltrating immune cells [250], and thereby directly linked to NF-κB mediated recruitment of these cells [251]. Thus, higher activation of NF-κB signaling in Rnf43 deficient mice can potentially increase STAT3 activity upon *H. pylori* infection through an increased recruitment of immune cells. Furthermore, STAT3 signaling has been linked to the Wnt pathway. A TCF binding domain was identified on the promoter of STAT3, indicating that it might be a direct Wnt target gene [252]. Additionally, it was shown that Wnt can mediate Src dependent phosphorylation of STAT3, thereby activating the pathway [253]. Therefore, it is possible that increased β-catenin levels in Rnf43$^{H292R/H295R}$ mice induced the elevated levels of pSTAT3 detected in these mice under basal conditions.

We further studied the effects of chronic inflammation by infecting Rnf43$^{H292R/H295R}$ mice with *H. pylori* for six months. Under inflammatory conditions, these mice developed hyperplasia and atrophy, while wild type mice only displayed some reactive changes. Parietal cell atrophy was shown to induce

intestinal metaplasia in mice [254]. As mentioned before, this type of metaplasia is characterized by the *de novo* expression of intestinal mucins such as MUC2 in the gastric epithelium. Upon infection, we could detect Muc2 expressing metaplastic cells in *Rnf43* mutant mice, but not in wild type mice. Intestinal Muc2 positive metaplasia has been described to occur in gerbils upon chronic *H. pylori* infection [36]. In human gastric tumors of the intestinal-type, MUC2 was shown to be highly expressed and to be associated with chronic inflammation as defined by infiltration of lymphocytes [255]. Indeed, we could observe that inflammation in Rnf43$^{H292R/H295R}$ mice upon long-term infection was rather driven by the infiltration of lymphocytes than neutrophils and mast cells, since numbers of CD3$^{+}$ cells were significantly increased compared to uninfected controls, while numbers of CAE$^{+}$ cells were not.

CD44 has been described as a putative gastric cancer stem cell marker, and it was shown to be upregulated during *H. pylori* infection [256] and to play a role in *H. pylori*-driven pathology. Cancer progression in infected gerbils depended on CD44 expression [257] and *H. pylori*-induced metaplasia as well as cancer progression was associated with CD44 expression in patients [258, 259]. Additionally, CD44 was shown to be upregulated by Wnt signaling [21, 260]. We detected increased expression levels of CD44 in the stomach of Rnf43$^{H292R/H295R}$ mice, which might be caused by increased Wnt activity in Rnf43$^{H292R/H295R}$ mice compared to wild type mice. This increased CD44 expression potentially contributes to the worsened pathology observed in these mice. Interestingly, CD44 was shown to be regulated by NF-κB signaling in breast and ovarian cancer cells [261-263]. Thus, elevated levels of CD44 in Rnf43$^{H292R/H295R}$ mice upon *H. pylori* infection might be additionally regulated by increased NF-κB signaling activity observed in these mice.

In contrast to our mouse model, most human individuals infected with *H. pylori* are infected at early age and acquire mutations in *RNF43* or other genes only much later during gastric carcinogenesis. *RNF43* germline mutations have been rarely described and were so far only linked to serrated polyposis of the colon [162, 264, 265]. This suggests that mutations in other genes than *RNF43* are responsible for the initiation of neoplastic changes of the stomach. However, it is possible that

acquired *RNF43* mutations in *H. pylori* infected individuals contribute to gastric carcinogenesis by the mechanisms we detected in our mouse models, since the pathways altered in Rnf43 loss of function mice are highly associated with the development of gastric cancer in humans [13, 266, 267]. To prove this, an animal model that develops gastric cancer upon *H. pylori* infection such as Mongolian gerbils could be used. Combining this model with an inducible knock out of Rnf43 could help to elucidate whether loss of Rnf43 function worsens pathology when infection has already established. Furthermore, comparative studies in patients with *H. pylori*-driven neoplasia in the stomach could show whether activity of carcinogenic pathways differs in patients carrying *RNF43* mutations compared to patients with wild-type *RNF43*.

As mentioned before, *RNF43* was described to be frequently mutated in gastric cancer patients suggesting an important role during carcinogenesis. These mutations were found to drive gastric carcinogenesis [167] and to occur in high-grade dysplasia and at the transition from adenoma to carcinoma [151]. In contrast, a more recent study found *RNF43* mutations in adenoma and carcinoma and also in low-grade dysplasia. However, patient number was limited in this study [169]. In line with the former study, our data suggest that *RNF43* mutations occur at later stages, since we could detect RNF43 mutations only in gastric cancer, but not in intestinal metaplasia. In total, we could detect mutations in 4 out of 28 gastric cancer samples, which account for 14.3 % of the analyzed cases. In literature, frequency of RNF43 mutations in gastric cancer varies drastically, ranging from 3 % [30] to 35 % [151, 168]. Interestingly, we found 2 mutations that were already detected before, R132X (COSM981870) and D628G (COSM3195615), while the third mutation R584fs has not been described yet. In gastric cancers, RNF43 expression was shown to be downregulated [159, 160], yet, how RNF43 is regulated during earlier stages of carcinogenesis has not been described. We found RNF43 expression to be upregulated in human gastric tissue samples presenting with chemoreactive as well as *H. pylori*-induced gastritis. This was in line with the observations made in Rnf43 wild type mice upon infection. As postulated in the mouse model, RNF43 upregulation might be due to enhanced levels of Wnt activity, that can be directly induced by *H. pylori* infection [43]. In IM, RNF43 expression was

significantly downregulated compared to gastritis, and was completely lost in some of the samples. Similarly, diffuse-type gastric cancers did either express high levels of RNF43 or were mostly negative for protein expression. In contrast, all intestinal-type tumors expressed RNF43 and expression was significantly higher than in healthy tissue. As mentioned before, RNF43 was described to be downregulated in gastric tumors; however, these studies did not distinguish between diffuse- and intestinal-type gastric cancer. Furthermore, samples were not analyzed for *RNF43* mutations [159, 160], and thus, it is not possible to distinguish whether these samples were truly negative for RNF43 or the protein was not detectable due to truncating mutations. In other cancer entities, such as hepatocellular carcinoma and colorectal cancer, RNF43 expression was also described to be upregulated [157, 268], indicating that RNF43 is expressed differentially in tumors. In our study, all tumors carrying RNF43 mutations displayed elevated expression of RNF43. It has to be noted that the truncated protein resulting from the R132X mutation could not be detected by the antibody used. Thus, the detected mutation is either heterozygous and the wild type copy was detected or only a subset of tumor cells is carrying this mutation. In a previous study, mutated RNF43 G659fs was still detected in gastric and colorectal cancer samples, while the second mutation R117fs could not be detected by the antibody used since the recognized epitope is lost in this early frameshift mutation [269]. In line with this study, our data showed that RNF43 expression is not lost in gastric cancers with mutations in this protein, but the truncated protein could be detected in these samples. However, whether this truncated protein would still be functional needs further investigation.

## 6.2 RNF43 exerts its tumor suppressive function in the stomach by regulating DNA damage response

Previous studies and our results showed that RNF43 has a tumor suppressive function in the stomach. However, how endogenous RNF43 could influence gastric tissue homeostasis and act as a tumor suppressor in the stomach was unclear, since previous studies were conducted under overexpression

conditions. This study aimed at deciphering through which signaling pathways endogenous RNF43 exerts its tumor suppressive function in the stomach.

In colon cancer cells, RNF43 was suggested to have a tumor suppressive function by negatively regulating Wnt signaling. Several studies have localized overexpressed RNF43 at the cellular membrane where it ubiquitinates Fz receptors, thereby targeting them for degradation [142]. Also, at the cellular membrane, it gets bound and internalized in a complex together with R-spondins and LGR receptors [143]. When located in the nucleus of intestinal cells, RNF43 was shown to sequester TCF4 to the nuclear membrane, thereby inhibiting Wnt target gene expression [157]. In gastric cells, it was shown that RNF43 overexpression enhanced protein levels of Wnt signaling components such as LGR5 and the Wnt target gene *c-MYC*. However, these proteins were shown to also be regulated by other pathways, such as EGFR signaling [270-272]. Furthermore, this study did not analyze the subcellular localization of RNF43, nor the expression of Fz receptors upon overexpression of RNF43. Therefore, a direct mechanistic link between RNF43 and Wnt signaling in gastric cells has not been established. We observed endogenous RNF43 in the nucleus of gastric cancer cells, thereby ruling out that RNF43 could interact with Fz receptors at the cellular membrane. Additionally, we could not observe changes in nuclear β-catenin in tumors derived from RNF43 depleted cells, indicating that RNF43 may not regulate this signaling pathway in gastric cells. When comparing expression levels of *Lgr5* and *Axin2* in our mouse models, we could not see a consistent upregulation of these Wnt target genes in the stomach of mice lacking Rnf43 function. Interestingly, $Rnf43^{H292R/H295R}$ mice displayed higher levels of nuclear β-catenin in the stomach compared to wild type mice, while $Rnf43^{\Delta Exon8}$ mice did not. Indeed, the mutated $RNF43^{H292R/H295R}$ variant was shown to transactivate Wnt signaling *in vitro* [157], which might account for elevated β-catenin levels, while the loss of the RING domain in $Rnf43^{\Delta Exon8}$ mice did not have an influence on Wnt activity. This suggests that loss of endogenous Rnf43 function does not elevate Wnt signaling in the stomach, but only transactivating mutations increase Wnt activity. However, why elevated β-catenin levels in $Rnf43^{H292R/H295R}$ mice did not translate into increased expression of *Axin2* and *Lgr5*, remains to be elucidated. Taken together, our results propose that

RNF43 exerts its tumor suppressive function through a different mechanism than regulating Wnt signaling in the gastric epithelium.

Considering its subcellular localization, RNF43 is suggested to exert its tumor suppressive function by a mechanism localized in the nucleus. Interestingly, other E3 ubiquitin ligases have been described to be involved in DDR signaling and were shown to be important for initiation [166, 228] as well as maintenance of DDR [230]. Phosphorylation of H2AX by ATM is mediated through monoubiquitination of the histone by RNF2/RNF51 at the lysine residue K119/K120 [166, 228], whereas recruitment of repair factors such as BRCA1 and 53BP1 are dependent on linkage of K63-linked ubiquitin chains by RNF8 and RNF168. Additionally, RNF168 was described to monoubiquitinate the histones H2A and H2AX at K13/K15 to drive DDR signaling [231]. A possible link between RNF43 and DDR was firstly proposed in pancreatic duct cells, where loss of RNF43 protein led to a decrease in DDR activation upon treatment of these cells with UV light [232]. However, this study did not investigate by which mechanism RNF43 might be involved in DDR. Additionally, UV-light was used here to induce DNA damage, which does not play a role during carcinogenesis in the gastrointestinal tract or cancer therapy. In our study, we used clinically relevant DNA damage-inducing agents such as γ-irradiation. Loss of RNF43 in gastric cancer cells changed the ubiquitination pattern of γH2AX at K48 and K63 residues upon irradiation. While K48-linked ubiquitination was described as the canonical signal for proteasomal degradation [273], K63 linkage of ubiquitin was described to be involved in protein kinase activation, for example in NF-KB signaling [274]. Therefore, whether RNF43-mediated K48 ubiquitination is involved in DDR signaling, remains to be elucidated. For K63-linkage, which is important in DDR, RNF43 could be a key ubiquitin ligase since loss of the protein reduces DDR signaling and especially H2AX phosphorylation. However, since DDR activation is not completely lost upon RNF43 depletion in gastric cells, other E3 ubiquitin ligases might serve as redundant proteins. So far, no data has been published that describes which lysines RNF43 preferentially ubiquitinates. Studies on ZNRF3 and RNF43 mediated Frizzled ubiquitination have not analyzed which residue is important for this modification, but have only used mutagenesis of all lysine residues at once [142, 156]. Thus,

whether RNF43 generates K48 and K63 linked ubiquitin chains and whether this could account for its involvement in DDR needs further investigation.

When DDR is impaired, two distinct outcomes are possible. This can either render cells more susceptible to DNA-damaging agents since repair mechanisms are not activated, or confer resistance to DNA damage, when apoptosis is not induced. When accumulation of DNA damage impairs cellular functions and leads to senescence or cell death for example by depletion of ATM function, cells show more sensitivity to radiotherapy in bladder cancer [275] as well as tumor endothelium [276]. In contrast, loss of DDR function can prevent p53-mediated apoptosis upon DNA damage, thereby conferring resistance to DNA damaging irradiation. This was shown in glioma cells, where loss of Chk2 induced reduced response to ionizing radiation *in vivo* [277]. Additionally, *p53* mutations were associated with resistance to radiotherapy in B-lineage chronic lymphocytic leukemia cells [278]. Similarly, we observed that impaired DDR activation in our model through loss of RNF43 led to enhanced cell viability in gastric cancer cell lines upon γ-irradiation. By AnnexinV/PI stainings, we could show that this was due to impaired activation of apoptosis in RNF43 depleted cells. Thus, our findings suggest that loss of RNF43 function confers resistance to treatment with γ-irradiation.

*H. pylori* was shown to directly induce DNA damage. Similar to our findings after ionizing radiation, we observed impaired DDR activation upon loss of RNF43 function in gastric cells as well as in *Rnf43*$^{\Delta Exon8}$ mice upon infection with *H. pylori*. *In vivo*, this resulted in reduced induction of apoptosis in the stomach. In gastric cells, it has been shown that ongoing infection leads to chronic DNA damage and that infected cells lose their proliferative capacity and display senescence [112]. Yet, whether loss of RNF43 function abolishes this senescent phenotype, remains to be elucidated. On a functional level, induction of DSBs was shown to be important for infection-mediated upregulation of NF-κB signaling [114]. When infecting mice with RNF43 loss of function, we observed enhanced levels of NF-κB target gene expression, such as *Il-1β* and *Cxcl10*. It is tempting to speculate that impaired DDR activation in these mice impedes efficient DNA repair which allows for sustained NF-κB target gene expression, thereby increasing inflammation and worsening pathology of *H. pylori* infection.

We confirmed a role for RNF43 in DDR activation in our human gastric biopsy cohort. To correlate RNF43 expression to DDR activation, tissue samples were stained for γH2AX. We detected that DDR was highly activated in all types of gastritis. As described above, *H. pylori* was shown to directly induce DDR in gastric cells *in vitro* [112], and DNA damage was also linked to *H. pylori*-induced gastritis in patients [279]. C-gastritis is often induced by influx of bile acids and these have been shown to induce DNA damage in cells of the gastrointestinal tract [280, 281]. Inflammatory-related DNA damage induced by ROS and RNS has also been linked to Barrett's esophagus [282, 283], which is also caused by chemically-induced inflammation, and thus, DDR activation in C-gastritis might be also caused by ROS and RNS. In a recent publication, γH2AX was shown to be slightly increased in biopsies with IM, and an increase in DDR activity was detected during the progression from IM to intestinal-type gastric cancer, which was in line with the observations made in our cohort of gastric biopsies. However, in this cohort, IM cases with low or no DDR activation was also detected [284]. In our study, we detected either high levels of γH2AX in one group of IM patients or no activation at all in the other group. In diffuse-type gastric cancer, components of the DDR were shown to be upregulated, indicating that the pathway is also activated in this cancer subtype [285]. However, we observed high variability in our cohort, since we could detect samples with high as well as samples with low DDR activation similar to what was observed in IM samples. Interestingly, we could detect a significant correlation between RNF43 expression and H2AX phosphorylation in samples with IM and diffuse-type gastric cancer supporting a link between RNF43 and DDR.

Upon treatment with γ-irradiation, RNF43 was upregulated in AGS and MKN45 cells in a dose-dependent manner, further supporting the involvement of RNF43 in DDR signaling. However, how RNF43 could be regulated upon DNA damage remains to be elucidated since so far, RNF43 has only been described as a Wnt target gene that is upregulated upon active Wnt signaling [157, 158]. DDR and Wnt signaling have been described to interact in different manners [286]. It was shown that active DDR signaling can downregulate Wnt activity by mediating β-catenin degradation [287]. Additionally, p53 was shown to interact with GSK3β, thereby blocking β-catenin ubiquitination, which in turn

increases Wnt activity [288]. Furthermore, DNA damage-binding protein 2 (DDB2), was shown to upregulate RNF43 through activation of Wnt signaling in colon cancer cells [289]. DDB2 was initially described to be a p53 target gene involved in NER [290], however, in a more recent study, it was also described to be involved in resistance to ionizing radiation [291]. Taken together, these studies support the assumption that RNF43 upregulation upon DNA damage might be regulated by crosstalk between DDR and Wnt signaling.

An involvement of RNF43 in DDR is further supported by the finding that depletion of RNF43 enhances resistance to DNA damage inducing chemotherapy. In a previous publication, RNF43 overexpression conferred sensitivity to chemotherapeutic treatment with 5-FU or oxaliplatin in gastric cells by increasing the number of apoptotic cells upon treatment. However, this study did not link this finding to DDR, but to decreased stemness in gastric cells overexpressing RNF43 [159]. Yet, our data suggest that RNF43 regulates sensitivity to chemotherapy by regulating DDR. We could show that loss of RNF43 function induced resistance to DNA damaging chemotherapy in gastric cancer cells. In xenograft tumors derived from RNF43 wild type cells, we could detect activation of DDR and apoptosis upon chemotherapeutic treatment, while activation of these pathways was decreased in RNF43 depleted cells. Additionally, the number of proliferating tumor cells was higher in gastric cells with RNF43 loss of function. This data suggest that RNF43 depletion leads to reduced activation of DDR upon treatment with chemotherapy, thereby preventing apoptosis and conferring resistance similarly as observed for ionizing radiation. In human gastric organoids, we could observe an inverse correlation between RNF43 expression and responsiveness to chemotherapy further suggesting a possible link between RNF43 and therapy resistance. In contrast, we did not detect any differences in sensitivity to chemotherapy between organoids from patients carrying wild type or SNPs of *RNF43*. It has been described for other genes, such as methylenetetrahydrofolate reductase (*MTHFR*) [292] or *TLR7* [293], that SNPs could be associated with survival of colorectal cancer patients after chemotherapy. For *RNF43,* one study showed that the SNP R117H correlated with longer overall survival compared to wild type R117R in colorectal cancer patients. Additionally, overexpression of this variant decreased

proliferation of colorectal cells compared to the wild type variant [294]. However, this study did not include patients treated with chemotherapy, and thus, no link between *RNF43* SNPs and response to chemotherapy has been established. Taken together, our data suggest that RNF43 loss of function as well as expression levels influence susceptibility to chemotherapy. Therefore, RNF43 might serve as a biomarker to predict response to chemotherapy in gastric cancer patients.

We further analyzed whether RNF43 mutations could influence susceptibility to radio- and chemotherapy in a more clinically relevant model. Thus, we used the CRISPR/Cas9 system to introduce the mutations found in human gastric tumors into gastric cancer cells. We analyzed the mutations A136fs as a surrogate for R132X and Q577fs for R584fs for their impact on sensitivity to radio- and chemotherapy. Interestingly, we observed that the early frameshift mutation conferred resistance to ionizing radiation as well as chemotherapy, while the late frameshift mutation did not. Since we could show that RNF43 depletion induced changes in γH2AX ubiquitination, it is tempting to speculate that the involvement of RNF43 in sensitivity to DNA damaging agents is dependent on a functional RING domain, which is still present in the Q577fs, but not in the A136fs mutation. Indeed, it was shown that the involvement of RNF2 and RNF8 in DDR also depended on their E3 ligase activity [228, 295]. Interestingly, the commonly occurring late frameshift mutation G659fs of RNF43 was shown to be fully functional in inhibiting Wnt signaling in colorectal cells, further supporting the finding that a functional RING domain is essential for RNF43 function [296, 297].

In summary, we could show that RNF43 regulated the susceptibility of gastric cells to DNA damage-inducing radio- and chemotherapy. Thus, mutations in *RNF43* that impede its function or downregulation of RNF43 in gastric cancer samples might predict response to these therapies commonly used for gastric cancer patients. Patients lacking RNF43 function might not only show resistance to DNA damage inducing chemotherapy, but also further accumulate mutations induced by the therapy, thereby contributing to cancer progression and worsening prognosis. Therefore, we propose RNF43 as a potential biomarker for neoadjuvant therapy selection in gastric cancer patients.

## 6.3 Conclusion

This study aimed at deciphering, whether RNF43 has a tumor suppressive function in the stomach and by which signaling pathway it acts as a tumor suppressor.

We found that RNF43 has a tumor suppressive function in the stomach and negatively regulates stemness in gastric cells.

Furthermore, we showed that RNF43 is involved in DDR and regulates susceptibility to DNA damage-inducing radio- and chemotherapy.

Thus, we propose RN43 as a new potential biomarker to stratify gastric cancer patients for therapy selection.

# 7 Registers

## 7.1 Abbreviations

| | |
|---|---|
| 53BP1 | Tumor Protein P53 Binding Protein 1 |
| 5-FU | 5-Fluorouracil |
| AID | Activation-Induced Cytidine Deaminase |
| ALDH1 | Aldehyde dehydrogenase 1 |
| APC | Adenomatosis Polyposis Complex |
| ARID1A | AT-Rich Interaction Domain 1A |
| ATM | Ataxia Telangiectasia Mutated |
| ATR | Ataxia Telangiectasia And Rad3-Related Protein |
| ATP | Adenosine Triphosphate |
| BabA | Blood Group Antigen Binding Adhesin |
| BAX | Bcl-2-Associated X Protein |
| BER | Base excision repair |
| BHI | Brain-heart infusion |
| BMP4 | Bone Morphogenetic Protein 4 |
| BP | Base pair |
| BRAF | B-Raf Proto-Oncogene |
| BRCA1/2 | Breast Cancer Type ½ Susceptibility Protein |
| βTRCP | β-Transducin Repeat Containing E3 Ubiquitin Ligase |
| CAE | Chloracetate Esterase |
| CagA | Cytotoxin-Associated Gene A |
| CCND1 | Cyclin D1 |
| CD44 | Cell Surface Glycoprotein CD44 |
| CD54 | Intercellular Adhesion Molecule 1 |
| CD133 | Prominin 1 |
| CDH1 | Cadherin 1 |
| CDKN2A | Cyclin-dependent Kinase Inhibitor 2A |
| cDNA | coding DNA |
| CDX2 | Caudal Type Homeobox 2 |
| CEACAM | Carcinoembryonic Antigen-Related Cell Adhesion Molecule |
| CHK1/2 | Checkpoint Kinase ½ |
| CIMP | CpG island methylator phenotype |
| CIN | Chromosomal instability |
| CMYC | Avian Myelocytomatosis Viral Oncogene Homolog |
| CRISPR | Clustered regularly interspaced short palindromic repeats |
| Cxcl | C-X-C Motif Chemokine Ligand |
| DAB | Diaminobenzidine |

| | |
|---|---|
| DAPI | 4’,6-diamidino-2-phenylindole |
| DC | Dendritic cell |
| DDB2 | DNA Damage-Binding Protein 2 |
| DDR | DNA damage response |
| DMEM | Dulbecco’s Modified Eagle Medium |
| DMSO | Dimethyl sulfoxide |
| DNA | Deoxyribonucleic acid |
| DNA-PK | DNA Dependent Protein Kinase |
| DSB | Double strand break |
| DSS | Dextran sulfate sodium |
| EBV | Epstein-Barr virus |
| ECL | Enterochromaffin-like cells |
| EDTA | Ethylenediaminetetraacetic acid |
| EGF | Epithelial Growth Factor |
| EMT | Epithelial-mesenchymal transition |
| ERCC1 | Excision Repair Cross-Complementation Group 1 |
| FAP | Familial adenomatous polyposis |
| FBXW7 | F-Box And WD Repeat Domain Containing 7 |
| FCS | Fetal calf serum |
| FZD | Frizzled |
| GAPDH | Glyceraldehyde-3-Phosphate Dehydrogenase |
| GC | Gastric cancer |
| GFP | Green Fluorescent Protein |
| GGT | γ-Glutamyltransferase |
| GSK3β | Glycogen Synthase Kinase 3 β |
| H2Ax | Histone Variant 2Ax |
| HA | Hemagglutinin |
| HCC | Hepatocellular carcinoma |
| HE | hematoxylin-eosin |
| HER2/ERBB2 | Human Epidermal Growth Factor Receptor 2 |
| HPF | High power field |
| HR | Homology directed repair |
| HRP | Horseradish peroxidase |
| HtrA | High-Temperature Requirement A |
| IARC | International Agency for Research on Cancer |
| IF | Immunofluorescence |
| IFNγ | Interferon γ |
| Ig | Immunoglobulin |
| IHC | Immunohistochemistry |
| IHH | Indian Hedgehog |
| IL | Interleukin |

| | |
|---|---|
| IM | Intestinal metaplasia |
| IMDM | Iscove's Modified Dulbecco's Medium |
| Indel | Insertion/deletion |
| Int1 | Integration 1 |
| IP | Immunoprecipitation |
| IRIF | Ionizing radiation-induced foci |
| KRAS | Kirsten Rat Sarcoma Viral Oncogene Homolog |
| LB | Luria Bertani |
| LD | Lethal dosis |
| LEF | Lymphoid Enhancing Factor |
| LGR4/5 | Leucin-rich repeat containing G-Protein coupled receptor 4/5 |
| LOH | Loss of heterozygosity |
| LPS | Lipopolysaccharide |
| LRP 5/6 | Lipoprotein Receptor-Related Protein |
| LTK | Homo Sapiens Leukocyte Receptor Tyrosine Kinase |
| MALT | Mucosa-associated lymphoid tissue lymphoma |
| MDM2 | Mouse Double Minute 2 Homolog |
| MHC | Major Histocompatibility Complex |
| MIST1 | Muscle, Intestine And Stomach Expression 1 |
| MLH1 | MutL Homolog 1 |
| MMR | Mismatch repair |
| MOI | Multiplicity of infection |
| MRE11 | Meiotic Recombination 11 Homolog 1 |
| MRN | MRE11-Rad50-Nbs1 |
| mRNA | Messenger RNA |
| MSI | Microsatellite instability |
| MSS | Microsatellite stable |
| MTHFR | Methylenetetrahydrofolate Reductase |
| MTOR | Mechanistic Target Of Rapamycin Kinase |
| MTT | 3-(4,5-dimethylthiazol-2-yl)-2,5-diphenyltetrazolium bromide |
| MUC | Mucin |
| NBS1 | Nibrin |
| NER | Nucleotide excision repair |
| NF-κB | Nuclear Factor Kappa-Light-Chain-Enhancer Of Activated B Cells |
| NHEJ | Non-homologous end joining |
| NK cell | Natural killer cell |
| OD | Optical density |
| P21 | Cyclin-Dependent Kinase Inhibitor 1 |
| P53 | Tumor Protein p53 |
| PAI | Pathogenicity island |
| PAGE | Polyacrylamide gel electrophoresis |

| | |
|---|---|
| PAM | Protospacer adjacent motif |
| PAMP | Pathogen-associated molecular pattern |
| PAS | Periodic acid Schiff |
| PBS | Phosphate-buffered saline |
| PCR | Polymerase chain reaction |
| PD-L1/2 | Programmed Death-Ligand ½ |
| PI | Propidium iodide |
| PIK3CA | Phosphatidylinositol-4,5-Bisphosphate 3-Kinase Catalytic Subunit Alpha |
| PORCN | Porcupine |
| PREX | Phosphatidylinositol-3,4,5-Trisphosphate Dependent Rac Exchange Factor 2 |
| PTEN | Phosphatase And Tensin Homolog |
| PTM | Posttranslational modification |
| PTPRT | Protein Tyrosine Phosphatase Receptor Type T |
| PUMA | P53 Upregulated Mediator of Apoptosis |
| qRT-PCR | Quantitative real time PCR |
| RHOA | Ras Homolog Gene Family, Member A |
| RNA | Ribonucleic acid |
| RNF | Ring Finger Protein |
| RNP | Ribonucleoprotein complex |
| RNS | Reactive nitrogen species |
| ROS | Reactive oxygen species |
| RPA | Replication Protein A |
| RSPO | Rspondin |
| RTK | Receptor Tyrosine Kinase |
| SabA | Sialic Acid–Binding Adhesin |
| SASP | Senescence-associated secretor phenotype |
| SD | Standard deviation |
| SDS | Sodium dodecyl sulfate |
| Sh | Short hairpin |
| SHH | Sonic Hedgehog |
| SLX4 | SLX4 Structure-Specific Endonuclease Subunit |
| SNP | Single nucleotide polymorphism |
| SOX2 | Sex Determining Region Y Box 2 |
| SPEM | Spasmolytic Polypeptide expressing metaplasia |
| SPF | Specific-pathogen-free |
| SSB | Single strand break |
| STAT3 | Signal Transducer And Activator Of Transcription 3 |
| T4SS | Type IV secretion system |
| TAE | Tris Acetate-EDTA |
| TBS | Tris buffered saline |
| TCF | T Cell Factor |

| | |
|---|---|
| TFF2 | Trefoil Factor 2 |
| TGFβ(R) | Transforming Growth Factor β (Receptor) |
| TLR | Toll-Like Receptor |
| TNF(-R) | Tumor Necrosis Factor (Receptor) |
| TNM | Tumor, nodes, metastasis |
| Treg | Regulatory T cell |
| UreA | Urease |
| UV | Ultraviolet |
| VacA | Vacuolating Cytotoxin A |
| VEGF | Vascular Endothelial Growth Factor |
| WC | Wilkins Chalgren |
| WES | Whole exome sequencing |
| Wg | Wingless |
| WGS | Whole genome sequencing |
| WHO | World Health Organization |
| Wnt | Wingless-Related Integration Site |
| WRE | Wnt responsive element |
| WWC2 | Homo Sapiens WW And C2 Domain Containing 2 |
| XPA/F/G | Xeroderma Pigmentosum, Complementation Group A/F/G |
| ZNRF3 | Zinc And Ring Finger 3 |

## 7.2 List of figures

## 7.3 List of tables

## 7.4 List of references


1. Ferlay, J., M. Colombet, and I. Soerjomataram, *Global and Regional Estimates of the Incidence and Mortality for 38 Cancers: GLOBOCAN 2018. Lyon: International Agency for Research on Cancer.* World Health Organization, 2018.
2. Krams, M., et al., *Kurzlehrbuch Pathologie*. 2013: Georg Thieme Verlag.
3. Wilk, M., *Anatomie und Physiologie des Gastrointestinaltraktes*, in *Magen-Darm-Trakt*. 2013, Springer. p. 1-22.
4. Lüllmann-Rauch, R. and F. Paulsen, *Taschenlehrbuch Histologie* 2012, Thieme Verlag.
5. Han, M.-E. and S.-O. Oh, *Gastric stem cells and gastric cancer stem cells.* Anatomy & cell biology, 2013. **46**(1): p. 8-18.
6. Karam, S.M. and C.P. Leblond, *Dynamics of epithelial cells in the corpus of the mouse stomach. II. Outward migration of pit cells.* The Anatomical Record, 1993. **236**(2): p. 280-296.
7. Shinohara, M., et al., *Bone morphogenetic protein signaling regulates gastric epithelial cell development and proliferation in mice.* Gastroenterology, 2010. **139**(6): p. 2050-2060. e2.
8. Hata, M., Y. Hayakawa, and K. Koike, *Gastric Stem Cell and Cellular Origin of Cancer.* Biomedicines, 2018. **6**(4): p. 100.
9. Barker, N., et al., *Lgr5(+ve) stem cells drive self-renewal in the stomach and build long-lived gastric units in vitro.* Cell stem cell, 2010. **6**(1): p. 25-36.
10. Matsuo, J., et al., *Identification of stem cells in the epithelium of the stomach corpus and antrum of mice.* Gastroenterology, 2017. **152**(1): p. 218-231. e14.
11. Sigal, M., et al., *Helicobacter pylori activates and expands Lgr5+ stem cells through direct colonization of the gastric glands.* Gastroenterology, 2015. **148**(7): p. 1392-1404. e21.
12. Sigal, M., et al., *Stromal R-spondin orchestrates gastric epithelial stem cells and gland homeostasis.* Nature, 2017. **548**(7668): p. 451.
13. Fischer, A.-S. and M. Sigal, *The Role of Wnt and R-spondin in the Stomach During Health and Disease.* Biomedicines, 2019. **7**(2): p. 44.
14. Tomita, H., et al., *Development of gastric tumors in Apc(Min/+) mice by the activation of the beta-catenin/Tcf signaling pathway.* Cancer research, 2007. **67**(9): p. 4079-4087.
15. Huh, W.J., et al., *Tamoxifen induces rapid, reversible atrophy, and metaplasia in mouse stomach.* Gastroenterology, 2012. **142**(1): p. 21-24. e7.
16. Leushacke, M., et al., *Lgr5-expressing chief cells drive epithelial regeneration and cancer in the oxyntic stomach.* Nature cell biology, 2017. **19**(7): p. 774-786.
17. Hayakawa, Y., et al., *Mist1 Expressing Gastric Stem Cells Maintain the Normal and Neoplastic Gastric Epithelium and Are Supported by a Perivascular Stem Cell Niche.* Cancer cell, 2015. **28**(6): p. 800-814.
18. Arnold, K., et al., *Sox2<sup>+</sup> Adult Stem and Progenitor Cells Are Important for Tissue Regeneration and Survival of Mice.* Cell Stem Cell, 2011. **9**(4): p. 317-329.
19. Kim, T.-H. and R.A. Shivdasani, *Stomach development, stem cells and disease.* Development (Cambridge, England), 2016. **143**(4): p. 554-565.
20. Reya, T., et al., *Stem cells, cancer, and cancer stem cells.* Nature, 2001. **414**(6859): p. 105-111.
21. Takaishi, S., et al., *Identification of gastric cancer stem cells using the cell surface marker CD44.* Stem cells, 2009. **27**(5): p. 1006-1020.
22. Mayer, B., et al., *De-novo expression of CD44 and survival in gastric cancer.* The Lancet, 1993. **342**(8878): p. 1019-1022.
23. Zhao, P., Y. Li, and Y. Lu, *Aberrant expression of CD133 protein correlates with Ki-67 expression and is a prognostic marker in gastric adenocarcinoma.* BMC cancer, 2010. **10**(1): p. 218.
24. Ishigami, S., et al., *Prognostic impact of CD133 expression in gastric carcinoma.* Anticancer research, 2010. **30**(6): p. 2453-2457.

25. Liu, W.-T., et al., *Expression of ALDH1A1 and CD133 is associated with the prognosis and effect of different chemotherapeutic regimens in gastric cancer.* Oncology letters, 2019. **18**(5): p. 4573-4582.
26. Katsuno, Y., et al., *Coordinated expression of REG4 and aldehyde dehydrogenase 1 regulating tumourigenic capacity of diffuse-type gastric carcinoma-initiating cells is inhibited by TGF-β.* The Journal of pathology, 2012. **228**(3): p. 391-404.
27. Aichler, M., et al., *Proteomic and metabolic prediction of response to therapy in gastric cancer.* World journal of gastroenterology, 2014. **20**(38): p. 13648-13657.
28. Bosman, F.T., et al., *WHO classification of tumours of the digestive system*. 2010: World Health Organization.
29. Lauren, P., *THE TWO HISTOLOGICAL MAIN TYPES OF GASTRIC CARCINOMA: DIFFUSE AND SO-CALLED INTESTINAL-TYPE CARCINOMA. AN ATTEMPT AT A HISTO-CLINICAL CLASSIFICATION.* Acta pathologica et microbiologica Scandinavica, 1965. **64**: p. 31-49.
30. Cancer Genome Atlas Research, N., *Comprehensive molecular characterization of gastric adenocarcinoma.* Nature, 2014. **513**(7517): p. 202-209.
31. Correa, P., et al., *A model for gastric cancer epidemiology.* Lancet (London, England), 1975. **2**(7924): p. 58-60.
32. Dixon, M.F., et al., *Classification and grading of gastritis. The updated Sydney System. International Workshop on the Histopathology of Gastritis, Houston 1994.* The American journal of surgical pathology, 1996. **20**(10): p. 1161-1181.
33. Bruner, S.D., D.P. Norman, and G.L. Verdine, *Structural basis for recognition and repair of the endogenous mutagen 8-oxoguanine in DNA.* Nature, 2000. **403**(6772): p. 859-66.
34. Dolcet, X., et al., *NF-kB in development and progression of human cancer.* Virchows Archiv : an international journal of pathology, 2005. **446**(5): p. 475-482.
35. Judd, L.M., et al., *Gastric cancer development in mice lacking the SHP2 binding site on the IL-6 family co-receptor gp130.* Gastroenterology, 2004. **126**(1): p. 196-207.
36. Yoshizawa, N., et al., *Emergence of spasmolytic polypeptide-expressing metaplasia in Mongolian gerbils infected with Helicobacter pylori.* Laboratory investigation; a journal of technical methods and pathology, 2007. **87**(12): p. 1265-1276.
37. Nozaki, K., et al., *A molecular signature of gastric metaplasia arising in response to acute parietal cell loss.* Gastroenterology, 2008. **134**(2): p. 511-522.
38. Mills, J.C. and R.A. Shivdasani, *Gastric epithelial stem cells.* Gastroenterology, 2011. **140**(2): p. 412-424.
39. Varon, C., et al., *Helicobacter pylori infection recruits bone marrow-derived cells that participate in gastric preneoplasia in mice.* Gastroenterology, 2012. **142**(2): p. 281-291.
40. Houghton, J., et al., *Gastric cancer originating from bone marrow-derived cells.* Science (New York, N.Y.), 2004. **306**(5701): p. 1568-1571.
41. Correa, P., *The biological model of gastric carcinogenesis.* IARC scientific publications, 2004(157): p. 301-310.
42. He, C., Z. Yang, and N. Lu, *Imbalance of Gastrointestinal Microbiota in the Pathogenesis of helicobacter pylori-associated Diseases.* Helicobacter, 2016. **21**(5): p. 337-348.
43. Murata-Kamiya, N., et al., *Helicobacter pylori CagA interacts with E-cadherin and deregulates the beta-catenin signal that promotes intestinal transdifferentiation in gastric epithelial cells.* Oncogene, 2007. **26**(32): p. 4617-4626.
44. Chan, A.O.O., et al., *Promoter methylation of E-cadherin gene in gastric mucosa associated with Helicobacter pylori infection and in gastric cancer.* Gut, 2003. **52**(4): p. 502-506.
45. Lim, J.W., H. Kim, and K.H. Kim, *Cell adhesion-related gene expression by Helicobacter pylori in gastric epithelial AGS cells.* The International Journal of Biochemistry & Cell Biology, 2003. **35**(8): p. 1284-1296.
46. Orditura, M., et al., *Treatment of gastric cancer.* World journal of gastroenterology, 2014. **20**(7): p. 1635-1649.

47. Yoo, C. and Y.S. Park, *Companion diagnostics for the targeted therapy of gastric cancer.* World journal of gastroenterology, 2015. **21**(39): p. 10948-10955.
48. Lianos, G.D., et al., *Identification of novel genes by whole-exome sequencing can improve gastric cancer precision oncology.* Future oncology (London, England), 2017. **13**(10): p. 883-892.
49. Fuchs, C.S., et al., *Safety and Efficacy of Pembrolizumab Monotherapy in Patients With Previously Treated Advanced Gastric and Gastroesophageal Junction Cancer: Phase 2 Clinical KEYNOTE-059 Trial.* JAMA oncology, 2018. **4**(5): p. e180013-e180013.
50. Kim, S.T., et al., *Comprehensive molecular characterization of clinical responses to PD-1 inhibition in metastatic gastric cancer.* Nature medicine, 2018. **24**(9): p. 1449-1458.
51. Parkin, D.M., *International variation.* Oncogene, 2004. **23**(38): p. 6329-40.
52. Warren, J.R. and B. Marshall, *Unidentified curved bacilli on gastric epithelium in active chronic gastritis.* Lancet (London, England), 1983. **1**(8336): p. 1273-1275.
53. Agents, B., *Volume 100 B. A review of human carcinogens.* IARC Monogr Eval Carcinog Risks Hum, 2012. **100**(Pt B): p. 1-441.
54. IARC, *Schistosomes, liver flukes and Helicobacter pylori. IARC Working Group on the Evaluation of Carcinogenic Risks to Humans. Lyon, 7-14 June 1994.* IARC monographs on the evaluation of carcinogenic risks to humans, 1994. **61**: p. 1-241.
55. Hunt, R.H., et al., *Helicobacter pylori in developing countries. World Gastroenterology Organisation Global Guideline.* J Gastrointestin Liver Dis, 2011. **20**(3): p. 299-304.
56. Posselt, G., S. Backert, and S. Wessler, *The functional interplay of Helicobacter pylori factors with gastric epithelial cells induces a multi-step process in pathogenesis.* Cell Commun Signal, 2013. **11**: p. 77.
57. Thews, G., E. Mutschler, and P. Vaupel, *Anatomie, Physiologie, Pathophysiologie des Menschen*. Vol. 4. 1999: Wissenschaftliche Verlagsgesellschaft Stuttgart.
58. Javed, S., E.C. Skoog, and J.V. Solnick, *Impact of Helicobacter pylori Virulence Factors on the Host Immune Response and Gastric Pathology.* Current topics in microbiology and immunology, 2019. **421**: p. 21-52.
59. Li, Q., et al., *Association of CagA EPIYA-D or EPIYA-C phosphorylation sites with peptic ulcer and gastric cancer risks: a meta-analysis.* Medicine, 2017. **96**(17).
60. Arnold, I.C., et al., *Helicobacter pylori infection prevents allergic asthma in mouse models through the induction of regulatory T cells.* J Clin Invest, 2011. **121**(8): p. 3088-93.
61. Oertli, M. and A. Muller, *Helicobacter pylori targets dendritic cells to induce immune tolerance, promote persistence and confer protection against allergic asthma.* Gut Microbes, 2012. **3**(6): p. 566-71.
62. Luther, J., et al., *Helicobacter pylori DNA decreases pro-inflammatory cytokine production by dendritic cells and attenuates dextran sodium sulphate-induced colitis.* Gut, 2011. **60**(11): p. 1479-1486.
63. Hidaka, E., et al., *Helicobacter pylori and two ultrastructurally distinct layers of gastric mucous cell mucins in the surface mucous gel layer.* Gut, 2001. **49**(4): p. 474-480.
64. Bansil, R., et al., *The Influence of Mucus Microstructure and Rheology in Helicobacter pylori Infection.* Front Immunol, 2013. **4**: p. 310.
65. Celli, J.P., et al., *Helicobacter pylori moves through mucus by reducing mucin viscoelasticity.* Proceedings of the National Academy of Sciences, 2009. **106**(34): p. 14321-14326.
66. Saha, A., et al., *Helicobacter pylori CagL activates ADAM17 to induce repression of the gastric H, K-ATPase alpha subunit.* Gastroenterology, 2010. **139**(1): p. 239-48.
67. Kobayashi, H., et al., *The effect of Helicobacter pylori on gastric acid secretion by isolated parietal cells from a guinea pig. Association with production of vacuolating toxin by H. pylori.* Scand J Gastroenterol, 1996. **31**(5): p. 428-33.
68. Gooz, M., et al., *Inhibition of human gastric H(+)-K(+)-ATPase alpha-subunit gene expression by Helicobacter pylori.* Am J Physiol Gastrointest Liver Physiol, 2000. **278**(6): p. G981-91.

69. Beales, I. and J. Calam, *Interleukin 1ß and tumour necrosis factor α inhibit acid secretion in cultured rabbit parietal cells by multiple pathways.* Gut, 1998. **42**(2): p. 227-234.
70. Padol, I. and R. Hunt, *Effect of Th1 cytokines on acid secretion in pharmacologically characterised mouse gastric glands.* Gut, 2004. **53**(8): p. 1075-1081.
71. Mahdavi, J., et al., *Helicobacter pylori SabA adhesin in persistent infection and chronic inflammation.* Science (New York, N.Y.), 2002. **297**(5581): p. 573-578.
72. Aspholm-Hurtig, M., et al., *Functional adaptation of BabA, the H. pylori ABO blood group antigen binding adhesin.* Science (New York, N.Y.), 2004. **305**(5683): p. 519-522.
73. Rad, R., et al., *The Helicobacter pylori blood group antigen-binding adhesin facilitates bacterial colonization and augments a nonspecific immune response.* Journal of immunology (Baltimore, Md. : 1950), 2002. **168**(6): p. 3033-3041.
74. Javaheri, A., et al., *Helicobacter pylori adhesin HopQ engages in a virulence-enhancing interaction with human CEACAMs.* Nature microbiology, 2016. **2**: p. 16189-16189.
75. Königer, V., et al., *Helicobacter pylori exploits human CEACAMs via HopQ for adherence and translocation of CagA.* Nature microbiology, 2016. **2**: p. 16188-16188.
76. Hoy, B., et al., *Helicobacter pylori HtrA is a new secreted virulence factor that cleaves E-cadherin to disrupt intercellular adhesion.* EMBO Rep, 2010. **11**(10): p. 798-804.
77. Wessler, S. and S. Backert, *A novel basolateral type IV secretion model for the CagA oncoprotein of Helicobacter pylori.* Microbial cell (Graz, Austria), 2017. **5**(1): p. 60-62.
78. Zhao, Q., et al., *Integrin but not CEACAM receptors are dispensable for Helicobacter pylori CagA translocation.* PLoS pathogens, 2018. **14**(10): p. e1007359-e1007359.
79. Yokota, S.-i., et al., *Highly-purified Helicobacter pylori LPS preparations induce weak inflammatory reactions and utilize Toll-like receptor 2 complex but not Toll-like receptor 4 complex.* FEMS immunology and medical microbiology, 2007. **51**(1): p. 140-148.
80. Gobert, A.P. and K.T. Wilson, *Human and Helicobacter pylori Interactions Determine the Outcome of Gastric Diseases.* Current topics in microbiology and immunology, 2017. **400**: p. 27-52.
81. Keates, S., et al., *Helicobacter pylori infection activates NF-kappa B in gastric epithelial cells.* Gastroenterology, 1997. **113**(4): p. 1099-109.
82. Lee, A. and F. Buck, *Vaccination and mucosal responses to Helicobacter pylori infection.* Alimentary pharmacology & therapeutics, 1996. **10**(Sup1): p. 129-138.
83. Necchi, V., et al., *Evidence for transepithelial dendritic cells in human H. pylori active gastritis.* Helicobacter, 2009. **14**(3): p. 208-222.
84. Shi, Y., et al., *Helicobacter pylori-induced Th17 responses modulate Th1 cell responses, benefit bacterial growth, and contribute to pathology in mice.* J Immunol, 2010. **184**(9): p. 5121-9.
85. Bamford, K.B., et al., *Lymphocytes in the human gastric mucosa during Helicobacter pylori have a T helper cell 1 phenotype.* Gastroenterology, 1998. **114**(3): p. 482-492.
86. Stoicov, C., et al., *T-bet knockout prevents Helicobacter felis-induced gastric cancer.* J Immunol, 2009. **183**(1): p. 642-9.
87. Moran, A.P., *Molecular structure, biosynthesis, and pathogenic roles of lipopolysaccharides*, in *Helicobacter pylori: Physiology and Genetics*. 2001, ASM Press.
88. Pachathundikandi, S.K., A. Müller, and S. Backert, *Inflammasome Activation by Helicobacter pylori and Its Implications for Persistence and Immunity.* Current topics in microbiology and immunology, 2016. **397**: p. 117-131.
89. Robinson, K., et al., *Helicobacter pylori-induced peptic ulcer disease is associated with inadequate regulatory T cell responses.* Gut, 2008. **57**(10): p. 1375-85.
90. Tanaka, H., et al., *The CagA protein of Helicobacter pylori suppresses the functions of dendritic cell in mice.* Archives of biochemistry and biophysics, 2010. **498**(1): p. 35-42.
91. Kim, J.M., et al., *Stimulation of dendritic cells with Helicobacter pylori vacuolating cytotoxin negatively regulates their maturation via the restoration of E2F1.* Clinical and experimental immunology, 2011. **166**(1): p. 34-45.

92. Sundrud, M.S., et al., *Inhibition of primary human T cell proliferation by Helicobacter pylori vacuolating toxin (VacA) is independent of VacA effects on IL-2 secretion.* Proceedings of the National Academy of Sciences, 2004. **101**(20): p. 7727-7732.
93. Wüstner, S., et al., *H elicobacter pylori γ-glutamyltranspeptidase impairs T-lymphocyte function by compromising metabolic adaption through inhibition of cMyc and IRF4 expression.* Cellular microbiology, 2015. **17**(1): p. 51-61.
94. Zabaleta, J., et al., *Helicobacter pylori arginase inhibits T cell proliferation and reduces the expression of the TCR zeta-chain (CD3zeta).* Journal of immunology (Baltimore, Md. : 1950), 2004. **173**(1): p. 586-593.
95. Adamsson, J., et al., *Gastric expression of IL-17A and IFNγ in Helicobacter pylori infected individuals is related to symptoms.* Cytokine, 2017. **99**: p. 30-34.
96. Jafarzadeh, A., et al., *T cell subsets play an important role in the determination of the clinical outcome of Helicobacter pylori infection.* Microbial pathogenesis, 2018. **116**: p. 227-236.
97. Robinson, K., D.P. Letley, and K. Kaneko, *The Human Stomach in Health and Disease: Infection Strategies by Helicobacter pylori.* Current topics in microbiology and immunology, 2017. **400**: p. 1-26.
98. Zavros, Y., et al., *Hypergastrinemia in response to gastric inflammation suppresses somatostatin.* American Journal of Physiology-Gastrointestinal and Liver Physiology, 2002. **282**(1): p. G175-G183.
99. Levi, S., et al., *Antral Helicobacter pylori, hypergastrinaemia, and duodenal ulcers: effect of eradicating the organism.* BMJ: British Medical Journal, 1989. **299**(6714): p. 1504.
100. Mejías-Luque, R., et al., *Lymphotoxin β receptor signalling executes Helicobacter pylori-driven gastric inflammation in a T4SS-dependent manner.* Gut, 2017. **66**(8): p. 1369-1381.
101. Wang, C.-Y., et al., *NF-κB antiapoptosis: induction of TRAF1 and TRAF2 and c-IAP1 and c-IAP2 to suppress caspase-8 activation.* Science, 1998. **281**(5383): p. 1680-1683.
102. Guttridge, D.C., et al., *NF-κB controls cell growth and differentiation through transcriptional regulation of cyclin D1.* Molecular and cellular biology, 1999. **19**(8): p. 5785-5799.
103. Sugimoto, M., et al., *Helicobacter pylori outer membrane proteins on gastric mucosal interleukin 6 and 11 expression in Mongolian gerbils.* J Gastroenterol Hepatol, 2011. **26**(11): p. 1677-84.
104. Piao, J.-Y., et al., *Helicobacter pylori Activates IL-6-STAT3 Signaling in Human Gastric Cancer Cells: Potential Roles for Reactive Oxygen Species.* Helicobacter, 2016. **21**(5): p. 405-416.
105. Chaturvedi, R., et al., *Activation of EGFR and ERBB2 by Helicobacter pylori results in survival of gastric epithelial cells with DNA damage.* Gastroenterology, 2014. **146**(7): p. 1739-51.e14.
106. Sierra, J.C., et al., *Epidermal growth factor receptor inhibition downregulates Helicobacter pylori-induced epithelial inflammatory responses, DNA damage and gastric carcinogenesis.* Gut, 2018. **67**(7): p. 1247-1260.
107. Neal, J.T., et al., *<em>H. pylori</em> virulence factor CagA increases intestinal cell proliferation by Wnt pathway activation in a transgenic zebrafish model.* Disease Models & Mechanisms, 2013. **6**(3): p. 802.
108. Hardbower, D.M., R.M. Peek, Jr., and K.T. Wilson, *At the Bench: Helicobacter pylori, dysregulated host responses, DNA damage, and gastric cancer.* J Leukoc Biol, 2014. **96**(2): p. 201-12.
109. Handa, O., Y. Naito, and T. Yoshikawa, *Redox biology and gastric carcinogenesis: the role of Helicobacter pylori.* Redox Rep, 2011. **16**(1): p. 1-7.
110. Matsumoto, Y., et al., *Helicobacter pylori infection triggers aberrant expression of activation-induced cytidine deaminase in gastric epithelium.* Nat Med, 2007. **13**(4): p. 470-6.
111. Matsumoto, T., et al., *Hepatic inflammation facilitates transcription-associated mutagenesis via AID activity and enhances liver tumorigenesis.* Carcinogenesis, 2015. **36**(8): p. 904-13.
112. Toller, I.M., et al., *Carcinogenic bacterial pathogen Helicobacter pylori triggers DNA double-strand breaks and a DNA damage response in its host cells.* Proceedings of the National Academy of Sciences of the United States of America, 2011. **108**(36): p. 14944-14949.

113. Hanada, K., et al., *Helicobacter pylori infection introduces DNA double-strand breaks in host cells.* Infection and immunity, 2014. **82**(10): p. 4182-4189.
114. Hartung, M.L., et al., *H. pylori-Induced DNA Strand Breaks Are Introduced by Nucleotide Excision Repair Endonucleases and Promote NF-κB Target Gene Expression.* Cell reports, 2015. **13**(1): p. 70-79.
115. Wei, J., et al., *Regulation of p53 tumor suppressor by Helicobacter pylori in gastric epithelial cells.* Gastroenterology, 2010. **139**(4): p. 1333-1343.
116. Koeppel, M., et al., *Helicobacter pylori Infection Causes Characteristic DNA Damage Patterns in Human Cells.* Cell Rep, 2015. **11**(11): p. 1703-13.
117. Machado, A.M., et al., *Helicobacter pylori infection induces genetic instability of nuclear and mitochondrial DNA in gastric cells.* Clin Cancer Res, 2009. **15**(9): p. 2995-3002.
118. Kim, J.J., et al., *Helicobacter pylori impairs DNA mismatch repair in gastric epithelial cells.* Gastroenterology, 2002. **123**(2): p. 542-53.
119. Nusse, R. and H.E. Varmus, *Many tumors induced by the mouse mammary tumor virus contain a provirus integrated in the same region of the host genome.* Cell, 1982. **31**(1): p. 99-109.
120. Nüsslein-Volhard, C. and E. Wieschaus, *Mutations affecting segment number and polarity in Drosophila.* Nature, 1980. **287**(5785): p. 795-801.
121. Rijsewijk, F., et al., *The Drosophila homolog of the mouse mammary oncogene int-1 is identical to the segment polarity gene wingless.* Cell, 1987. **50**(4): p. 649-657.
122. Clevers, H., *Wnt/beta-catenin signaling in development and disease.* Cell, 2006. **127**(3): p. 469-480.
123. McMahon, A.P. and R.T. Moon, *int-1--a proto-oncogene involved in cell signalling.* Development (Cambridge, England), 1989. **107 Suppl**: p. 161-167.
124. Alonso, L. and E. Fuchs, *Stem cells in the skin: waste not, Wnt not.* Genes & development, 2003. **17**(10): p. 1189-1200.
125. Reya, T., et al., *A role for Wnt signalling in self-renewal of haematopoietic stem cells.* Nature, 2003. **423**(6938): p. 409-414.
126. Hartmann, C., *A Wnt canon orchestrating osteoblastogenesis.* Trends in cell biology, 2006. **16**(3): p. 151-158.
127. Reya, T. and H. Clevers, *Wnt signalling in stem cells and cancer.* Nature, 2005. **434**(7035): p. 843.
128. Willert, K., et al., *Wnt proteins are lipid-modified and can act as stem cell growth factors.* Nature, 2003. **423**(6938): p. 448.
129. Zhai, L., D. Chaturvedi, and S. Cumberledge, *Drosophila wnt-1 undergoes a hydrophobic modification and is targeted to lipid rafts, a process that requires porcupine.* Journal of Biological Chemistry, 2004. **279**(32): p. 33220-33227.
130. Aberle, H., et al., *β-catenin is a target for the ubiquitin–proteasome pathway.* The EMBO journal, 1997. **16**(13): p. 3797-3804.
131. Pinson, K.I., et al., *An LDL-receptor-related protein mediates Wnt signalling in mice.* Nature, 2000. **407**(6803): p. 535.
132. Behrens, J., et al., *Functional interaction of β-catenin with the transcription factor LEF-1.* Nature, 1996. **382**(6592): p. 638.
133. Van de Wetering, M., et al., *Armadillo coactivates transcription driven by the product of the Drosophila segment polarity gene dTCF.* Cell, 1997. **88**(6): p. 789-799.
134. Molenaar, M., et al., *XTcf-3 transcription factor mediates β-catenin-induced axis formation in Xenopus embryos.* Cell, 1996. **86**(3): p. 391-399.
135. Cavallo, R.A., et al., *Drosophila Tcf and Groucho interact to repress Wingless signalling activity.* Nature, 1998. **395**(6702): p. 604.
136. Daniels, D.L. and W.I. Weis, *β-catenin directly displaces Groucho/TLE repressors from Tcf/Lef in Wnt-mediated transcription activation.* Nature structural & molecular biology, 2005. **12**(4): p. 364.

137. Tetsu, O. and F. McCormick, *Beta-catenin regulates expression of cyclin D1 in colon carcinoma cells.* Nature, 1999. **398**(6726): p. 422-426.
138. He, T.C., et al., *Identification of c-MYC as a target of the APC pathway.* Science (New York, N.Y.), 1998. **281**(5382): p. 1509-1512.
139. Yan, D., et al., *Elevated expression of axin2 and hnkd mRNA provides evidence that Wnt/beta -catenin signaling is activated in human colon tumors.* Proceedings of the National Academy of Sciences of the United States of America, 2001. **98**(26): p. 14973-14978.
140. Nam, J.-S., et al., *Mouse cristin/R-spondin family proteins are novel ligands for the Frizzled 8 and LRP6 receptors and activate β-catenin-dependent gene expression.* Journal of Biological Chemistry, 2006. **281**(19): p. 13247-13257.
141. Zebisch, M., et al., *Structural and molecular basis of ZNRF3/RNF43 transmembrane ubiquitin ligase inhibition by the Wnt agonist R-spondin.* Nature communications, 2013. **4**: p. 2787-2787.
142. Koo, B.-K., et al., *Tumour suppressor RNF43 is a stem-cell E3 ligase that induces endocytosis of Wnt receptors.* Nature, 2012. **488**(7413): p. 665-669.
143. Park, S., et al., *Differential activities and mechanisms of the four R-spondins in potentiating Wnt/β-catenin signaling.* The Journal of biological chemistry, 2018. **293**(25): p. 9759-9769.
144. Kinzler, K.W. and B. Vogelstein, *Lessons from hereditary colorectal cancer.* Cell, 1996. **87**(2): p. 159-170.
145. Kinzler, K.W., et al., *Identification of FAP locus genes from chromosome 5q21.* Science (New York, N.Y.), 1991. **253**(5020): p. 661-665.
146. Su, L.-K., et al., *Multiple intestinal neoplasia caused by a mutation in the murine homolog of the APC gene.* Science, 1992. **256**(5057): p. 668-670.
147. Clements, W.M., et al., *beta-Catenin mutation is a frequent cause of Wnt pathway activation in gastric cancer.* Cancer research, 2002. **62**(12): p. 3503-3506.
148. Saitoh, T., T. Mine, and M. Katoh, *Frequent up-regulation of WNT5A mRNA in primary gastric cancer.* International journal of molecular medicine, 2002. **9**(5): p. 515-519.
149. Kirikoshi, H., H. Sekihara, and M. Katoh, *Up-regulation of WNT10A by tumor necrosis factor alpha and Helicobacter pylori in gastric cancer.* International journal of oncology, 2001. **19**(3): p. 533-536.
150. Ebert, M.P.A., et al., *Increased β-catenin mRNA levels and mutational alterations of the APC and β-catenin gene are present in intestinal-type gastric cancer.* Carcinogenesis, 2002. **23**(1): p. 87-91.
151. Min, B.-H., et al., *Dysregulated Wnt signalling and recurrent mutations of the tumour suppressor RNF43 in early gastric carcinogenesis.* The Journal of pathology, 2016. **240**(3): p. 304-314.
152. Radulescu, S., et al., *Acute WNT signalling activation perturbs differentiation within the adult stomach and rapidly leads to tumour formation.* Oncogene, 2013. **32**(16): p. 2048-2057.
153. Kurayoshi, M., et al., *Expression of Wnt-5a Is Correlated with Aggressiveness of Gastric Cancer by Stimulating Cell Migration and Invasion.* Cancer Research, 2006. **66**(21): p. 10439.
154. Huang, T., et al., *The prognostic role of Leucine-rich repeat-containing G-protein-coupled receptor 5 in gastric cancer: A systematic review with meta-analysis.* Clinics and Research in Hepatology and Gastroenterology, 2016. **40**(2): p. 246-253.
155. Xing, C., et al., *Reversing effect of ring finger protein 43 inhibition on malignant phenotypes of human hepatocellular carcinoma.* Molecular cancer therapeutics, 2013. **12**(1): p. 94-103.
156. Jiang, X., et al., *Inactivating mutations of RNF43 confer Wnt dependency in pancreatic ductal adenocarcinoma.* Proceedings of the National Academy of Sciences of the United States of America, 2013. **110**(31): p. 12649-12654.
157. Loregger, A., et al., *The E3 ligase RNF43 inhibits Wnt signaling downstream of mutated β-catenin by sequestering TCF4 to the nuclear membrane.* Science signaling, 2015. **8**(393): p. ra90-ra90.

158. Takahashi, N., et al., *Identification of two Wnt-responsive elements in the intron of RING finger protein 43 (RNF43) gene.* PloS one, 2014. **9**(1): p. e86582-e86582.
159. Gao, Y., et al., *Ring finger protein 43 associates with gastric cancer progression and attenuates the stemness of gastric cancer stem-like cells via the Wnt-β/catenin signaling pathway.* Stem cell research & therapy, 2017. **8**(1): p. 98-98.
160. Niu, L., et al., *RNF43 Inhibits Cancer Cell Proliferation and Could be a Potential Prognostic Factor for Human Gastric Carcinoma.* Cellular Physiology and Biochemistry, 2015. **36**(5): p. 1835-1846.
161. Sekine, S., et al., *Frequent PTPRK-RSPO3 fusions and RNF43 mutations in colorectal traditional serrated adenoma.* The Journal of pathology, 2016. **239**(2): p. 133-138.
162. Yan, H.H.N., et al., *RNF43 germline and somatic mutation in serrated neoplasia pathway and its association with BRAF mutation.* Gut, 2017. **66**(9): p. 1645-1656.
163. Bond, C.E., et al., *RNF43 and ZNRF3 are commonly altered in serrated pathway colorectal tumorigenesis.* Oncotarget, 2016. **7**(43): p. 70589-70600.
164. Giannakis, M., et al., *RNF43 is frequently mutated in colorectal and endometrial cancers.* Nature genetics, 2014. **46**(12): p. 1264-1266.
165. Hashimoto, K., et al., *Expression of CD133 in the cytoplasm is associated with cancer progression and poor prognosis in gastric cancer.* Gastric Cancer, 2014. **17**(1): p. 97-106.
166. Wu, C.-Y., et al., *Critical role of monoubiquitination of histone H2AX protein in histone H2AX phosphorylation and DNA damage response.* The Journal of biological chemistry, 2011. **286**(35): p. 30806-30815.
167. Wang, K., et al., *Whole-genome sequencing and comprehensive molecular profiling identify new driver mutations in gastric cancer.* Nature genetics, 2014. **46**(6): p. 573-582.
168. Maruvka, Y.E., et al., *Analysis of somatic microsatellite indels identifies driver events in human tumors.* Nature biotechnology, 2017. **35**(10): p. 951-959.
169. Jung, S.-H., et al., *Clonal Structures of Regionally Synchronous Gastric Adenomas and Carcinomas.* Clinical cancer research : an official journal of the American Association for Cancer Research, 2018. **24**(19): p. 4715-4725.
170. Cho, J., et al., *Four distinct immune microenvironment subtypes in gastric adenocarcinoma with special reference to microsatellite instability.* ESMO open, 2018. **3**(3): p. e000326-e000326.
171. Lindahl, T. and D. Barnes. *Repair of endogenous DNA damage*. in *Cold Spring Harbor symposia on quantitative biology*. 2000. Cold Spring Harbor Laboratory Press.
172. Valko, M., et al., *Free radicals, metals and antioxidants in oxidative stress-induced cancer.* Chemico-biological interactions, 2006. **160**(1): p. 1-40.
173. Kawanishi, S., et al., *Oxidative and nitrative DNA damage in animals and patients with inflammatory diseases in relation to inflammation-related carcinogenesis.* Biological chemistry, 2006. **387**(4): p. 365-372.
174. Ward, J.F., *DNA damage produced by ionizing radiation in mammalian cells: identities, mechanisms of formation, and reparability*, in *Progress in nucleic acid research and molecular biology*. 1988, Elsevier. p. 95-125.
175. Kastan, M.B. and J. Bartek, *Cell-cycle checkpoints and cancer.* Nature, 2004. **432**(7015): p. 316.
176. Douki, T., et al., *Formation of the main UV-induced thymine dimeric lesions within isolated and cellular DNA as measured by high performance liquid chromatography-tandem mass spectrometry.* The Journal of biological chemistry, 2000. **275**(16): p. 11678-11685.
177. Jackson, S.P. and J. Bartek, *The DNA-damage response in human biology and disease.* Nature, 2009. **461**(7267): p. 1071-1078.
178. Tibbetts, R.S., et al., *Functional interactions between BRCA1 and the checkpoint kinase ATR during genotoxic stress.* Genes & development, 2000. **14**(23): p. 2989-3002.
179. Matsuoka, S., et al., *ATM and ATR substrate analysis reveals extensive protein networks responsive to DNA damage.* Science (New York, N.Y.), 2007. **316**(5828): p. 1160-1166.

180. Falck, J., et al., *The DNA damage-dependent intra-S phase checkpoint is regulated by parallel pathways.* Nature genetics, 2002. **30**(3): p. 290-294.
181. Haupt, Y., et al., *Mdm2 promotes the rapid degradation of p53.* Nature, 1997. **387**(6630): p. 296-299.
182. Liang, S.H. and M.F. Clarke, *Regulation of p53 localization.* European journal of biochemistry, 2001. **268**(10): p. 2779-2783.
183. Reinke, V. and G. Lozano, *Differential activation of p53 targets in cells treated with ultraviolet radiation that undergo both apoptosis and growth arrest.* Radiat Res, 1997. **148**(2): p. 115-22.
184. Wu, L. and A.J. Levine, *Differential regulation of the p21/WAF-1 and mdm2 genes after high-dose UV irradiation: p53-dependent and p53-independent regulation of the mdm2 gene.* Mol Med, 1997. **3**(7): p. 441-51.
185. Bartek, J. and J. Lukas, *DNA damage checkpoints: from initiation to recovery or adaptation.* Current opinion in cell biology, 2007. **19**(2): p. 238-245.
186. Bernstein, C., et al., *DNA repair/pro-apoptotic dual-role proteins in five major DNA repair pathways: fail-safe protection against carcinogenesis.* Mutation research, 2002. **511**(2): p. 145-178.
187. Müller, M., et al., *p53 activates the CD95 (APO-1/Fas) gene in response to DNA damage by anticancer drugs.* The Journal of experimental medicine, 1998. **188**(11): p. 2033-2045.
188. Nakano, K. and K.H. Vousden, *PUMA, a novel proapoptotic gene, is induced by p53.* Molecular cell, 2001. **7**(3): p. 683-694.
189. Yu, J., et al., *PUMA induces the rapid apoptosis of colorectal cancer cells.* Molecular cell, 2001. **7**(3): p. 673-682.
190. Reed, J.C., *Bcl-2 family proteins.* Oncogene, 1998. **17**(25): p. 3225-36.
191. Nicholson, D.W. and N.A. Thornberry, *Caspases: killer proteases.* Trends in Biochemical Sciences, 1997. **22**(8): p. 299-306.
192. Plati, J., O. Bucur, and R. Khosravi-Far, *Apoptotic cell signaling in cancer progression and therapy.* Integrative biology : quantitative biosciences from nano to macro, 2011. **3**(4): p. 279-296.
193. Jiricny, J., *The multifaceted mismatch-repair system.* Nature reviews Molecular cell biology, 2006. **7**(5): p. 335.
194. Drummond, J.T., et al., *Isolation of an hMSH2-p160 heterodimer that restores DNA mismatch repair to tumor cells.* Science, 1995. **268**(5219): p. 1909-12.
195. David, S.S., V.L. O'Shea, and S. Kundu, *Base-excision repair of oxidative DNA damage.* Nature, 2007. **447**(7147): p. 941.
196. Fromme, J.C., et al., *Structural basis for removal of adenine mispaired with 8-oxoguanine by MutY adenine DNA glycosylase.* Nature, 2004. **427**(6975): p. 652-656.
197. Hoeijmakers, J.H., *Genome maintenance mechanisms for preventing cancer.* nature, 2001. **411**(6835): p. 366.
198. Almeida, K.H. and R.W. Sobol, *A unified view of base excision repair: lesion-dependent protein complexes regulated by post-translational modification.* DNA repair, 2007. **6**(6): p. 695-711.
199. Huang, J.C., et al., *Human nucleotide excision nuclease removes thymine dimers from DNA by incising the 22nd phosphodiester bond 5' and the 6th phosphodiester bond 3' to the photodimer.* Proceedings of the National Academy of Sciences, 1992. **89**(8): p. 3664-3668.
200. Moggs, J.G., et al., *Analysis of Incision Sites Produced by Human Cell Extracts and Purified Proteins during Nucleotide Excision Repair of a 1,3-Intrastrand d(GpTpG)-Cisplatin Adduct.* Journal of Biological Chemistry, 1996. **271**(12): p. 7177-7186.
201. San Filippo, J., P. Sung, and H. Klein, *Mechanism of eukaryotic homologous recombination.* Annu. Rev. Biochem., 2008. **77**: p. 229-257.
202. Filippo, J.S., et al., *Recombination Mediator and Rad51 Targeting Activities of a Human BRCA2 Polypeptide.* Journal of Biological Chemistry, 2006. **281**(17): p. 11649-11657.

203. Chen, P.L., et al., *The BRC repeats in BRCA2 are critical for RAD51 binding and resistance to methyl methanesulfonate treatment.* Proceedings of the National Academy of Sciences of the United States of America, 1998. **95**(9): p. 5287-5292.
204. Bekker-Jensen, S., et al., *Spatial organization of the mammalian genome surveillance machinery in response to DNA strand breaks.* The Journal of cell biology, 2006. **173**(2): p. 195-206.
205. Adachi, N., et al., *DNA ligase IV-deficient cells are more resistant to ionizing radiation in the absence of Ku70: Implications for DNA double-strand break repair.* Proceedings of the National Academy of Sciences, 2001. **98**(21): p. 12109-12113.
206. Lieber, M.R., *The mechanism of human nonhomologous DNA end joining.* Journal of Biological Chemistry, 2008. **283**(1): p. 1-5.
207. Giglia-Mari, G., A. Zotter, and W. Vermeulen, *DNA damage response.* Cold Spring Harbor perspectives in biology, 2011. **3**(1): p. a000745-a000745.
208. Rogakou, E.P., et al., *Megabase chromatin domains involved in DNA double-strand breaks in vivo.* The Journal of cell biology, 1999. **146**(5): p. 905-916.
209. Rogakou, E.P., et al., *DNA double-stranded breaks induce histone H2AX phosphorylation on serine 139.* The Journal of biological chemistry, 1998. **273**(10): p. 5858-5868.
210. Reiman, A., et al., *Lymphoid tumours and breast cancer in ataxia telangiectasia; substantial protective effect of residual ATM kinase activity against childhood tumours.* British journal of cancer, 2011. **105**(4): p. 586-591.
211. Malkin, D., et al., *Germ line p53 mutations in a familial syndrome of breast cancer, sarcomas, and other neoplasms.* Science (New York, N.Y.), 1990. **250**(4985): p. 1233-1238.
212. Petitjean, A., et al., *Impact of mutant p53 functional properties on TP53 mutation patterns and tumor phenotype: lessons from recent developments in the IARC TP53 database.* Human mutation, 2007. **28**(6): p. 622-629.
213. Cho, J., et al., *Bridging genomics and phenomics of gastric carcinoma.* International journal of cancer, 2019. **145**(9): p. 2407-2417.
214. Gisselsson, D., et al., *Telomere dysfunction triggers extensive DNA fragmentation and evolution of complex chromosome abnormalities in human malignant tumors.* Proceedings of the National Academy of Sciences, 2001. **98**(22): p. 12683-12688.
215. Rudolph, K.L., et al., *Telomere dysfunction and evolution of intestinal carcinoma in mice and humans.* Nature Genetics, 2001. **28**(2): p. 155-159.
216. de Lange, T., *Shelterin: the protein complex that shapes and safeguards human telomeres.* Genes & development, 2005. **19**(18): p. 2100-2110.
217. Verdun, R.E. and J. Karlseder, *Replication and protection of telomeres.* Nature, 2007. **447**(7147): p. 924.
218. di Fagagna, F.d.A., S.-H. Teo, and S.P. Jackson, *Functional links between telomeres and proteins of the DNA-damage response.* Genes & development, 2004. **18**(15): p. 1781-1799.
219. Gorgoulis, V.G., et al., *Activation of the DNA damage checkpoint and genomic instability in human precancerous lesions.* Nature, 2005. **434**(7035): p. 907-13.
220. Umbenhauer, D.R. and A.E. Pegg, *Alkylation of intracellular and extracellular DNA by dimethylnitrosamine following activation by isolated rat hepatocytes.* Cancer research, 1981. **41**(9 Pt 1): p. 3471-3474.
221. Bartkova, J., et al., *Oncogene-induced senescence is part of the tumorigenesis barrier imposed by DNA damage checkpoints.* Nature, 2006. **444**(7119): p. 633-637.
222. Rodier, F., et al., *Persistent DNA damage signalling triggers senescence-associated inflammatory cytokine secretion.* Nature cell biology, 2009. **11**(8): p. 973-979.
223. Smyth, E.C., et al., *Gastric cancer: ESMO Clinical Practice Guidelines for diagnosis, treatment and follow-up.* Annals of oncology : official journal of the European Society for Medical Oncology, 2016. **27**(suppl 5): p. v38-v49.
224. Sherman, S.E., et al., *X-ray structure of the major adduct of the anticancer drug cisplatin with DNA: cis-[Pt(NH3)2(d(pGpG))].* Science (New York, N.Y.), 1985. **230**(4724): p. 412-417.

225. Dasari, S. and P.B. Tchounwou, *Cisplatin in cancer therapy: molecular mechanisms of action.* European journal of pharmacology, 2014. **740**: p. 364-378.
226. Santi, D.V., C.S. McHenry, and H. Sommer, *Mechanism of interaction of thymidylate synthetase with 5-fluorodeoxyuridylate.* Biochemistry, 1974. **13**(3): p. 471-81.
227. Kufe, D.W. and P.P. Major, *5-Fluorouracil incorporation into human breast carcinoma RNA correlates with cytotoxicity.* J Biol Chem, 1981. **256**(19): p. 9802-5.
228. Pan, M.-R., et al., *Monoubiquitination of H2AX protein regulates DNA damage response signaling.* The Journal of biological chemistry, 2011. **286**(32): p. 28599-28607.
229. Huen, M.S.Y., et al., *RNF8 transduces the DNA-damage signal via histone ubiquitylation and checkpoint protein assembly.* Cell, 2007. **131**(5): p. 901-914.
230. Doil, C., et al., *RNF168 Binds and Amplifies Ubiquitin Conjugates on Damaged Chromosomes to Allow Accumulation of Repair Proteins.* Cell, 2009. **136**(3): p. 435-446.
231. Mattiroli, F., et al., *RNF168 ubiquitinates K13-15 on H2A/H2AX to drive DNA damage signaling.* Cell, 2012. **150**(6): p. 1182-1195.
232. Gala, M.K., et al., *Germline mutations in oncogene-induced senescence pathways are associated with multiple sessile serrated adenomas.* Gastroenterology, 2014. **146**(2): p. 520-529.
233. Heyer, W.-D., K.T. Ehmsen, and J. Liu, *Regulation of homologous recombination in eukaryotes.* Annual review of genetics, 2010. **44**: p. 113-139.
234. Bartfeld, S. and H. Clevers, *Organoids as Model for Infectious Diseases: Culture of Human and Murine Stomach Organoids and Microinjection of Helicobacter Pylori.* Journal of visualized experiments : JoVE, 2015(105): p. 53359.
235. Neumeyer, V., et al., *Loss of RNF43 Function Contributes to Gastric Carcinogenesis by Impairing DNA Damage Response.* Cellular and Molecular Gastroenterology and Hepatology, 2021. **11**(4): p. 1071-1094.
236. Neumeyer, V., *The Role of RNF43 in DNA damage response*. 2015.
237. Neumeyer, V., et al., *Loss of endogenous RNF43 function enhances proliferation and tumour growth of intestinal and gastric cells.* Carcinogenesis, 2019. **40**(4): p. 551-559.
238. Neumeyer, V., et al., *Mutated Rnf43 Aggravates Helicobacter Pylori-Induced Gastric Pathology.* Cancers, 2019. **11**(3).
239. Yagyu, R., et al., *A novel oncoprotein RNF43 functions in an autocrine manner in colorectal cancer.* International journal of oncology, 2004. **25**(5): p. 1343-1348.
240. Eto, T., et al., *Impact of loss-of-function mutations at the RNF43 locus on colorectal cancer development and progression.* The Journal of pathology, 2018. **245**(4): p. 445-455.
241. Tsai, J.-H., et al., *RNF43 Is an Early and Specific Mutated Gene in the Serrated Pathway, With Increased Frequency in Traditional Serrated Adenoma and Its Associated Malignancy.* The American journal of surgical pathology, 2016. **40**(10): p. 1352-1359.
242. Mishra, A., et al., *Generation of focal mutations and large genomic deletions in the pancreas using inducible in vivo genome editing.* Carcinogenesis, 2019: p. bgz108.
243. Semper, R.P., et al., *Helicobacter pylori-induced IL-1β secretion in innate immune cells is regulated by the NLRP3 inflammasome and requires the cag pathogenicity island.* Journal of immunology (Baltimore, Md. : 1950), 2014. **193**(7): p. 3566-3576.
244. Eaton, K.A., M. Mefford, and T. Thevenot, *The role of T cell subsets and cytokines in the pathogenesis of Helicobacter pylori gastritis in mice.* The Journal of Immunology, 2001. **166**(12): p. 7456-7461.
245. Jang, J., et al., *LPS-induced inflammatory response is suppressed by Wnt inhibitors, Dickkopf-1 and LGK974.* Scientific reports, 2017. **7**: p. 41612-41612.
246. Schön, S., et al., *β-catenin regulates NF-κB activity via TNFRSF19 in colorectal cancer cells.* International journal of cancer, 2014. **135**(8): p. 1800-1811.
247. Wang, X., et al., *The Role of β-Transducin Repeat-Containing Protein (β-TrCP) in the Regulation of NF-κB in Vascular Smooth Muscle Cells.* Arteriosclerosis, Thrombosis, and Vascular Biology, 2004. **24**(1): p. 85-90.

248. Bronte-Tinkew, D.M., et al., *Helicobacter pylori Cytotoxin-Associated Gene A Activates the Signal Transducer and Activator of Transcription 3 Pathway In vitro and In vivo.* Cancer Research, 2009. **69**(2): p. 632-639.
249. Jenkins, B.J., et al., *Hyperactivation of Stat3 in gp130 mutant mice promotes gastric hyperproliferation and desensitizes TGF-beta signaling.* Nature medicine, 2005. **11**(8): p. 845-852.
250. Bimczok, D., et al., *Human primary gastric dendritic cells induce a Th1 response to H. pylori.* Mucosal Immunol, 2010. **3**(3): p. 260-9.
251. Grivennikov, S., et al., *IL-6 and Stat3 are required for survival of intestinal epithelial cells and development of colitis-associated cancer.* Cancer cell, 2009. **15**(2): p. 103-113.
252. Yan, S., et al., *beta-Catenin/TCF pathway upregulates STAT3 expression in human esophageal squamous cell carcinoma.* Cancer letters, 2008. **271**(1): p. 85-97.
253. Villarroel, A., et al., *Src and Fyn define a new signaling cascade activated by canonical and non-canonical Wnt ligands and required for gene transcription and cell invasion.* Cellular and molecular life sciences : CMLS, 2019: p. 10.1007/s00018-019-03221-2.
254. Liu, W., et al., *Dynamic characterization of intestinal metaplasia in the gastric corpus mucosa of Atp4a-deficient mice.* Bioscience reports, 2020: p. BSR20181881.
255. Mejías-Luque, R., et al., *Inflammation modulates the expression of the intestinal mucins MUC2 and MUC4 in gastric tumors.* Oncogene, 2010. **29**(12): p. 1753-1762.
256. Khurana, S.S., et al., *The Hyaluronic Acid Receptor CD44 Coordinates Normal and Metaplastic Gastric Epithelial Progenitor Cell Proliferation.* Journal of Biological Chemistry, 2013. **288**(22): p. 16085-16097.
257. Bertaux-Skeirik, N., et al., *CD44 plays a functional role in Helicobacter pylori-induced epithelial cell proliferation.* PLoS pathogens, 2015. **11**(2).
258. Garay, J., et al., *The homing receptor CD44 is involved in the progression of precancerous gastric lesions in patients infected with Helicobacter pylori and in development of mucous metaplasia in mice.* Cancer Letters, 2016. **371**(1): p. 90-98.
259. Fang, M., et al., *CD44 and CD44v6 are Correlated with Gastric Cancer Progression and Poor Patient Prognosis: Evidence from 42 Studies.* Cellular physiology and biochemistry : international journal of experimental cellular physiology, biochemistry, and pharmacology, 2016. **40**(3-4): p. 567-578.
260. Zhang, C., et al., *Identification of CD44+CD24+ gastric cancer stem cells.* Journal of cancer research and clinical oncology, 2011. **137**(11): p. 1679-1686.
261. Smith, S.M. and L. Cai, *Cell specific CD44 expression in breast cancer requires the interaction of AP-1 and NFκB with a novel cis-element.* PloS one, 2012. **7**(11): p. e50867-e50867.
262. Smith, S.M., Y.L. Lyu, and L. Cai, *NF-κB affects proliferation and invasiveness of breast cancer cells by regulating CD44 expression.* PloS one, 2014. **9**(9): p. e106966-e106966.
263. Haria, D., et al., *The Homeoprotein DLX4 Stimulates NF-κB Activation and CD44-Mediated Tumor–Mesothelial Cell Interactions in Ovarian Cancer.* The American journal of pathology, 2015. **185**(8): p. 2298-2308.
264. Quintana, I., et al., *Evidence suggests that germline RNF43 mutations are a rare cause of serrated polyposis.* Gut, 2018. **67**(12): p. 2230-2232.
265. Taupin, D., et al., *A deleterious RNF43 germline mutation in a severely affected serrated polyposis kindred.* Human genome variation, 2015. **2**: p. 15013-15013.
266. Sasaki, N., et al., *Nuclear factor-kappaB p65 (RelA) transcription factor is constitutively activated in human gastric carcinoma tissue.* Clinical cancer research : an official journal of the American Association for Cancer Research, 2001. **7**(12): p. 4136-4142.
267. Fan, Y., R. Mao, and J. Yang, *NF-κB and STAT3 signaling pathways collaboratively link inflammation to cancer.* Protein & cell, 2013. **4**(3): p. 176-185.
268. Xie, H., et al., *Association of RNF43 with cell cycle proteins involved in p53 pathway.* International journal of clinical and experimental pathology, 2015. **8**(11): p. 14995-15000.

269. Jo, Y.S., et al., *Frequent frameshift mutations in 2 mononucleotide repeats of RNF43 gene and its regional heterogeneity in gastric and colorectal cancers.* Human pathology, 2015. **46**(11): p. 1640-1646.
270. Morgan, R.G., et al., *LGR5 expression is regulated by EGF in early colorectal adenomas and governs EGFR inhibitor sensitivity.* British journal of cancer, 2018. **118**(4): p. 558-565.
271. Rollins, B.J. and C.D. Stiles, *Regulation of c-myc and c-fos proto-oncogene expression by animal cell growth factors.* In vitro cellular & developmental biology : journal of the Tissue Culture Association, 1988. **24**(2): p. 81-84.
272. Meyer, N. and L.Z. Penn, *Reflecting on 25 years with MYC.* Nature reviews. Cancer, 2008. **8**(12): p. 976-990.
273. Grice, G.L. and J.A. Nathan, *The recognition of ubiquitinated proteins by the proteasome.* Cellular and molecular life sciences : CMLS, 2016. **73**(18): p. 3497-3506.
274. Chen, Z.J. and L.J. Sun, *Nonproteolytic Functions of Ubiquitin in Cell Signaling.* Molecular Cell, 2009. **33**(3): p. 275-286.
275. Zhang, T., et al., *The ATM inhibitor KU55933 sensitizes radioresistant bladder cancer cells with DAB2IP gene defect.* International journal of radiation biology, 2015. **91**(4): p. 368-378.
276. Moding, E.J., et al., *Atm deletion with dual recombinase technology preferentially radiosensitizes tumor endothelium.* The Journal of clinical investigation, 2014. **124**(8): p. 3325-3338.
277. Squatrito, M., et al., *Loss of ATM/Chk2/p53 Pathway Components Accelerates Tumor Development and Contributes to Radiation Resistance in Gliomas.* Cancer Cell, 2010. **18**(6): p. 619-629.
278. Sturm, I., et al., *Mutation of p53 and consecutive selective drug resistance in B-CLL occurs as a consequence of prior DNA-damaging chemotherapy.* Cell Death & Differentiation, 2003. **10**(4): p. 477-484.
279. Ladeira, M.S.P., et al., *DNA damage in patients infected by Helicobacter pylori.* Cancer epidemiology, biomarkers & prevention : a publication of the American Association for Cancer Research, cosponsored by the American Society of Preventive Oncology, 2004. **13**(4): p. 631-637.
280. Perez, M.-J. and O. Briz, *Bile-acid-induced cell injury and protection.* World journal of gastroenterology, 2009. **15**(14): p. 1677-1689.
281. Jiang, B., et al., *Controlled bile acid exposure to oesophageal mucosa causes up-regulation of nuclear γ-H2AX possibly via iNOS induction.* Bioscience reports, 2016. **36**(4): p. e00357.
282. Farinati, F., et al., *Oxidative stress and inducible nitric oxide synthase induction in carcinogenesis.* Digestive diseases (Basel, Switzerland), 2010. **28**(4-5): p. 579-584.
283. Ferguson, H.R., et al., *Cyclooxygenase-2 and inducible nitric oxide synthase gene polymorphisms and risk of reflux esophagitis, Barrett's esophagus, and esophageal adenocarcinoma.* Cancer epidemiology, biomarkers & prevention : a publication of the American Association for Cancer Research, cosponsored by the American Society of Preventive Oncology, 2008. **17**(3): p. 727-731.
284. Krishnan, V., et al., *DNA damage signalling as an anti-cancer barrier in gastric intestinal metaplasia.* Gut, 2020: p. gutjnl-2019-319002.
285. Manoel-Caetano, F.S., et al., *Upregulation of the APE1 and H2AX genes and miRNAs involved in DNA damage response and repair in gastric cancer.* Genes & diseases, 2019. **6**(2): p. 176-184.
286. Karimaian, A., et al., *The crosstalk between Wnt/β-catenin signaling pathway with DNA damage response and oxidative stress: Implications in cancer therapy.* DNA repair, 2017. **51**: p. 14-19.
287. Matsuzawa, S.I. and J.C. Reed, *Siah-1, SIP, and Ebi collaborate in a novel pathway for beta-catenin degradation linked to p53 responses.* Molecular cell, 2001. **7**(5): p. 915-926.

288. Watcharasit, P., et al., *Direct, activating interaction between glycogen synthase kinase-3beta and p53 after DNA damage.* Proceedings of the National Academy of Sciences of the United States of America, 2002. **99**(12): p. 7951-7955.
289. Huang, S., et al., *DDB2 Is a Novel Regulator of Wnt Signaling in Colon Cancer.* Cancer research, 2017. **77**(23): p. 6562-6575.
290. Wittschieben, B.Ø., S. Iwai, and R.D. Wood, *DDB1-DDB2 (xeroderma pigmentosum group E) protein complex recognizes a cyclobutane pyrimidine dimer, mismatches, apurinic/apyrimidinic sites, and compound lesions in DNA.* The Journal of biological chemistry, 2005. **280**(48): p. 39982-39989.
291. Zou, N., et al., *DDB2 increases radioresistance of NSCLC cells by enhancing DNA damage responses.* Tumour biology : the journal of the International Society for Oncodevelopmental Biology and Medicine, 2016. **37**(10): p. 14183-14191.
292. Yeh, C.-C., et al., *Polymorphisms of MTHFR C677T and A1298C associated with survival in patients with colorectal cancer treated with 5-fluorouracil-based chemotherapy.* International Journal of Clinical Oncology, 2017. **22**(3): p. 484-493.
293. Okazaki, S., et al., *Predictive value of TLR7 polymorphism for cetuximab-based chemotherapy in patients with metastatic colorectal cancer.* International Journal of Cancer, 2017. **141**(6): p. 1222-1230.
294. Wen, D., et al., *Reduced Frequency and Prognostic Significance of Ring Finger Protein 43 Nucleotide Polymorphisms in a Chinese Colorectal Cancer Cohort.* DNA and Cell Biology, 2019. **38**(6): p. 541-548.
295. Mailand, N., et al., *RNF8 ubiquitylates histones at DNA double-strand breaks and promotes assembly of repair proteins.* Cell, 2007. **131**(5): p. 887-900.
296. Tu, J., et al., *The most common RNF43 mutant G659Vfs*41 is fully functional in inhibiting Wnt signaling and unlikely to play a role in tumorigenesis.* Scientific reports, 2019. **9**(1): p. 18557-18557.
297. Li, S., et al., *Commonly observed RNF43 mutations retain functionality in attenuating Wnt/β-catenin signaling and unlikely confer Wnt-dependency onto colorectal cancers.* Oncogene, 2020: p. 10.1038/s41388-020-1232-5.

# 8 Publications

Victoria Neumeyer*, Martina Grandl*, Alisa Dietl, Anna Brutau-Abia, Michael Allgäuer, Behnam Kalali, Yang Zhang, Kai-Feng Pan, Katja Steiger, Michael Vieth, Martina Anton, Raquel Mejías-Luque*, Markus Gerhard*.; Loss of Endogenous RNF43 Function Enhances Proliferation and Tumour Growth of Intestinal and Gastric Cells.; Carcinogenesis 40 (4), 551-559, 2019 Jun 10.; DOI: 10.1093/carcin/bgy152

Victoria Neumeyer, Michael Vieth, Markus Gerhard, Raquel Mejías-Luque.; Mutated Rnf43 Aggravates Helicobacter Pylori-Induced Gastric Pathology.; Cancers (Basel) 11 (3), 2019 Mar 16.; DOI: 10.3390/cancers11030372

Victoria Neumeyer, Anna Brutau-Abia, Michael Allgäuer, Nicole Pfarr, Wilko Weichert, Christina Falkeis-Veits, Elisabeth Kremmer, Michael Vieth, Markus Gerhard, Raquel Mejías-Luque.; Loss of RNF43 Function Contributes to Gastric Carcinogenesis by Impairing DNA Damage Response.; Cellular and Molecular Gastroenterology and Hepatology. 2021;11(4):1071-1094. doi: 10.1016/j.jcmgh.2020.11.005

# 9 Declaration

I, Victoria Neumeyer, hereby declare that I independently prepared the present thesis, using only the references and resources stated. This work has not been submitted to any examination board yet. Parts of this work have already been published in the scientific journals Carcinogenesis (Title: “Loss of Endogenous RNF43 Function Enhances Proliferation and Tumour Growth of Intestinal and Gastric cells”), Cancers (Basel) (Title: “Mutated Rnf43 Aggravates *Helicobacter Pylori*-Induced Gastric Pathology”), and Cellular and Molecular Gastroenterology and Hepatology (Title: “Loss of RNF43 Function Contributes to Gastric Carcinogenesis by Impairing DNA Damage Response”).

# 10 Acknowledgements

First of all, I would like to thank my mentor, Dr. Raquel Mejías Luque for this interesting project, and her guidance and support during my dissertation. She always believed in me and encouraged me to become a self-reliant and open minded scientist. She has taught me so many things, including a lot of Spanish and just the right amount of perfectionism.

I would like to thank my first supervisor, Prof. Dr. Markus Gerhard for the opportunity to work on this project in his group, and for his enthusiasm and motivation. Furthermore, I am deeply grateful for his continuous support and scientific input.

My thanks also go to my second supervisor, Prof. Dr. Percy Knolle, for his critical feedback and constructive discussions in the committee meetings.

Furthermore, I would like to thank Andreas Wanisch for his support in the lab, and more importantly, for his friendship that has definitely helped to survive the more difficult times of the past years.

Special thanks also go to Anna Brutau Abia for joining me in the fight of introducing mutations into RNF43, for her support in this project, her friendship, and her patience in teaching me Spanish.

I would also like to thank Karin Taxauer and Karin Mink for their inspiring teamwork on the organoid project, Dr. Raphaela Semper for her support on a scientific and experimental level, and Martin Skerhut for his support in the animal experiments. Furthermore, I owe my thanks to our technical assistant students, Nicolai Buse, Monika Schön and Levi Thumm for their excellent support in the lab. I would like to thank all former and current members of the AG Gerhard for their assistance, inspiration and the great working atmosphere.

I am very grateful for all other friends I have made at the institute, especially Wichtl, Julia, Marten, the Simons and Monika who made lunch and coffee breaks a lot more enjoyable.

Most importantly, I would like to thank my family and friends for their endless support throughout this thesis, for their unconditional love and their patience. Lastly, I would like to thank my husband Florian for his love and support and for being by my side all those years.